9-2010

Catalytic Fast Pyrolysis of Biomass for the Production of Fuels and Chemicals

Torren Ryan Carlson
University of Massachusetts Amherst, tcarlson@ecs.umass.edu

CATALYTIC FAST PYROLYSIS OF BIOMASS FOR THE PRODUCTION OF FUELS AND CHEMICALS

A Dissertation Presented

by

TORREN R. CARLSON

Submitted to the Graduate School of the
University of Massachusetts Amherst in partial fulfillment
of the requirements for the degree of

DOCTOR OF PHILOSOPHY

September 2010

Chemical Engineering

CATALYTIC FAST PYROLYSIS OF BIOMASS FOR THE PRODUCTION OF FUELS AND CHEMICALS

A Dissertation Presented

by

TORREN R. CARLSON

Approved as to style and content by:

_____
George W. Huber, Chair

_____
W. Curt Conner, Member

_____
Scott M. Auerbach, Member

_____
T. J. (Lakis) Mountziaris, Department Head
Chemical Engineering

DEDICATION

To skateboarding. The best stress relief.

ACKNOWLEDGMENTS

First and foremost I would like to thank George Huber for his guidance and support. I'm very excited to be his first graduate and am lucky to have witnessed and been a part of the building of his successful career. I would also like to thank Curt Conner and Scott Auerbach for their guidance as well. Curt has been a huge help with planning of many of the experiments. He is a seasoned experimentalist and when he would tell me "yeah I tried that before" I was not discouraged but rather comforted that he had been down the same road. Scott has helped greatly with many enlightening discussions. He is also a great dancer (as long as the Grateful Dead are playing). I would like to thank Geoff Tompsett, Tushar Vispute, Jungho Jae, Yu-Ting Cheng, Huiyan Zhang and Yu-Chuan Lin for co-authoring several papers with me. Their help, hard work and countless hours of discussion were vital to the quality of our publications. I would also like to thank the other members of the Huber research group for help with equipment and their insight. I would like to thank my family for their support. I'm very grateful that my father passed on his mechanical knowledge to me. Without his help and encouragement I don't think I ever could have turned out to be a successful experimentalist. I would also like to thank my girlfriend Elli Schmidt for her love and support. I'm very lucky to have such a wonderful woman in my life. Lastly, I would like to acknowledge the funding agencies that made this research possible. This work was supported by the National Science Foundation (CBET division) through a CAREER grant and an MRI award, John and Elizabeth Armstrong, the Department of Energy through an EFRC grant and the Defense Advanced Research Project Agency through the Defense Science Office Cooperative Agreement 30 W911NF-09-2-0010.

ABSTRACT

CATALYTIC FAST PYROLYSIS OF BIOMASS FOR THE PRODUCTION OF FUELS AND CHEMICALS

SEPTEMBER 2010

TORREN R. CARLSON, B.S., UNIVERSITY OF MINNESOTA

Ph.D., UNIVERSITY OF MASSACHUSETTS AMHERST

Directed by: Professor George W. Huber

Due to its low cost and large availability lignocellulosic biomass is being studied worldwide as a feedstock for renewable liquid biofuels. Currently there are several routes being studied to convert solid biomass to a liquid fuel, which involve multiple steps at long residence times thus greatly increasing the cost of biomass processing. Catalytic fast pyrolysis (CFP) is a new promising technology to convert directly solid biomass to gasoline-range aromatics. CFP involves the rapid heating of biomass (~500˚C sec^{-1}) in an inert atmosphere to intermediate temperatures (400 to 600 ˚C) in the presence of zeolite catalysts. During CFP, biomass is converted in a single step to produce gasoline-range aromatics which are compatible with the gasoline of the current market. CFP has many advantages over other conversion processes including short residence times (2-10 s) and inexpensive catalysts. The major impediment to the further development of CFP is the lack of fundamental understanding of the underlying chemistry of the process. The first goal of this thesis is to study the underlying chemistry of the CFP process using model compounds to aid in catalyst and reactor design. The second goal is to optimize the CFP process for real biomass feeds in a larger continuous fluidized bed reactor.

The production of aromatics from glucose by catalytic fast pyrolysis occurs in two steps. First glucose is thermally decomposed to smaller oxygenates through retro-aldol fragmentation, Grob fragmentation and dehydration reactions. At low temperatures (<300 ^{o}C) retro-aldol and Grob fragmentation reactions are favored with d-glyceraldehyde, hydroxyacetone and hydroxyacetaldehyde being the primary products. At higher temperatures (>300 ^{o}C) dehydration is favored with levoglucosan as the major product. The addition of ZSM-5 catalyst into the pyrolysis reactor lowers the temperature at which the fragmentation and dehydration reactions occur to 206 ^{o}C and 312 ^{o}C, from 282 ^{o}C and 369 ^{o}C, respectively. In the second step of catalytic fast pyrolysis, the dehydrated products enter into the catalyst pores where they are converted into aromatics, olefins, CO, CO_2, and water. The catalytic conversion step is significantly slower than the initial pyrolysis reaction. The aromatic product selectivity is a function of catalyst-to-glucose weight ratio, heating rate and reaction temperature. At 600 ˚C, a maximum carbon yield of 32% aromatics is realized after 240 s with catalysts-to-feed ratio of 19. The major competing reaction to aromatic production is the formation of coke. Coke is most likely formed by polymerization of the furans on the external catalyst surface.

Catalytic fast pyrolysis of pine wood saw dust and furan (a model biomass compound) with ZSM-5 based catalysts was studied with three different reactors: a bench scale bubbling fluidized bed reactor, a fixed bed reactor and a semi-batch pyroprobe reactor. The highest aromatic yield from sawdust of 14 % carbon in the fluidized bed reactor was obtained at low biomass weight hourly space velocities (less than 0.5 hr^{-1}) and high temperature (600 ^{o}C). The aromatic product consists mainly of benzene (24.8 %

carbon), toluene (34.1% carbon), xylene (15.4% carbon) and naphthalene (14.9 % carbon). Olefins (primarily ethylene and propylene) were also produced with a carbon yield of 5.4 %. The biomass weight hourly space velocity and the reactor temperature can be used to control both aromatic yield and selectivity. At low biomass WHSV the more valuable monocyclic aromatics such as toluene and xylene are produced and the formation of less valuable polycyclic aromatics such as naphthalene is inhibited. Lowering the reaction temperature also results in more valuable monocyclic aromatics. The olefins produced during the reaction can be recycled to the reactor to produce additional aromatics. Propylene is more reactive than ethylene. Co-feeding propylene to the reactor results in a higher aromatic yield in both continuous reactors and higher conversion of the intermediate furan in the fixed bed reactor. When olefins are recycled, the aromatic yield from wood of 20 % carbon can be obtained. After ten reaction regeneration cycles there were metal impurities deposited on the catalyst, however, the acid sites on the zeolite are not affected. Of the three reactors tested the batch pyroprobe reactor yielded the most aromatics, however, the aromatic product is largely naphthalene. The continuous reactors produce less naphthalene and the sum of aromatics plus olefin products is higher than the pyroprobe reactor.

TABLE OF CONTENTS

LIST OF TABLES

Table Page

LIST OF FIGURES

Figure Page

CHAPTER 1

INTRODUCTION

Due to its low cost and large availability, lignocellulosic biomass is being studied worldwide as a feedstock for renewable liquid biofuels.[1-4] Lignocellulosic biomass is not currently used as a liquid fuel feedstock because the economical processes for its conversion has yet to be developed.[1] Currently there are several routes being studied to convert solid biomass to a liquid fuel, which involve multiple steps thus greatly increasing the cost of biomass conversion.[5] For example, ethanol production from lignocellulosic biomass, involves multiple steps including: pretreatment, enzymatic or acid hydrolysis, fermentation, and distillation.[2] Dumesic and co-workers have demonstrated that diesel range alkanes can be produced by aqueous-phase processing (APP) of aqueous carbohydrate solutions at low temperatures (100-300°C).[6] APP first requires that solid lignocellulosic biomass be converted into aqueous carbohydrates which would require pretreatment and hydrolysis steps. Dauenhauer et al. have shown that solid biomass can be reformed at high temperatures (~800°C) to produce synthesis gas through partial oxidation in an auto thermal packed bed reactor over Rh catalysts.[7] The ideal process for solid biomass conversion involves the production of liquid fuels directly from solid biomass in a single step at short residence times. Fast pyrolysis of biomass comes very close to this ideal process since solid biomass is converted directly into liquid fuels, called bio-oils or pyrolysis oils, in a single reactor at short residence times. Fast pyrolysis involves rapidly heating biomass (>500°C sec^{-1}) to intermediate temperatures (400-600°C) followed by rapid cooling (vapor residence times 1-2 s).[8] The importance of pyrolysis heating rate is well known as several researches have shown

the yield of bio-oil is increased when high heating rates are used.[9, 10] This technology is economical on the smaller scale where smaller distributed plants can be built close to the location of the biomass.[11, 12] However, the bio-oils are of poor fuel quality. They are thermally unstable, degrade with time, are acidic, have a low heating value, and are not compatible with existing petroleum-derived oils.[13] Bio-oils must be catalytically upgraded and/or stabalized if they are to be used as a conventional liquid transportation fuel.[14-16] Catalytic fast pyrolysis (CFP) is a promising method for the direct conversion of solid biomass into gasoline range aromatic products.[14, 17-23] CFP involves the pyrolysis of biomass in the presence of zeolites. In the first step of this reaction, the solid biomass is rapidly heated (>500 °C s^{-1}) to intermediate temperatures (400-600°C). At these high temperatures, the biomass readily decomposes into pyrolysis vapors. These pyrolysis vapors then enter into the zeolite catalyst pores where they are converted into aromatics, CO, CO_2, and H_2O.[24] One advantage of CFP is that solid biomass is directly converted into liquid aromatic fuel in a single reactor with short residence times without the need for additional upgrading steps. Hence, conversion is rapid, continuous and uncomplicated. All the reaction chemistry occurs in one single reactor which is advantageous compared to gasification and fermentation technologies which all require a number of different reactors. The major challenge with catalytic fast pyrolysis is to avoid undesired coke formation, which can be produced from both homogeneous and heterogeneous reactions.[18]

The focus of this thesis is to study the key reaction parameters, chemistry and kinetics of catalytic fast pyrolysis. The mechanism of catalytic conversion of biomass to aromatics over a zeolite catalyst is not fully understood, however, there is evidence of

many of the general reaction steps. CFP involves the homogeneous thermal decomposition of the biomass to smaller oxygenates.[25-27] These oxygenates are then dehydrated. The dehydrated oxygenates diffuse into the zeolite catalyst pores where they undergo a series of oligomerization, decarbonylation and dehydration reactions to produce aromatics, CO, CO_2 and water at the active sites.[28] Isotopic studies of CFP for ^{13}C and ^{12}C glucose have shown that the oxygenates are all monoisotopic and the aromatics produced are a random mixture of ^{13}C and ^{12}C.[28] This indicates that the aromatics are produced from a hydrocarbon pool composed of the decomposed oxygenated compounds.

Several researchers have used zeolite catalysts for conversion of biomass-derived feedstocks into aromatics. This includes the early work in the 1980s by Chen et al., Haniff et al. on the conversion of carbohydrate feeds.[29-31] Chen et al. reported that aqueous glucose solutions can be converted to hydrocarbons in an atmospheric pressure fixed bed reactor operated at 510 °C. [29] Hanniff also reported that glucose could be converted in a micro reactor with ZSM-5 as well as MnZSM-5 and ZnZSM-5. However, they reported low yields of hydrocarbons as polymerization of the carbohydrate feed was favored at temperatures above 350 °C.[31]

In addition to direct conversion of carbohydrates, several researches have studied the upgrading of pyrolysis oils with zeolite catalysts.[15, 32-36] Horne et al. reported a three fold increase in aromatic yield when the pyrolysis vapors from a fluidized bed reactor where passed over a secondary fixed bed of ZSM-5 catalyst.[15] More recently high aromatic yields have been obtained from lignocellulosic biomass in one step by introducing zeolite catalysts directly into various types of pyrolysis reactors. [17, 19, 20, 22,

[23]. Pattiya et al. used a fixed bed micro reactor to study the catalytic pyrolysis of cassava rhizome. Out of the four catalysts tested; ZSM-5, Al-MCM-41 and Al-MSU-F and a proprietary alumina-stabilised ceria MI-575, ZSM-5 yielded the most aromatics in the resulting bio-oil.[22]

Several researchers have also performed catalytic pyrolysis in continuous fluidized bed reactors.[19, 20, 23] Olazar et al. reported high yields of aromatics (28% of the theoretical yield) in a canonical spouted bed reactor using ZSM-5 catalyst.[20] Aho et al. tested several types of zeolites for the catalytic pyrolysis of softwood in a fluidized bed reactor.[23] They reported that β-zeolite, mordenite, Y-zeolite, and ZSM-5 all produced different product spectra in the resulting bio-oil. The addition of ZSM-5 significantly decreased the amount of acids and alcohols in the bio-oil while the amount of ketones was increased. Lappas et al. reported on the use of a lab scale FCC unit for the catalytic pyrolysis of pine wood with a commercial fluid catalytic cracking catalyst and a commercial ZSM-5 additive.[19] They reported that addition of catalyst increased the yield of water, non-condensable gases and char. The bio-oil obtained was of lower oxygen content and therefore of better quality.

The objective of this thesis is to develop a single step process to convert biomass to aromatics by integrating zeolite catalyst into the fast pyrolysis process. In this thesis I will specifically study the chemistry for the conversion of biomass to aromatics over zeolite catalysts and how process parameters (e.g. temperature, reactor type) affect the hydrocarbon selectivity. These basic studies will aid in the design of new reactors and catalyst properties specifically tailored to optimize aromatic production in the catalytic fast pyrolysis process.

CHAPTER 2

EXPERIMENTAL METHODS

2.1 Feed

Furan (Sigma-Aldrich) was used as feedstock without any pretreatment. The wood for the pyroprobe and fluidized bed studies was eastern pine sawdust. The elemental analysis of the wood feed is shown in Table 2.1.1. The chemical formula for the untreated wood used is therefore approximately $C_4H_6O_3$. The moisture content of the feed was determined to be 4 wt% by the mass difference between a 5 g sample of feed before and after drying in a 95 °C oven overnight. On a dry basis the approximate chemical formula of the wood is $C_{3.8}H_{5.8}O_{2.7}$. The ash content was determined by the mass difference between a 1 g sample of feed before and after burning in air at 600 °C for 5 hours in a muffle oven.

Table 2.1.1 Elemental analysis of eastern pine wood.

Elemental analysis (wt%)			
C	H	O[a]	Ash
46.19	6.02	47.29	0.47

[a] By balance.

2.2 Catalyst

For the fixed bed studies, ZSM-5 powder in the proton form (Zeolyst CBV 3024E, Si/Al = 60) was used. The as received ZSM-5 catalyst was sieved to 425 – 800 μm before reaction. Prior to reaction, the catalyst was calcined for 5 hours in the fixed bed reactor at 600 °C with flowing air (Airgas) at 60 mL/min. The catalyst used in the fluidized bed experiments was a commercial spray dried ZSM-5 catalyst (BioCat1, Grace

Davison). The catalyst was calcined in the reactor for 4 hours at 600 °C in 1200 mL min^{-1} flowing air prior to reaction. For reactions in the pyroprobe batch reactor, both catalysts were calcined in a muffle oven at 600 °C for 5 hours. The Grace Davison catalyst was characterized before and after ten reaction/regeneration cycles by XRD (PANalytical X'Pert Pro Material Research Diffractometer) and SEM (JEOL JSM-5400 Scanning electron microscope). Ammonia TPD curves of the fresh and spent catalyst were measured using a ChemBET Pulsar TPR/TPD system (Quantachrome Instruments). The samples were degassed at 450 °C in 60 ml min^{-1} of flowing helium. Ammonia was adsorbed at 100 °C for 20 minutes followed by purging with helium for one hour. TPD was performed from 100 to 600 °C with a temperature ramp rate of 10 °C min^{-1}. FTIR spectra of adsorbed ammonia at 150 °C were taken using a DRIFTS cell (Harrick Scientific) with an Equinox 55 FTIR spectrometer (Bruker).

2.3 Pyroprobe

Fast pyrolysis experiments were conducted using a model 2000 pyroprobe analytical pyrolizer (CDS Analytical Inc.). The probe is a computer controlled resistively heated element which holds an open ended quartz tube (pictured in Figure 2.1.1). Powdered samples are held in the tube with loose quartz wool packing; during pyrolysis vapors flow from the open ends of the quartz tube into a larger cavity (the pyrolysis interface) with a helium carrier gas stream.

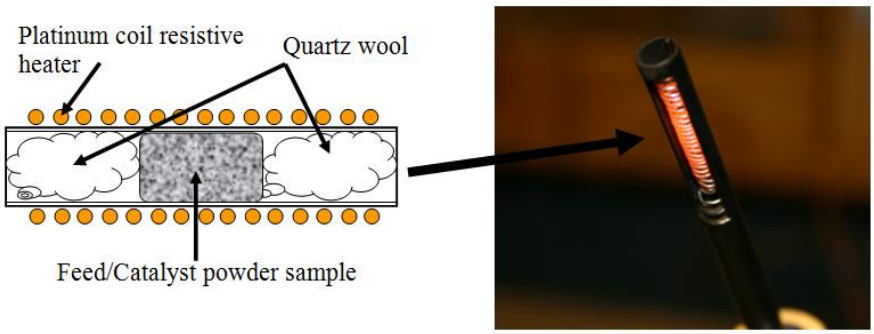

Figure 2.3.1 Diagram of the pyroprobe reactor setup. On the left a schematic cross-section of the prepared sample is pictured (not to scale). Powdered reactants and catalysts are held with loose quartz wool packing. Pictured on the right is the resistively heated element which holds the sample tube (2 mm x 25 mm). During reaction, product vapors flow from the open ends of the sample tube into the GC/MS interface via a helium sweeper gas stream.

The carrier gas stream is routed to a model 5890 gas chromatograph (GC) interfaced with a Hewlett Packard model 5972A mass spectrometer (MS). The pyrolysis interface was held at 100 °C and the GC injector temperature used was 275 °C. Helium was used as the inert pyrolysis gas as well as the carrier gas for the GC/MS system. A 0.5 ml min^{-1} constant flow program was used for the GC capillary column (Restek Rtx-5sil MS). The GC oven was programmed with the following temperature regime: hold at 50 °C for 1 min, ramp to 200 °C at 10 °C min^{-1}, hold at 200 °C for 15 min. Products were quantified by injecting calibration standards into the GC/MS system. All yields are reported in terms of molar carbon yield where the moles of carbon in the product are divided by the moles of carbon in the reactant. The aromatic selectivity reported is defined as the moles of carbon in an aromatic species divided by the total moles aromatic species carbon. Similarly, the oxygenate selectivity is defined as the moles of carbon in an oxygenated species divided by the total moles oxygenated species carbon.

Powdered reactants were prepared by physically mixing the glucose feed and the catalyst. For a typical run 8-15 mg of reactant-catalyst mixture was used. Both the feed

and the catalyst were sifted to <140 mesh before mixing. The physical mixtures of glucose were prepared with a ZSM-5 (Si/Al = 60, WR Grace) to D-glucose (Fisher) ratio of 19, 9, 4, 2.3, and 1.5. Xylitol (Fisher) /ZSM-5. Cellobiose (Acros) /ZSM-5, and cellulose (Whatnam) /ZSM-5 with a catalyst to feed ratio of 19 were also tested. The ^{13}C labelled carbon experiments were conducted using a mixture of ^{12}C glucose (Fisher) and ^{13}C labelled glucose (Cambridge Isotope Labs) in a weight ratio of 1:1. Both the feed and the catalyst were sifted to <140 mesh before mixing. The physical mixtures of glucose were prepared with a ZSM-5 (Si/Al = 60, WR Grace) to feed ratio of 19 and 2.3. A 1:1 weight ratio mix of 12C naphthalene (fisher) and 13C labelled glucose was prepared and physically mixed with ZSM-5 to a ZSM-5 to feed weight ratio of 19. A ^{12}C benzene (fisher) and ^{13}C labelled glucose was prepared by first physically mixing glucose and ZSM-5 to a glucose to ZSM-5 weight ratio of 38. Benzene was then added to the catalyst-glucose mixture until a 1:1 glucose to benzene weight ratio was obtained thus resulting in a final ZSM-5 to feed ratio of 19. ZSM5 was calcined at 500°C in air for 5 hours prior to reaction. Samples with a catalyst:glucose ratio of 19 were also prepared with the following catalysts: Silicalite (Grace), β-zeolite, Y-zeolite (Si/Al = 50, Degussa) , and mesoporous SiO_2/Al_2O_3 (Si/Al = 8, Davison).

For the speciation and quantification of pure glucose pyrolysis products (which are mostly thermally unstable), an in-house designed trap was employed. The trap consists of a 25 mL pyrex vial, a screw-tight frame with plug-valve controlled gas inlet and outlet, and the pyroprobe pyrolizer. A 1/4 inch channel allows the pyroprobe pyrolizer to be inserted from the top of frame into the center of vial. Prior to each trial, the vial was flushed with ultra-high purity helium at 50 mL min^{-1} flow rate for 10 minutes. After

purging, the vial is made gastight by closing the outlet and inlet valves. The trap is then transferred in a dewar flask with a liquid nitrogen bath at 77 K, which allows rapid quenching of volatiles evolved during reaction. After reaction the condensed products on the walls of the vial are quantitatively removed with 1 mL of methanol. The methanol solution is then analyzed using a GC-MS (Shimadzu GC-2010 and QP2010S, analytes separated by Restek RTX-VMS).

2.4 Thermogravimetric Analysis with Mass Spectrometry (TGA-MS)

Thermogravimetric analysis was performed with a Q600 TGA system (TA Instruments). A quadruple mass spectrometer (Extorr XT 300) was coupled via a heated line to the TGA to measure the volatile species produced during pyrolysis. The heated transfer line was held at 250 ^{o}C to circumvent condensation of the product vapors. A low electron ionization voltage of 29 eV was used to suppress sondary fragmentation. The total pressure of ion source was 10^{-6} Torr. The ions measured for each run include 2, 16, 18, 28, 44, 78, 91, and 128 m/z. Ultra-high-purity helium (AirGas, NH) was used as the sweeper gas with a flow rate of 100 mL min^{-1}. External and internal mass transfer limitations were investigated by varying sweeper gas flow rates (from 50 to 200 mL min^{-1}) and particle sizes (from 40 to 325 mesh). Both were found to be negligible. For a typical run approximately 5 mg of powdered sample was used for pure glucose pyrolysis and about 30 mg for the glucose-ZSM-5 mixture. Prior to all trials, samples were preheated to 110 °C for 30 minutes, under helium flow, to remove physically adsorbed water. Pyrolysis was then carried out from 50 °C to 600 °C with a designated heating rate (0.017, 0.25, or 2.5 °C s^{-1}).

2.5 Fourier-Transform Infrared (FTIR)

FTIR spectra were obtained from the zeolite samples using a Bruker Equinox 55 infrared spectrometer. The KBr method was employed using spectroscopic grade KBr mixed with the zeolite/glucose in a 100: 5 weight ratio. An average of 50 scans at 4 cm^{-1} resolution were obtained for each KBr pellet. This method is as used by Bilba et al. [37] and Sharma et al.[38] KBr pellet method was used due to the low quantity of samples prepared using the pyroprobe reactor.

2.6 Elemental Analysis (EA)

Carbon on the spent catalyst was quantified by elemental analysis (performed by Schwarzkopf Microanalytical Lab, Inc., NY). The missing carbon can be attributed to: non quantified thermally unstable oxygenated species (which cannot be detected in our experimental setup), and coking of the pyrolysis interface or transfer lines.

2.7 Nitrogen Adsorption

Nitrogen adsorption experiments was carried out at the normal boiling point of N_2 (-196 °C) for the determination of external surface area and micropore volume (t-method) using an AUTOSORB®-1-MPC (Quantachrome Instruments; Boynton Beach, FL) gas adsorption system. Prior to the measurement, the samples were outgassed at 300 °C for 24 h under vacuum. Coked catalyst sample were prepared by using the catalyst after reaction at 600 °C for 240s, mixing fresh glucose at 5wt% and 30wt% and running a second pyrolysis treatment at 600 °C for 240 s.

2.8 Fluidized Bed Reactor

A schematic of the fluidized bed reactor system is shown in Figure 2.8.1 The fluidized bed reactor is a 2 in 316 stainless steel tube 10 in tall. The wood feed was injected by a stainless steel auger into the side of the reactor from a sealed feed hopper. To maintain an inert environment in the reactor, the hopper is swept with helium at a rate of 200 mL min^{-1}. The wood used was sieved to a particle size of 0.25-1 mm before loading it into the hopper. The catalyst bed is supported by a distributor plate made from stacked 316 stainless steel mesh (300 mesh). During the reaction, catalyst is fluidized via a helium gas stream controlled by a mass flow controller to a flow rate of 1200 sccm. The gas flow rate and catalyst used resulted in a bubbling fluidized bed flow regime. [39] Both the reactor and the inlet gas stream are resistively heated to reaction temperature. During reaction, product gases exit the top of the reactor and pass through a cyclone wherein entrained solids are removed and collected. The vapor then passes through a condenser train. The first three condensers are operated at 0 °C in an ice bath and the following three condensers are operated at -55 °C in a dry ice/acetone bath. The non-condensed vapors exiting the condenser train are collected in a tedlar gas sampling bag for GC/MS and GC/FID analysis. Liquids collected in the condensers are quantitatively removed after reaction with an ethanol solvent and analyzed with GC/MS and GC/FID. For a typical run, wood is fed to the reactor for 30 min. After the feed is stopped the reactor is purged with 1200 sccm of helium for another 30 min at reaction temperature to strip any remaining product from the catalyst.

For the olefin co-feed experiments, the secondary gas (T2 in Figure 2.8.1) was switched to either ethylene or propylene and controlled at the desired flow rate. The

helium fluidization gas flow rate was adjusted to hold the total inlet gas flow rate constant at 1200 mL min^{-1}.

After reaction and purge, the secondary gas is switched to air to regenerate the catalyst. For a typical run, the catalyst was regenerated for approximately three hours to ensure no organic species remained on the. The combustion effluent during regeneration is passed over a copper catalyst (Sigma Aldrich) held at 250 °C to convert carbon monoxide to carbon dioxide. The carbon dioxide stream then passes over a dryrite trap to remove water vapor. The dry carbon dioxide is collected a pre weighted ascarite trap. The total moles of carbon dioxide collected in the trap are equal to the moles of carbon in coke on the catalyst bed.

The gas residence time distribution of the reactor was measured at room temperature by switching the fluidization gas from pure helium to a 2 mol % CO in helium mixture in a step change fashion. After the gas was switched, the gas samples were collected every 30 sec at the reactor. The concentration of the outlet gas was measured by GC-TCD. Three separate runs were conducted starting at different times (5, 10 and 15 sec after the gas switch) to obtain a measurement every 5 seconds.

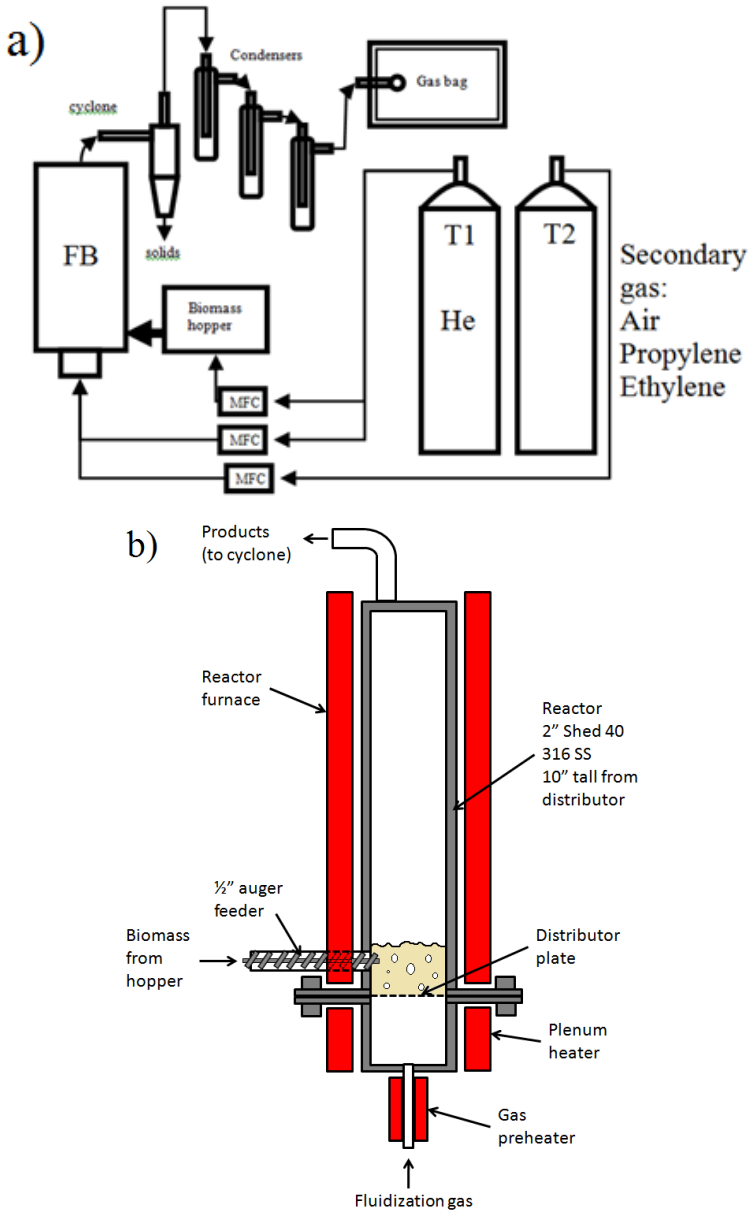

Figure 2.8.1 The experimental setup of the fluidized bed reactor system. a) schematic of the fluidized bed system, b) detailed drawing of the reactor.

2.9 Fixed bed

The fixed bed reactor was built from a ½ inch diameter quartz tube. Sieved ZSM-5 powders were held in the reactor by quartz beads (250 – 425 μm) and quartz wool. Typically ~26 mg of catalyst are used in the catalyst bed. The reactor temperature was measured using a thermocouple inserted on top of the catalyst bed. Prior to reactions, the

catalyst bed was calcined as described above. After calcinations, the reactor was flushed by helium (Airgas, ultra-high purity) for 10 min. The helium then was switched to bypass the reactor, and the inlet and outlet valves of the reactor were closed. Furan was pumped into the helium stream by a syringe pump (Fisher, KDS100) at a rate of 0.29 mL/h. The carrier gas was controlled at 204 mL/min yielding a furan partial pressure 6 torr. Prior to the run, the furan bypassed the reactor for 30 min before switching the helium stream to go through the reactor. An ice-water bath condenser was used to trap the heavy products. Gas phase products were collected by air bags. All runs were done at atmospheric pressure. After reaction, the reactor was flushed by helium with the flow rate of 30 mL/min for 20 min at the reaction temperature. Again, the effluent was collected by an air bag, and the heavy hydrocarbons were condensed in the condenser.

After flushing the reactor was cooled to room temperature with 10 mL/min helium flow. Condensed products were extracted by 10 mL ethanol from the condensers to obtain the liquid products. Both liquid and gas products were identified by GC-MS (Shimadzu-2010) and quantified by GC-FID (Shimadzu 2014 for gas samples, and HP-7890 for liquid samples). The spent catalyst was removed from the reactor and was subjected to TGA analysis to obtain coke amount. Because of the inefficiency of the condenser, less than 0.05% carbon or the products were collected in the liquid trap. The majority of the products produced during the reaction were in either the gas phase or as coke deposited on the catalyst.

CHAPTER 3

KEY REACTION PARAMETERS IN CATALYTIC FAST PYROLYSIS

3.1 Model Feedstock Selection

Ligno-cellulosic biomass is composed of three components: cellulose, hemicellulose, and lignin[13]. For this study we used the compounds glucose, cellobiose (dimer of glucose), cellulose and xylitol. The overall stoichiometry for conversion of xylitol and glucose to toluene, CO and H_2O is shown in Equation 3.1.1 and 3.1.2 respectively. Oxygen must be removed from the biomass as a combination of CO (or CO_2), and H_2O when aromatics are produced. The maximum theoretical molar carbon yield of toluene from xylitol and glucose is 76 and 63 % respectively when CO and H_2O are produced as by-products.

$$C_5O_5H_{12} \rightarrow 12/22\ C_7H_8\ (76\ \%\ \text{carbon yield}) + 26/22\ CO\ (24\ \%\ \text{carbon yield}) + 84/22\ H_2O \quad (3.1.1)$$

$$C_6O_6H_{12} \rightarrow 12/22\ C_7H_8\ (63\ \%\ \text{carbon yield}) + 48/22\ CO\ (36\ \%\ \text{carbon yield}) + 84/22\ H_2O \quad (3.1.2)$$

The hydrogen to carbon effective ratio (H/C_{eff}) as defined in Equation 3.1.3 is a way of comparing the relative amounts of hydrogen in different feeds[29, 40]. This metric can be used to classify biomass feedstocks. Feedstocks with the same H/C_{eff} ratio will have similar theoretical yields of aromatics. For example, cellulose, glucose and cellobiose all have a H/C_{eff} ratio of 0. All feedstocks with a H/C_{eff} ratio of 0 will have a molar carbon toluene yield of 63 % if CO and water are the byproducts. The H/C_{eff} ratio of biomass-derived feedstocks is significantly lower than petroleum feedstocks. For example, glucose, sorbitol and glycerol (all biomass-derived compounds) have H/C_{eff}

ratios of 0, 1/3 and 2/3 respectively. The H/C_{eff} ratio of petroleum-derived feeds ranges from slightly larger than 2 (for liquid alkanes) to 1 (for benzene).

$$H/C_{eff} = \frac{H - 2O}{C} \qquad (3.1.3)$$

Figure 3.1.1a shows the carbon yields for catalytic fast pyrolysis of xylitol, glucose, cellobiose and cellulose with ZSM-5 in the pyroprobe at the optimized reaction conditions. The major products include aromatics, CO, CO_2 and coke. No olefins were detected during catalytic fast pyrolysis in our reactor system. Olefins have been observed when glycerol and sugars where passed over ZSM-5 catalysts in previous studies.[19, 20] Xylitol has a higher yield of aromatics than the other feeds. Xylitol also has a higher H/Ceff ratio (2/5) than the other feeds (0 for cellulose, glucose, and cellobiose). The aromatic yields of these reactions are about half the theoretical yield given by Equations 2 and 3. The yield of coke is over 30 % for all of these feeds.

The grouped aromatic distribution from catalytic fast pyrolysis of biomass-derived oxygenates with ZSM-5 is shown in Figure 3.1.1b. Similar molecules are grouped together e.g. naphthalene, methyl-naphthalene and dimethyl-naphthalene are grouped at "naphthalenes". The feedstocks had a similar aromatic product distribution when tested under the same reaction conditions. The similarity of the aromatic distributions for the various feeds suggests a common intermediate forms all of these products. The aromatic selectivity decreases as napthalene >> toluene > xylenes > benzene > substituted benzene ~ indane. Naphthalene is the aromatic that is made in the highest yield. From these results glucose is selected as a model feedstock for cellulose in order to optimize reactor conditions. Cellobiose would be a good candidate for a model feedstock, however, glucose is far less expensive.

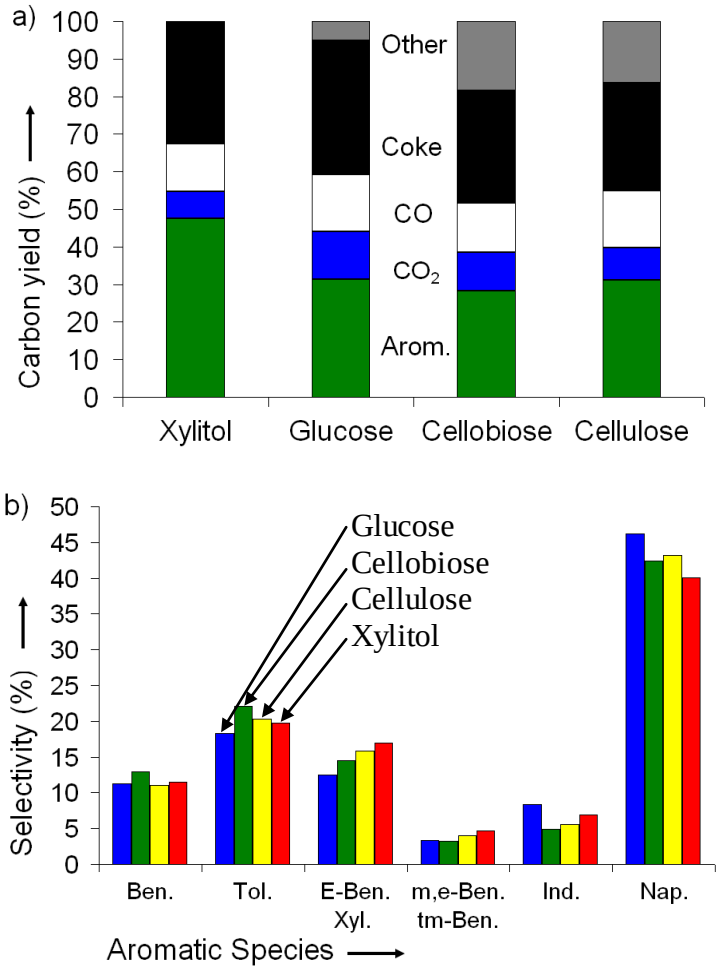

Figure 3.1.1 Catalytic fast pyrolysis of solid cellulose, cellobiose, glucose and xylitol. Reaction conditions: catalyst to feed weight ratio 19, catalyst ZSM5 (Si/Al = 60), nominal heating rate 1000 °C s-1, reaction temperature 600 °C, reaction time 240 s. a) Carbon yields for various biomass-derived feedstocks. Key for Figure 1a: Aromatics: green, CO2: blue, CO: white, coke: black, and unidentified: grey. b) Aromatic selectivity for different feeds. Key for Figure 1b: glucose feed: blue, cellulose feed: yellow, cellobiose feed: green, and xylitol feed: red. Aromatics quantified include: (Ben.) benzene, (Tol.) toluene, (E-Ben., Xyl.) xylenes, ethyl-benzene, (m,e-Ben., tm-Ben.) methyl-ethyl-benzene, trimethyl-benzene, (Ind.) indanes, (Nap.) naphthalenes.

Table 3.1.1 shows the complete list of aromatics produced from catalytic fast pyrolysis of glucose in the presence of ZSM-5 at 600 °C. It can be seen that the primary aromatics produced include benzene, toluene, 1,3-dimethyl-benzene, naphthalene, 1-methyl- naphthalene and 1,5-dimethyl- Naphthalene. Very large molecules such as methyl-phenanthrene are observed only in trace amounts. Naphthalenes are the largest

molecules produced in significant quantities, which maybe due to the size selectivity of the zeolite catalyst. Naphthalene has a kinetic diameter of ~6.0 Å[41] which is similar to the ZSM-5 pore size of ~6.2 Å (Norman radii adjusted[42]).

Table 3.1.1 Carbon yields of aromatics produced from catalytic fast pyrolysis of glucose with ZSM-5. Reaction conditions: catalyst to feed weight ratio = 19; catalyst ZSM-5 (Si/Al = 60), nominal heating rate 1000 °C s-1, reaction temperature 600 °C, reaction time 240 s.

Aromatic Component	Yield (% carbon)	Selectivity (% carbon)
Benzene	4.07	12.59
Toluene	7.53	23.29
Ethylbenzene	0.18	0.57
Xylene (m or p)	3.72	11.50
o-Xylene	1.17	3.61
Benzene, 1-methy-2-ethyl	0.20	0.61
Benzene, 1-ethyl-3-methyl	0.11	0.35
1,2,4-Trimethylbenzene	0.48	1.47
Benzene, 1-ethyl-3-methyl	0.03	0.11
Indane	0.14	0.44
Indene	0.10	0.30
Indane, 1-methyl	0.10	0.31
1H-Indene, 1-methyl	0.07	0.22
Naphthalene	4.28	13.23
Naphthalene, 1-methyl	4.25	13.15
Naphthalene, 2-methyl	2.13	6.58
Naphthalene, 1-ethyl	0.22	0.67
Naphthalene, dimethyl (isomer unknown)	1.05	3.24
Naphthalene, dimethyl (isomer unknown)	0.73	2.24
Naphthalene, dimethyl (isomer unknown)	0.55	1.71
Naphthalene, 1,3-dimethyl	0.21	0.64
Naphthalene, 1,4,6-trimethyl	0.12	0.36
Dibenzofuran	0.06	0.18
Naphthalene, 2,3,6-trimethyl	0.05	0.15
Naphthalene, 1,4,6-trimethyl	0.04	0.12
Naphthalene, trimethyl (isomer unknown)	0.03	0.08
Naphthalene, trimethyl (isomer unknown)	0.03	0.08
Fluorene	0.10	0.30
9H-Fluorene, 4-methyl	0.03	0.10
Anthracene	0.06	0.19
Phenanthrene	0.25	0.76
Anthracene, 2-methyl	0.02	0.07
Phenanthrene, 3-methyl	0.13	0.39
Phenanthrene, 2-methyl-	0.12	0.37

3.2 Catalyst Selection

Proper catalyst selection is crucial for high aromatic selectivity. Figure 3.2.1 shows catalytic fast pyrolysis of glucose with different catalysts. The catalyst that had the highest aromatic yield was ZSM-5. When no catalyst is used, the primary product is coke. The catalytic parameters that have an effect on the product distribution are pore structure and the type of acid sites. We tested ZSM-5, silicalite and mesoporous Silica-Alumina to test the relationship between catalytic parameters and catalytic activity. Silicalite and ZSM-5 have the same pore structure, but silicalite does not have acid sites. ZSM-5 contains Brønsted acid sites while silicalite does not. Silica-Alumina contains Brønsted acid sites, but is an amorphous material. Silicalite produces primarily coke indicating that Brønsted acid sites are needed for aromatic production. Silica-Alumina also produces mainly coke indicating that the pore structure of the zeolite is also needed to produce aromatics selectively. Figure 3.2.1 also includes catalytic fast pyrolysis with β-Zeolite and Y-zeolite catalysts which both produce large amounts of coke. The pore structures of the catalysts tested are quite different in nature. The ZSM-5 catalyst is a system of intersecting channels. The larger of the two channels has a near circular pore structure with dimensions of 0.54 x 0.56 nm. The smaller channels have a geometry of 0.51 x 0.54 nm. Based on the crystal structure, the intersection of these channels which contains the proposed active site is approximately a 0.9 nm cavity. Y-zeolite has a three dimensional faujasite structure. The supercages have a 1.2-1.3 nm diameter while the channels connecting the supercages have a diameter of 0.8-0.9 nm.[43] β-zeolite has intersecting channels similar to ZSM-5, however, this zeolite is a mixture of three polymorphs which have pore diameters of ~0.7 nm.[44]

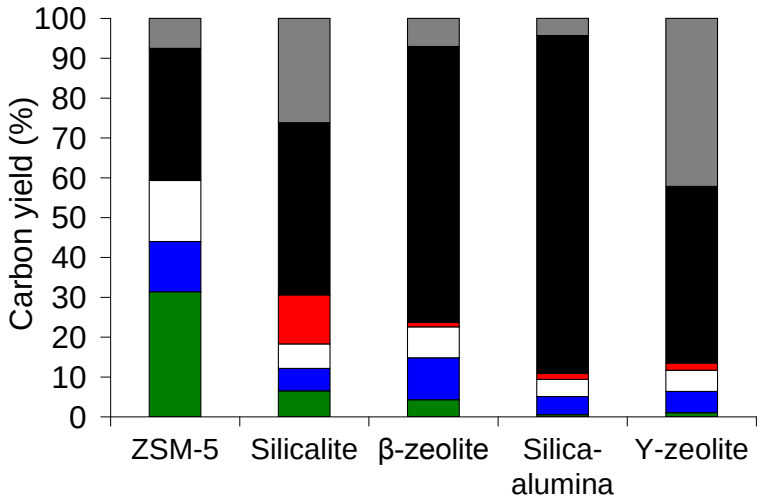

Figure 3.2.1 Catalytic fast pyrolysis of glucose with various catalysts. Reaction conditions: catalyst to feed weight ratio = 19; nominal heating rate 1000°C s-1, reaction temperature 600°C, reaction time 240 s. Key: aromatics: green, CO2: blue, CO: white, partially deoxygenated species: red, coke: black, and unidentified species: grey. Partially deoxygenated species quantified include: hydroxyacetylaldehyde, acetic acid, furan, 2-methyl furan, 2,5-dimethyl furan, furfural, 4-methyl-furfural, furan-2-methanol.

As seen in Figure 3.2.2, the aromatic selectivity can be modified with proper catalyst selection. If smaller aromatics are desired, such as benzene and toluene, then the best catalysts are Y-zeolite, β-zeolite and SiO_2-Al_2O_3. If the larger aromatics are desired, including napthalene and indane, then ZSM-5 and silicalite are the optimal catalysts. However, Y-zeolite, β-zeolite and SiO_2-Al_2O_3 produce large amounts of coke. Therefore, a significant challenge with these catalysts is to try and figure out how to minimize coke formation. Our results suggest that aromatic production is a shape selective reaction where the selectivity is a function of the structure of the zeolite catalyst.

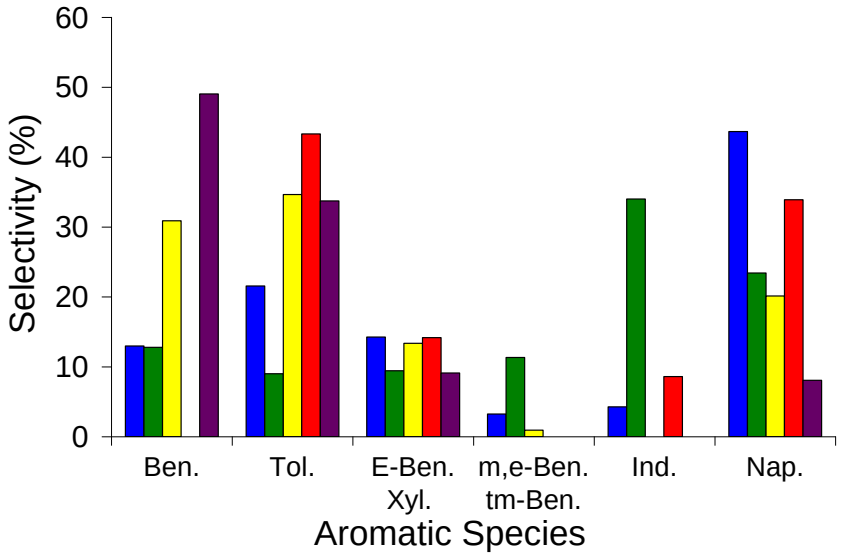

Figure 3.2.2 Aromatic selectivity for catalytic fast pyrolysis of glucose with various catalysts. Reaction conditions: catalyst to feed weight ratio = 19; nominal heating rate 1000°C s-1, reaction temperature 600°C, reaction time 240 s. Key: ZSM-5: blue, silicalite: green, β-zeolite: yellow, SiO2-Al2O3: red, Y-zeolite: purple. Aromatics quantified include: (Ben.) benzene, (Tol.) toluene, (E-Ben., Xyl.) xylenes, ethyl-benzene, (m,e-Ben., tm-Ben.) methyl-ethyl-benzene, trimethyl-benzene, (Ind.) indanes, (Nap.) naphthalenes.

3.3 Heating Rate: Pyroprobe Results

We used glucose as a model compound for cellulose to determine how the reaction parameters affect the product selectivity. As shown in Figure 3.3.1, the aromatic distribution is similar for the all feeds suggesting that the other feeds will be similar to glucose. High heating rates are needed to increase aromatic formation, as shown in Figure 3.3.1. This figure shows product yields as a function of nominal heating rate with ZSM-5 as the catalyst and glucose as the feed. As can be observed from Figure 3.3.1, the maximum aromatic yield and the lowest coke yield are obtained at the highest heating rate (1000°C sec^{-1}). The aromatic yield decreases by half and the coke yield increases from 35 to 40 % when the heating rate decreases from 1000°C s^{-1} to 1°C s^{-1}. The aromatic selectivity is not a function of heating rate, for heating rates greater than 50°C/s

as shown in Figure 3.3.2. However, for lower heating rates, the aromatic selectivity is a function of heating rate. The naphthalene selectivity decreases from 57 to 44% when the heating rate increases from 1°C s^{-1} to 50°C s^{-1}. At high heating rates, the biomass spends a maximum amount of time at the reaction temperature thus maximizing the liquid yield. These results show the importance of the heating rate in obtaining high yields of aromatics. The heating rate in continuous catalytic fast pyrolysis reactors can be controlled by proper reaction engineering.

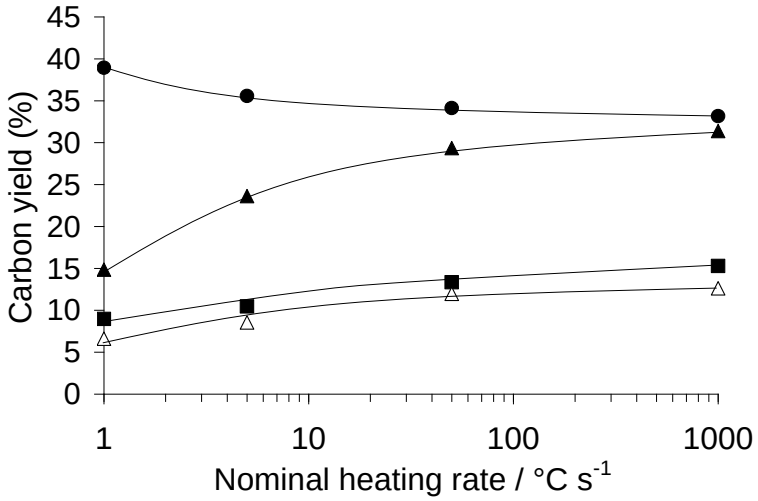

Figure 3.3.1 Carbon yield as a function of nominal heating rate for catalytic fast pyrolysis of glucose with ZSM-5. Reaction conditions: catalyst to feed weight ratio = 19; catalyst ZSM-5 (Si/Al = 60), reaction temperature 600°C, reaction time 240 s. Key: ■: carbon monoxide ▲: aromatics Δ: carbon dioxide ●: coke.

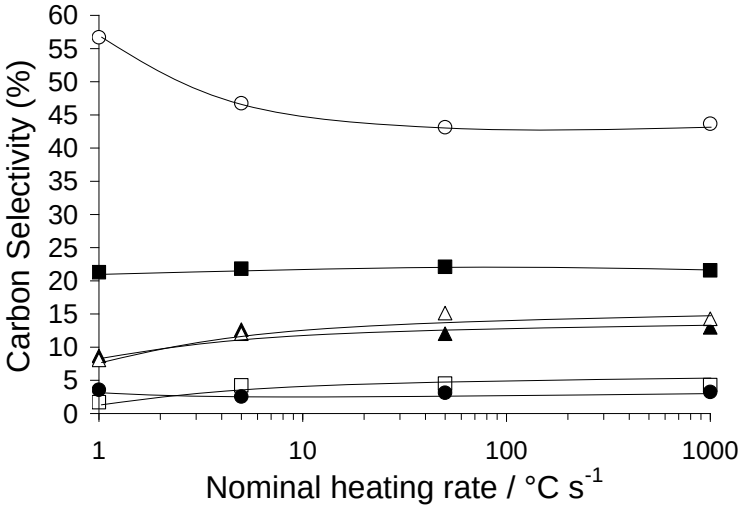

Figure 3.3.2 Aromatic selectivity as a function of nominal heating rate for catalytic fast pyrolysis of glucose with ZSM-5. Reaction conditions: catalyst to feed weight ratio = 19; catalyst ZSM-5 (Si/Al = 60), reaction temperature 600°C, reaction time 240 s. Key: ■: toluene ▲: benzene Δ: xylenes, ethyl-benzene ●: methyl-ethyl-benzene trimethyl-benzene □: indanes ○: naphthalenes.

3.4 Catalyst to Feed Ratio Pyroprobe Results

In addition to high heating rates, the product yields are also a function of the catalyst to biomass ratio. Figure 3.4.1 shows the product selectivity for catalytic fast pyrolysis of

glucose with ZSM5 as a function of the catalyst to glucose weight ratio. The coke yield increases and the aromatic yield decreases as the catalyst to glucose ratio decreases. Using a catalyst to feed ratio 19 produces the highest aromatic yield and lowest coke yield. Under thesis conditions thermally stable oxygenates form as the catalyst to glucose ratio decreases. The yield of oxygenated species decreases from 15% to ~0% with increasing catalyst to feed ratio from 1.5 to 19. The oxygenates quantified include: furan, 2-methyl furan, furfural, 4-methyl-furfural, furan-2-methanol, hydroxyacetylaldehyde, and acetic acid. Only trace amounts of anhydro sugars were also detected as the GC/MS does not allow us to detect thermally unstable compounds which are also formed in the pyrolysis process. The distribution of the partially deoxygenated species as a function of catalyst to glucose ratio for catalytic fast pyrolysis is shown in Figure 3.4.2. At high catalyst to glucose ratios, the major oxygenated products are hydroxyacetaldehyde and acetic acid. The furan selectivity increases as the catalyst to glucose ratio decreases.

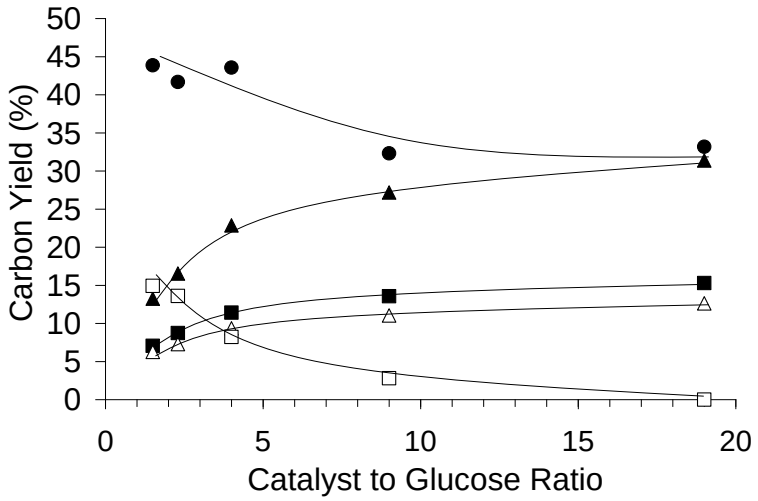

Figure 3.4.1 Effect of catalyst to glucose ratio for catalytic fast pyrolysis. Reaction conditions: nominal heating rate 1000°C s-1, final reaction temperature 600°C, reaction time 240 s. a) Carbon yield as a function of catalyst to glucose ratio. Key: ■: carbon monoxide ▲: aromatics Δ: carbon dioxide □: partially deoxygenated species ●: coke.

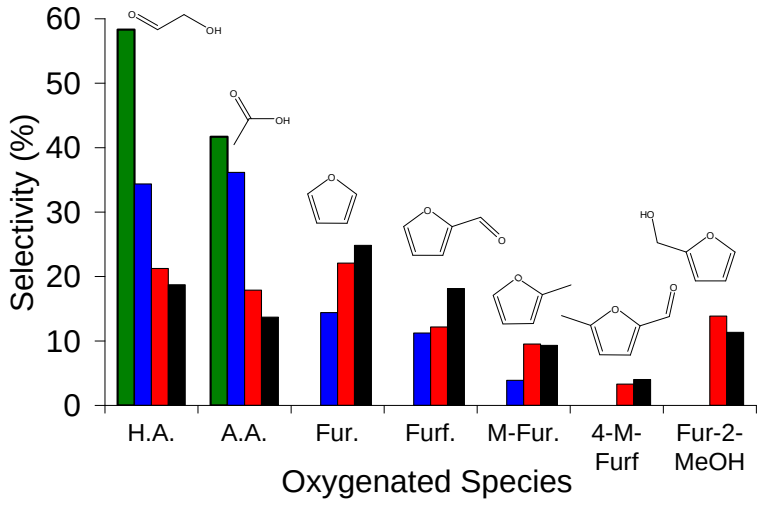

Figure 3.4.2 Distribution of partially deoxygenated species as a function of catalyst to glucose ratio for catalytic fast pyrolysis. Reaction conditions: nominal heating rate 1000°C s-1, final reaction temperature 600°C, reaction time 240 s. Key: catalyst:glucose ratio = 9 (green), catalyst:glucose ratio = 4 (blue), catalyst:glucose ratio = 2.3 (red), catalyst:glucose ratio = 1.5 (black). The species quantified include: (H.A.) hydroxyacetylaldehyde, (A.A.) acetic acid, (Fur.) furan, (Furf) furfural, (M-Fur) methyl furan, (4-M-Furf) 4-methyl furfural, (Fur-2-MeoH) furan-2-methanol.

As shown in Figure 3.4.3, the aromatic selectivity is not a strong function of the catalyst to glucose ratio. Increasing the catalyst to feed ratio slightly increases the selectivity for toluene, xylenes, and ethyl-benzene while slightly decreasing the selectivity for benzene, methyl-ethyl-benzene, trimethyl-benzene, indanes and naphthalenes. The largest change in selectivity is for the decrease of indanes from 12 to 4% and the increase of toluene from 13 to 22%.

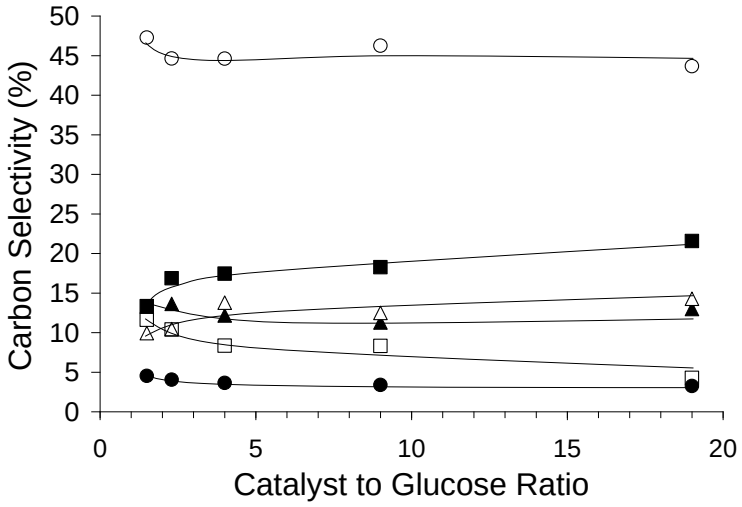

Figure 3.4.3 Distribution of aromatic species as a function of catalyst to glucose ratio for catalytic fast pyrolysis. Reaction conditions: nominal heating rate 1000°C s-1, final reaction temperature 600°C, reaction time 240 s. Key: ■: toluene ▲: benzene Δ: xylenes, ethyl-benzene ●: methyl-ethyl-benzene trimethyl-benzene □: indanes ○: naphthalenes.

3.5 Effect of Temperature on Catalytic Fast Pyrolysis of Glucose Pyroprobe Results

To investigate the effect of temperature on catalytic fast pyrolysis of glucose, final reaction temperatures of 400 °C, 500 °C, 600 °C, 700 °C and 800 °C were tested. A catalyst to feed ratio of 19:1 and heating rate of 1000 ˚C s^{-1} were used. These reaction conditions were previously determined to maximize the aromatic yield[18] at 600 ^{o}C. It can be seen in Figure 3.5.1 that increasing reaction temperature from 400 to 800 °C increases aromatic yield up to 30% at 600 °C. At temperatures higher than 600 °C, there

is little change in aromatic yield. Coke yield significantly decreases from 400 to 800 °C. Carbon monoxide and carbon dioxide yield increase slightly over the temperature range tested. Aromatic production and coke formation vary inversely suggesting they are competing reactions.

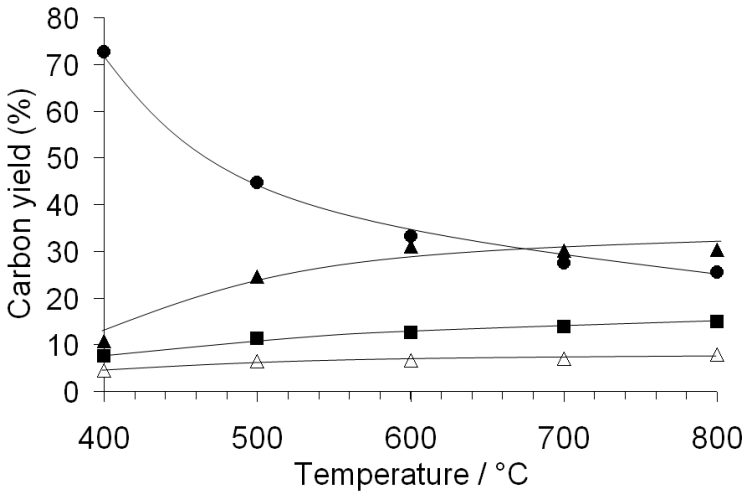

Figure 3.5.1 Carbon yield as a function of reaction temperature for catalytic fast pyrolysis of glucose with ZSM-5. Reaction conditions: catalyst to feed weight ratio = 19; catalyst ZSM-5 (Si/Al = 15), nominal heating rate 1000 °C s-1, reaction time 240 s. Key: ■: carbon monoxide ▲: aromatics Δ: carbon dioxide ●: coke □: total carbon.

Figure 3.5.2 shows the effect of temperature on the aromatic species selectivity. For simplicity similar aromatic species are grouped together, for example, naphthalenes include: naphthalene, methyl-naphthalenes and ethyl-naphthalenes. As the temperature is increased from 400 to 800 °C, the selectivity to benzene increases from 10 to 30% carbon while the selectivity for xylene and naphthalene decreases only a small amount. Changing the reaction temperature has little effect on the selectivity for toluene and the C_9 aromatics.

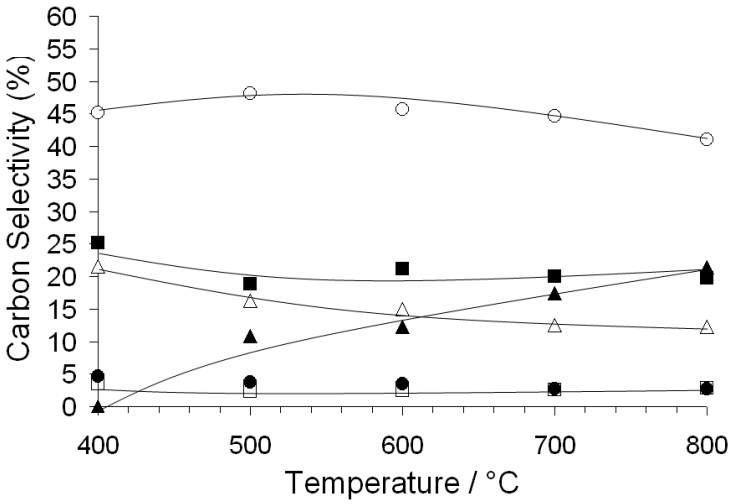

Figure 3.5.2 Aromatic selectivity as a function of reaction temperature for catalytic fast pyrolysis of glucose with ZSM-5. Reaction conditions: catalyst to feed weight ratio = 19; catalyst ZSM-5 (Si/Al = 15), nominal heating rate 1000 °C s-1, reaction time 240 s. Key: ■: toluene ▲: benzene Δ: xylenes and ethyl-benzene ●: methyl-ethyl-benzene and trimethyl-benzene □: indanes ○: naphthalenes.

3.6 Disscussion

3.6.1 Comparison to Previous Studies of Zeolite Conversion With Biomass-derived Feedstocks

Zeolite catalysts have been tested for conversion of biomass-derived feedstocks to aromatics in both fluidized bed reactors and fixed bed reactors. Table 3.6.1 shows previous groups who have added catalysts to fluidized bed reactors. The yields from the previous studies are all reported in wt% without characterizing the bio-oil effluent. When aromatics are produced (instead of oxygenated bio-oils), the wt% yield of the bio-oils decreases because oxygen is being removed as water, CO and CO_2. The aromatics have a higher heating value than the typical bio-oil because of there reduced oxygen content. A number of these previous studies report that catalyst addition to fast pyrolysis reactor is detrimental because it decreases the wt% yield of the resultant bio-oil. While the wt% yield does decrease, the advantage of catalyst addition is that a higher quality bio-oil is

produced. Olazar et. al.[20], used a spouted bed reactor with saw dust, and showed that a high percentage of aromatics (12 % carbon yield) in the product oils could be obtained when high catalyst to feed ratios were employed. The aromatic yield they obtained is about half the aromatic yield we obtained in this study, however, pine sawdust was used as a feed instead of pure cellulose. Horne et. al.[45] reported low organic liquid yields using a low catalyst to feed ratio. The result of low organic yield with low catalyst to feed ratio is in agreement with our study; although, it is difficult to make a direct comparison since no specific aromatic yields were reported in this study. Furthermore, the reactor used was a two stage type where the outlet of a fluidized bed was passed over a packed bed of ZSM-5. Lappas et. al.[19] did not observe increasing organic liquid yield with increasing catalyst to feed ratio, however, they observed a decrease in coke on the spent catalyst at the higher catalyst to feed ratios. We also observed a decrease in coke with increasing catalyst to feed ratio, however, the aromatic yield also increased.

Table 3.6.1 Effect of catalyst to feed ratio for several catalytic fast pyrolysis studies.

Study	Catalyst to feed ratio (WHSV)	Feed	catalyst type (Si/Al ratio)	Reactor Type	Temperature (°C)	Yield
Olazar et. al.	12.0-36.0	pine wood	ZSM-5 (24)	cononical spouted bed	450	30.8 wt% total organic liquid yield, 6.3 wt% yield aromatics (12% carbon yield aromatics)[a]
Horne et. al.	1.16	mixed wood	ZSM-5 (50)	fluidized bed coupled to a fixed catalyst bed	550	5.7 wt% organic liquid yield
Lappas et. al.	2.9-18	Lignocell HBS	ZSM-5 based FCC additive (10 wt% ZSM-5)	circulating fluidized bed	405	30.6, 44.4, 36.4 wt% total organic liquid yield for 18, 4.9 and 2.3 cat/feed ratio, respectively
This study	9.9	Cellulose	ZSM-5 (60)	fixed bed pyroprobe	600	31.1% carbon yield aromatics (13.5 wt% aromatic yield)
This study	9.9	Glucose	ZSM-5 (60)	fixed bed pyroprobe	600	31.4% carbon yield aromatics (13.6 wt% aromatic yield)

a. The WHSV for this run was not directly reported. The range of 12-36 WHSV was reported in the experimental.

The first work on conversion of biomass feedstocks over zeolite catalysts was done by researchers at Mobil[46] who showed that ZSM-5 could be used to convert biomass feedstocks such as latex and seed oils to hydrocarbons. A high degree of conversion (>74%) of these biomass feedstocks over ZSM-5 to form hydrocarbons (including aromatics) was achieved. They also showed that aqueous glucose feedstocks can also be converted to aromatics. Since this early report, there have been an increasing number of publications using zeolites catalysts, predominately ZSM-5, to upgrade biomass feestocks. These studies have indicated that ZSM-5 is the preferred zeolite catalyst for biomass conversion. For example, Olazar et al.[20] reported 30.8wt% total organic yield (12% carbon aromatics) for the pyrolysis of pine wood at 450˚C using ZSM-5. Further, Lappas et al.[19] report in excess of 30wt% total organic yield depending on the catalyst to feed ratio.

The literature on the catalytic pyrolysis of lignocellulosic model compounds and biomass feedstocks is summarized in the Supplementary Material. Dao and coworkers[30, 31, 36, 47, 48] carried out several studies on aqueous fructose and glucose feeds with ZSM-5 catalysts and metal doped ZSM-5 catalysts (ZnZSM-5 and MnZSM-5) in a fixed bed reactor at 350-500˚C. They found that increased yields of aromatics were realized using ZnZSM-5 and MnZSM-5 compared to undoped ZSM-5 catalysts with fructose and glucose feeds. Samolada et al.[32] used HZSM-5, fluid catalytic cracking (FCC) catalysts, transition metal catalysts (Fe/Cr), and aluminas in a fixed bed catalytic reactor using a mixture of model compounds (2-furaldehyde: 2.86; acetic acid: 17.14; cyclohexanone: 11.4; guaiacol: 17.1; vanillin: 8.6, and H_2O: 42.8 wt% ratio) to simulate biomass flash

pyrolysis vapors. HZSM-5 lead to the production of aromatics, while transition metal catalysts (Fe/Cr) lead to the production of phenol and light phenolics.

The catalytic pyrolysis of cellulose was reported by Fabbri et al.[21] using zeolites and nanopowder metal oxides. Zeolite catalysts were found to reduce the overall yields of anhydrosugars with respect to pure cellulose while all nanopowder oxides except silicon oxide provided higher yields. Fabbri et al.[21] carried out the catalytic pyrolysis experiments using a similar pyroprobe system employed in this work. To date, few other workers have utilized the pyroprobe system in order to screen potential catalyst materials for the pyrolysis of biomass. Nokkosmaki et al.[16] used a pyroprobe reactor to investigate zinc oxide as a potential catalyst for the conversion of sawdust pyrolysis vapors. They pyrolysed pine sawdust with ZnO catalyst at 600°C with 30 ms residence time and found that ZnO was a mild catalyst for producing bio-oils showing only a small reduction in the liquid yield with only a 2% gas increase. More recently, Bridgwater and coworkers[22] reported the use of a pyroprobe reactor to screen several microporous (HZSM-5), and mesoporous (Al-MCM-41, Al-MSU-F, alumina-stabilized ceria MI-575) catalysts for the fast pyrolysis of cassava rhizome to gasoline. They heated the biomass/catalyst mixtures to 600°C at a rate of 3000°C/s and held at the reaction temperature for 30s. All catalysts produced aromatic hydrocarbons and reduced oxygenated lignin derivatives. Bridgwater and coworkers[22] report ZSM-5 (Si/Al = 50) was the most effective catalyst for producing hydrocarbons from biomass (cassava rhizome). This activity was linked to the high quantity and strength of acids sites, together with the shape and size selectivity of the pores. These findings corroborate our results above. Furthermore, the larger pore mesoporous materials Al-MCM-41 and Al-

MSU-F (31 and 150 Å, respectively) could facilitate reactions of larger molecules such as lignin and derivatives. Al-MSU-F produced higher yields of xylenes than ZSM-5, whereas alumina stabilized ceria favored the formation of benzene and toluene.[22]

Aho et al. [49] studied the influence of catalyst (Beta zeolite) acidity on the pyrolysis of wood chips to aromatics. These workers found that increasing the catalyst acidity (Si/Al = 25 to 300) increased the gas yield of compounds such as aldehydes, but also increased the coking. While the formation of polyaromatic hydrocarbons was only observed when using a catalyst in the pyrolysis reactor. We observe lower aromatic yields using Beta zeolite compared to ZSM-5 (Si/Al = 60). Further, Iliopoulou et al.[50] also found increasing the acidity of Al-MCM-41 catalysts increased the conversion of biomass at 500˚C. This shows increasing the catalyst acidity while avoiding the formation of coke is an important step in optimizing hydrocarbon yield.

Several workers have utilized mesoporous acidic catalysts for the conversion of biomass using pyrolysis.[14, 22, 50] due to the high surface areas, large pore size (>2 nm) and moderate acidity. In general, these mesoporous catalysts showed less activity compared to ZSM-5 under the same conditions. However, careful tuning of the pore size and acidity could improve product selectivity.[50]

Metal exchanged zeolites for the catalytic pyrolysis of biomass have also been reported.[51-53] Park et al.[51] used Ga-ZSM-5 in the catalytic pyrolysis of sawdust at 500˚C in a fluidized bed reactor. GaZSM-5 produced a greater amount of aromatic hydrocarbons compared to ZSM-5 under the same conditions. Sulman and coworkers[52, 53] studied the catalytic pyrolysis of peat at 410˚C, using zeolites (Beta, Mordinite, HY, ZSM-5) catalysts and their iron impregnated counterparts. Iron impregnation was found

to decrease the acidity by decreasing the number of Brønsted and Lewis sites. In general, all catalysts increased the light hydrocarbon yields of the gas released compared to no catalyst. Catalyst modification with iron decreased the hydrocarbon yields by 2 to 3-fold compared to catalyst without iron impregnation, under the same conditions.

Predominately, solid acid catalysts (e.g. ZSM-5) have been used for the conversion of biomass to oils using pyrolysis. Only, Nokkosmaki et al.[16] and Fabbri et al.[21] applied basic oxides in catalytic pyrolysis, ZnO and MgO respectively. Base catalytic activity has been shown to lead to much higher conversions compared to acid catalysts in other biofuel reactions, such as aldol condensation and transesterification.[54] Recently, strongly basic zeolites have been synthesized from reaction of zeolites with ammonia at elevated temperatures.[55] These basic zeolites provide unique activity and selectivity for base catalyzed reactions. The application of basic zeolites, for example amine-substituted ZSM-5, to biomass pyrolysis could be a promising candidate for conversion to hydrocarbons.

In summary, we can infer from the aromatic product ratios, that the conversion of biomass model compounds and cellulose undergo the same mechanism during catalytic pyrolysis. Hence, modification of the catalyst will affect the overall conversion. Specific catalysts could in theory be used to produce selective compounds from a range of feedstocks. Further studies are required to optimize the catalyst to maximize the yield of gasoline range hydrocarbons, these studies include:

(a) the effect of acid strength

(b) incorporation of metals in the zeolites,

(c) use of varying pore size catalysts in order to utilize a larger fraction of the biomass composition e.g. lignin, and

(d) the use of microporous basic catalysts.

3.6.2 Potential of Catalytic Fast Pyrolysis

As we have shown aromatics can be directly produced from lignocellulosic biomass in a single step reactor at short residence times without the co-feeding of hydrogen. The motor octane number, based on summation of the individual aromatic components, of the aromatic products is approximately 111. The octane number and vapor pressure of the aromatic products and gasoline is shown in Table 3.7.1. The ideal gasoline fuel will have the proper combination of octane and vapor pressure, and will also have low toxicity. The vapor pressure of gasoline range is around 5.2-11.6 mmHg at 25 °C. All the aromatics we produce have a high octane number. However, the aromatics larger than xylene have low volatility which limits the amount that can be blended with gasoline. Also in the U.S. aromatics are currently limited to 25 % volume in gasoline.[56] Benzene is further limited to 0.8 vol % in gasoline because of its carcinogenic properties. Benzene can be converted to toluene by an alkylation process. Napthalene and the larger alkanes could be hydrogenated to cyclic alkanes in a secondary process. These cyclic alkane could be used as a diesel fuel. The hydrogen could potentially come from steam reforming of coke deposits or from water-gas shift of product carbon monoxide.

Table 3.6.2 Properties of the quantified aromatic species.

Compound	Boiling Point (°C)[a]	Research octane number (RON)[b]	Motor octane number (MON)[b]	(R+M)/2	Vapor Pressure (mmHg @ 25 C)[a]
Benzene	84.35	98	90	94	100.84
Toluene	112.29	124	112	118	28.47
Ethyl-Benzene	135.17	124	107	115.5	9.51
o-Xylene	140.15	120	102	111	6.62
m-Xylene	140.15	145	124	134.5	8.29
p-Xylene	140.15	146	126	136	8.75
Ethyl-methyl Benzene	163.03	126-155	112-138	119-147	2.89
Tri-methyl Benzene	168.01	118-170	104-136	111-153	1.87
Indan	174.44	161	140	150.5	1.48
Naphthalene	199.91	not reported	90	-	0.23
Methyl-Naphthalene	227.77	123-127	114-116	119-122	0.053
Gasoline	35-200	-	-	87-91	5.2-11.6[c]

a. [57], b. [58] c. [59]

The aromatics also have wide spread uses across the chemical industry. Figure 3.1.1b shows the primary product from the pyrolysis of biomass-derived compounds with ZSM-5 is naphthalene. The primary use of naphthalene (62 % of the total U.S. consumption) is in the production of Phthalic anhydride. The second major use for naphthalene (20 % of the total) is in the production of surfactants and plasticizers such as naphthalene sulfonate and naphthalene sulfonate-formaldehyde condensate.[39] Xylenes, toluene, and benzene produced during catalytic fast pyrolysis are also of chemical importance. Toluene and mixed xylenes are primarily used as an octane enhancer in motor gasoline. However, the pure para and ortho isomers of xylene are also important chemical precursors of terephthalic acid and phthalic anhydride, respectively. Almost all of the para and ortho xylenes produced in the U.S. go into these chemicals for the

production of platicizers and polymers.[39] Benzene was primarily used as an octane enhancing fuel additive until recent EPA regulations limited benzene to 0.8 vol % in gasoline.[56] Now almost all of the benzene produced in the U.S. is used for the manufacture of polymers such as polystyrene.[39]

The yield of aromatics that can be produced from biomass is a function of the composition of the biomass and the type of catalysts used. If the biomass contains 75 wt% carbohydrates then 240 L of aromatics per metric ton of biomass can be produced assuming that the remaining fraction of the biomass (which will be lignin and ash) is not converted. This also assumes that the oxygen is rejected as a combination of CO and H_2O as shown in Equation 2 (Section 3.1). Theoretically 63% percent of the carbon in the carbohydrate can be converted to aromatics. Figure 3.7.1 shows the yield of aromatics as a function of the theoretical yield. Our current data shows we can obtain a 50 % of the theoretical yield with model compounds which corresponds to an output of 120 L of aromatics per metric ton of biomass. The yield of cellulosic ethanol in the first cellulosic ethanol plant (built in 1910) was 83 $L_{ethanol}$/metric ton of biomass, which is significantly lower than the yield of our process. Current targets for cellulosic ethanol production are over 300 $L_{ethanol}$ per metric ton of biomass. [54] However, ethanol has an energy density two-thirds that of toluene. Therefore, 120 $L_{aromatics}$/metric ton of biomass corresponds to an ethanol yield of 180 $L_{ethanol}$/metric ton of biomass. Furthermore, catalytic fast pyrolysis occurs in a single step, whereas cellulosic ethanol production requires multiple steps (including: pretreatment of the biomass, enzymatic hydrolysis, fermentation of both glucose and xylose, and distillation). The multiple steps of cellulosic ethanol production result in a plant capital cost that is 10 times larger than fast

pyrolysis.[12] It is likely that future advances in design of new catalysts, combined with proper reaction engineering will leader to even further improvements in the production of aromatics from cellulosic biomass.

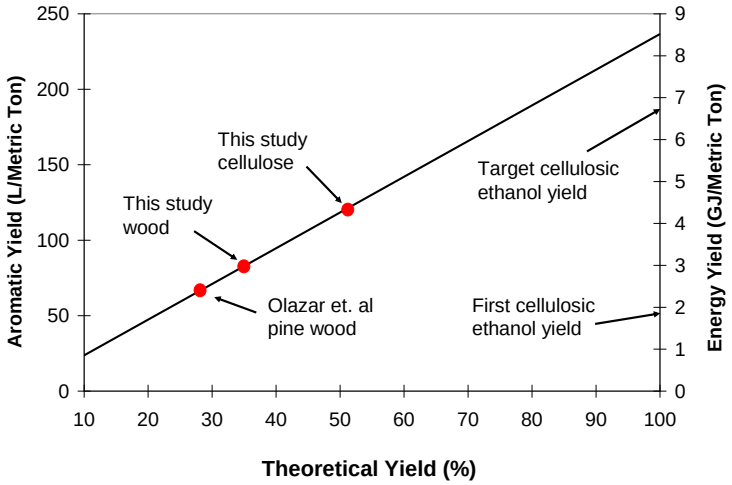

Figure 3.6.1 Aromatic yield as a function of theoretical yield. Included in the figure are the results from Olazar et. al[20], the results from this study and our preliminary results using mixed wood as a feed (same reaction conditions as reported in Figure 3.1.1.)

3.6.3 Challenges with Catalytic Fast Pyrolysis

Our results indicate the two important reactor parameters to maximize aromatic yields are fast heating rates and high catalyst to feed ratios. Therefore, the optimal reactor for catalytic fast pyrolysis will be designed to allow for fast heating of the biomass while maintaining a high feed to catalyst ratio. As described in the literature[9, 10], the heating rate is known to be an important parameter to control the product distribution in pyrolysis. Fast (>500°C sec^{-1}) heating rates produce high grade bio-oil and gasoline range compounds, particularly in the presence of a catalyst. Theoretically, microwaves could heat biomass materials at very high rates due to the volumetric heating and this process is likely to offer significant efficiencies over conventional resistively heated reactors. There have been few reports microwave catalytic pyrolysis in the

literature[60, 61], however only non-catalytic microwave pyrolysis of biomass materials such as cellulose[62-64] and lignin/wood[61, 65, 66] have been reported. Early work by Baysar et al.[60] described a microwave heated fluidized bed reactor used to convert biomass feedstocks to bio-fuel. Heating rates of 17 K min^{-1} were achieved. Further, Kriegler-Brockett[61] investigated the microwave pyrolysis of lignin,, with catalyst additives of NaOMe, NaOH, $NaHCO_3$, SiO_2 and $Ca(OH)_2$. Yu et al.[67] report the microwave pyrolysis of corn stover and the bio-oils properties were determined. Stover was heated for 40 minutes at 600W but no heating rate was recorded. The addition of NaOH as a homogeneous catalyst dramatically increased the syngas yield.

Conventionally heated fluidized beds may also be suitable for catalytic fast pyrolysis. These reactors have been successfully used with non-catalytic and catalytic fasy pyrolysis since this reactor type provides easy control of heating rates and product collection.[9] Furthermore, as shown in Table 3.3.1, high catalyst to feed ratios are obtainable with fluidized bed reactors.

One of the biggest challenges in catalytic fast pyrolysis is suppressing the formation of undesired coke. As seen in Figure 3.1.1, all of the runs yield more than 30 % coke. However, the coke can be burned to provide process heat for the catalytic fast pyrolysis reaction. Using dry glucose reacted at 600°C as a basis, we calculate that 12 % of the carbon of the biomass feedstock would need to be burned to provide the process heat for catalytic fast pyrolysis. Real biomass feedstocks (e.g., wood and grasses.) would require more carbon to be combusted, which would depend on the water content of the feed and the composition of the biomass. Zeolite catalysts can also be completely regenerated by burning the coke if the proper zeolite with proper pre-conditioning is

chosen. Corma and co-workers demonstrated that zeolite catalysts (including ZSM-5) can be completely regenerated by high temperature oxygen treatments after they have been exposed to aqueous biomass-derived oxygenates (including glycerol and sorbitol) feedstocks.[40]

Due to the moderate amounts of coke produced, the aromatic yields obtained are currently about half of the theoretical yield. Future work in this area will focus on elucidating the reaction kinetics of catalytic fast pyrolysis. As eluded to earlier, the similarity of product distribution for similar feedstocks suggests there are common dehydrated intermediate products that form aromatics. By determining the way in which aromatics are formed from these common intermediates, the role of the structure and nature of the active sites of the catalyst can be further understood. Once these parameters are understood new catalyst specifically tailored for biomass conversion can be synthesized.

3.7 Conclusions

The general conclusion from this study is that high quality aromatic fuel additives can be produced directly from solid biomass feedstocks by catalytic fast pyrolysis in a single catalytic reactor at short residence times. This reaction involves homogeneous thermal decomposition of the biomass to smaller oxygenates through dehydration reactions. The dehydrated oxygenates then diffuse into the zeolite catalysts where they undergo a series of oligomerization, decarbonylation, and dehydration reactions to produce aromatics, CO, CO_2, and water. The major challenge with catalytic fast pyrolysis is to avoid undesired coke formation, which can be produced from both homogeneous or heterogeneous

reactions. Coke formation can be minimized and aromatic formation can be maximized by three important parameters:

(1) fast heating rates

(2) high catalyst to feed ratios, and

(3) proper catalyst selection (both active site and pore structure).

The fast heating rates and high catalyst feed ratios with close contact are necessary to avoid undesired thermal decomposition reactions in the homogeneous phase. The pore structure and active sites of the catalyst can be tuned to control the product selectivity. The aromatics produced include benzene, toluene, xylenes, substituted benzenes, indanes, and naphthalenes. The pyroprobe reactor used in this study offers a convenient method to study the fundamental science of catalytic fast pyrolysis and for screening catalysts in order to scale up to real systems. It is likely that advances in understanding the chemistry of catalytic fast pyrolysis combined with the development of improved catalytic materials, which are specifically designed for biomass conversion, will lead to further process improvements.

CHAPTER 4

CHEMISTRY OF CATALYTIC FAST PYROLYSIS

The chief challenge with using zeolite catalysts is controlling the complicated chemistry that occurs inside the catalyst pores. The objective of this study is to elucidate the reaction mechanism for conversion of glucose to aromatics by CFP. The initial thermal decomposition of pure glucose and glucose in the presence of ZSM-5 will be studied with TG/DTG, ex situ FTIR and visual observation. The mechanism for aromatic formation will be studied with the pyroprobe GC/MS system by reacting isotopically (^{12}C and ^{13}C) labeled feeds. The pyroprobe reactor will also be used to study how yield and selectivity for aromatics changes with different reaction conditions as well as to study the conversion of reaction intermediates. Ex situ FTIR will also be used to determine which species are involved in the undesired coke formation reactions. Furthermore, nitrogen adsorption will be used to determine whether these undesired reactions occur on the surface or within the pores of the catalyst. These findings give us insight into how we might control zeolite chemistry for the conversion of biomass into aromatics. Glucose is used as a model compound for cellulosic biomass in this study.[54] As shown in section 3.1 both glucose and cellulose yield similar product distributions when pyrolized in the presence of ZSM-5 catalyst.[18] These findings suggest that both cellulose and glucose decompose to common intermediates. Therefore the mechanistic conclusions from glucose pyrolysis may be extended to more complicated cellulosic type feedstocks.

4.1 Thermal Decomposition of Glucose: Pyroprobe Results

Figure 4.1.1 shows the detailed quantification of glucose pyrolysis with 1000, 2.5, and 0.25 °C s^{-1} heating rates carried out with the in-house designed trap. The dehydration product levoglucosan (LGA, 1,6-anhydro-β-D-glucopyranose, $C_6H_{10}O_5$) was found to be the most abundant product. Other anhydrosugars such as; levoglucosanone (LGO, 6,8-dioxabicyclo[3.2.1]oct-2-en-4-one, $C_6H_6O_3$), 1,4:3,6-dianhydro-β-D-glucopyranose (DGP, $C_6H_8O_4$), and 1,6-anhydro-β-d-glucofuranose (AGF, $C_6H_{10}O_5$) were present in lower amounts. Products that are likely formed from the retro-aldol condensation of glucose such as d-glyceraldehyde, hydroxyacetone and hydroxyacetaldehyde were also observed. The selectivity for coke ranges from 30 to 40 carbon %. As the pyrolysis rate increases, the LGA yield increases while the coke yield is suppressed. A lower heating rate increases the amount of dehydration reactions, with greater DGP, LGO, and coke.

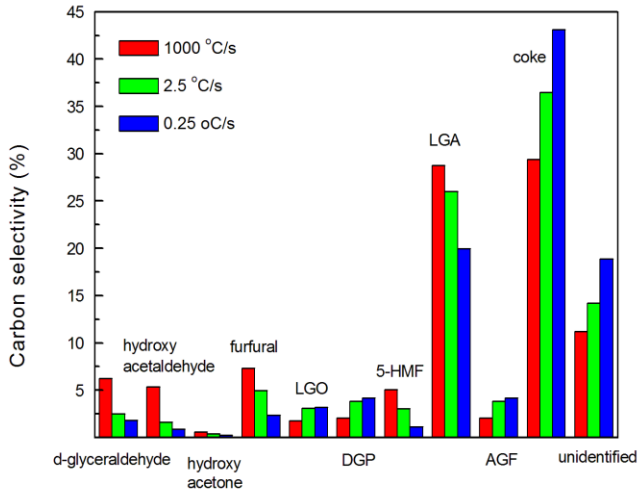

Figure 4.1.1 Product distribution pattern of glucose pyrolysis with 1000, 2.5, and 0.25oC s-1 heating rates; final temperature at 600 °C with reaction time for 240 seconds

4.2 Thermal Decomposition of Glucose: Themogravimetric Analysis with Mass Spectrometry (TGA-MS)

Table 4.2.1 summarizes the approximate and elemental analysis of glucose pyrolysis products after a 2.5 °C s^{-1} heating rate. Around 89 wt% of glucose can be volatilized, with 11% of fixed carbon and trace ash. Water, CO, and CO_2 are the major species identified by the TGA-MS. Only small amounts of these primary pyrolysis products are observed in our TGA-MS system. It is likely that some of the CO and CO_2 are formed from degradation of the primary pyrolysis products (e.g. levoglucosan, hydroxyacetaldehyde) in the line leading from the TGA to the MS. These primary pyrolysis products can only be observed if they are quickly condensed out, as with the liquid nitrogen trap in Section 4.1.

Table 4.2.1 Proximate and elemental analysis of glucose pyrolysis.

Proximate analysis (wt%)			Elemental analysis (wt%)		
Volatile	Fixed C.	Ash	C	H	O[a]
89.0	10.9	0.1	42.9	6.5	50.6

[a] By balance.

Figure 4.2.1 (a) and (b) shows the DTG and MS signals of pure glucose pyrolysis with 0.017, 0.25, and 2.5 °C s^{-1} heating rates. Glucose pyrolysis initiates at 150, 200, and 250 ^{o}C, respectively. The DTG curves of all pyrolysis rates are composed of two major peaks. For a heating rate of 0.017 °C s^{-1} the peaks are located at 198 and 290 ^{o}C, with almost equivalent intensity of the two peaks. For 0.25 °C s^{-1}, the first peak is at 228 ^{o}C; the second, 312^{o}C. For 2.5 °C s^{-1}, the first peak is at 282 ^{o}C; the second, 369 ^{o}C. The intensity of the first DTG peak diminishes as the heating rate is increased. Figure 4.2.1(b) shows the corresponded Mass Spec responses at a 2.5 ^{o}C s^{-1} heating rate. The ion fragments, including hydrogen (*m/z*=2), methane (*m/z*=16), water (*m/z*=18), carbon monoxide/ethylene (*m/z*=28) and carbon dioxide (*m/z*=44) were recorded with time. From the 28 m/z and 44 m/z signals it is seen that decarboxylation and water removal begins around 200 ^{o}C while decarbonylation, methane production and hydrogen production do not initiate until above 250 ^{o}C. Water is removed during two separate reactions the first taking place at ~300 ^{o}C and the second at ~410 ^{o}C. The water MS signal corresponds to the two separate DTG peaks indicating both of these reactions involve the removal of water. In Figure 4.2.1(c) the DTG curves for the pyrolysis of glucose with ZSM-5 (19:1 catalyst to glucose wt. ratio) are shown. The DTG responses for different heating rates show similar peaks to the non-catalyzed pyrolysis, however, the two peaks shift to lower temperature. For the heating rates of 0.017, 0.25, and 2.5 ^{o}C s^{-1} the first DTG peak shifts to 154, 171, and 206 ^{o}C, respectively. The second DTG

peaks also shift downward to 275, 282, and 312 ^{o}C for the 0.017, 0.25, and 2.5 ^{o}C s^{-1} heating rates, respectively. When glucose was pyrolized in the presence of ZSM-5 a third peak appears. This new peak is located at 327, 363, and 402 ^{o}C for the 0.017, 0.25, and 2.5 ^{o}C s^{-1} heating rates, respectively. In Figure 4.2.1(d) the MS responses for the pyrolysis of glucose with ZSM-5 at a heating rate of 2.5 ^{o}C s^{-1} are shown. Compared to pure glucose pyrolysis, the MS signals initiate at a lower temperature (*m/z*=28 at 50 ^{o}C; *m/z*=18 at 100 ^{o}C). At around 350 ^{o}C, where the newly formed third DTG peak is located, *m/z*=78 (benzene) and *m/z*=91 (toluene) signals are observed. The response of *m/z*=28 shows a second peak around the same temperature. The second m/z=28 peak is most likely from ethylene. It is well documented in the literature for the methanol to hydrocarbons process with ZSM-5 catalyst that ethylene is formed concurrently with benzene and toluene.[68]

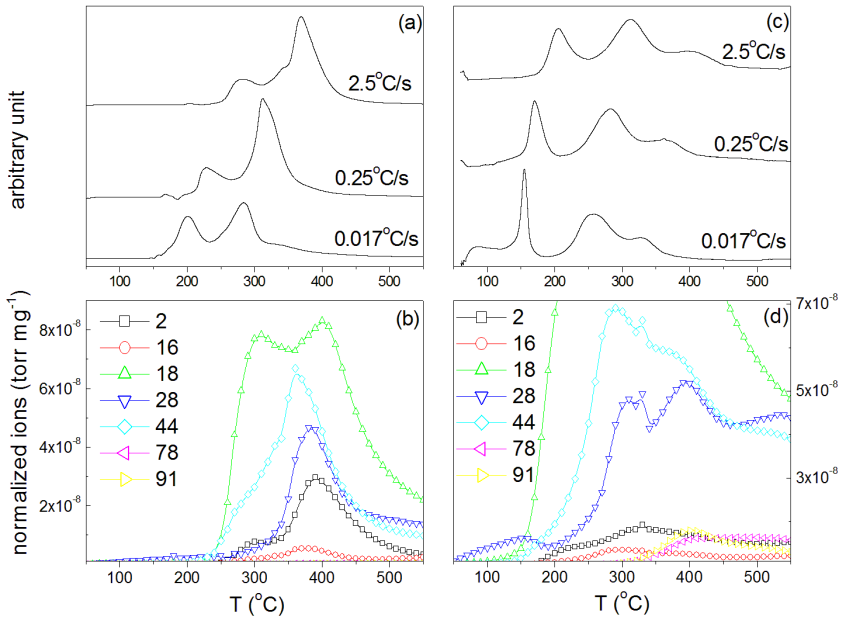

Figure 4.2.1 (a) DTG signals of glucose pyrolysis; (b) MS responses of selected ions of glucose pyrolysis at a 2.5 ^{o}C s^{-1} heating rate; (c) DTG signals of glucose pyrolysis with ZSM-5; (d) MS responses of selected ions of glucose pyrolysis with ZSM-5 at a 2.5 ^{o}C s^{-1} heating rate.

The two separate peaks in the DTG response for glucose pyrolysis imply two separate decomposition reactions. To identify the species that are present for each peak separate pyrolysis runs were carried out using identical reaction conditions, however, the temperature ramp was stopped at the onset of the peak of interest. At this designated temperature the reaction was rapidly quenched by cooling the furnace to room temperature with flowing air. The quenched reaction residue was then quantitatively dissolved in methanol and analyzed by GC/MS. For low-temperature products, the final temperatures were 180, 200 and 250 ^{o}C for the 0.017, 0.25 and 2.5 ^{o}C s^{-1} heating rate runs, respectively. At these temperatures, the residues of all samples are ~98% of the initial sample mass. 4.2.2 shows the distribution of the species within the methanol-dissolved residue for the three different heating rates. The primary products observed for

the low temperature peak were hydroxyl-acetaldehyde, hydroxyl acetone, and dihydroxyacetone. These products are likely from retro-aldol and Grob fragmentation of glucose.[26, 27] For the high-temperature peak, the final temperatures were 280, 300 and 380 ^{o}C for the 0.017, 0.25 and 2.5 ^{o}C s^{-1} heating rate runs, respectively. At these temperatures, only non-dissolvable coke and tar remained in the crucible.

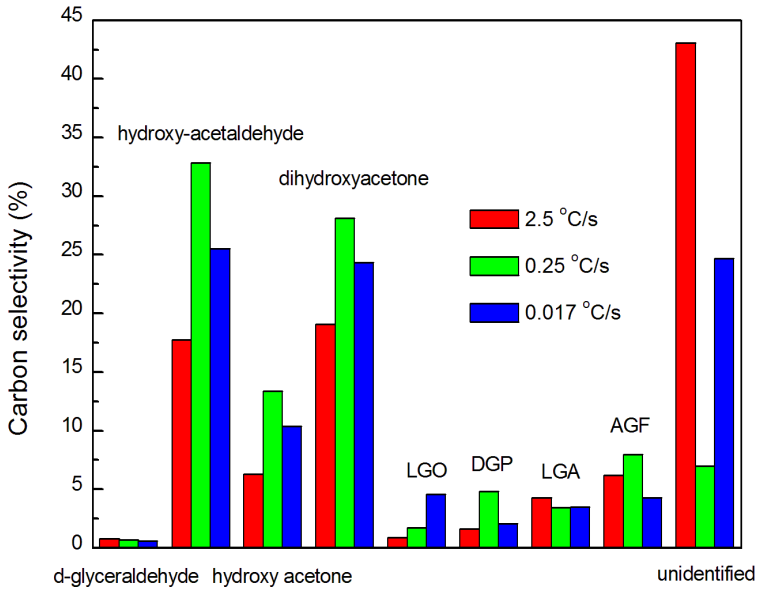

Figure 4.2.2 Carbon yields of glucose pyrolysis with three pyrolysis rates, final temperatures at 180 (0.017^{o}C s^{-1}), 200 (0.25^{o}C s^{-1}), and 250^{o}C (2.5 ^{o}C s^{-1}), respectively.

4.3 Thermal Decomposition of Glucose: Visual Observations

To provide a clear view of glucose fast pyrolysis and catalytic fast pyrolysis, a series of snapshots of these experiments are shown in Figure 4.3.1. Both trials were carried out in the pyrex trap with a 1000 ^{o}C s^{-1} heating rate and final temperature at 600 ^{o}C. Instead of immersing collectors into the liquid nitrogen dewar the pyrex vial was set on the bench top and filmed with a video camera at room temperature. Figure 4.3.1 shows the solid pure glucose (a) and glucose-ZSM-5 mixture (e) at room temperature before

reaction. Figure 3.3.1 (b) and (f) show snapshots at ~210 ^{o}C during pyrolysis of the glucose and glucose-ZSM-5 mixture, respectively. At 210 ^{o}C glucose transforms into a transparent liquid phase because such a pyrolysis temperature surpasses the boiling point (~145 ^{o}C).[69] As seen in Figure 3.3.1 (f) at 210 ^{o}C black spots (coke) are clearly visible. At this same temperature no coke is observed when the catalyst is not present during pyrolysis. This indicates that coke forms at a lower temperature when catalysts are present. At a temperature of 600 ^{o}C (Figure 4.3.1 (c) and (g)), vapors can be seen coming from the ends of the quartz tube. At 600 ^{o}C the coke formation becomes more severe for the glucose/ ZSM-5 sample (Figure 4.3.1 (g)). After 5 seconds at the final temperature, the residual of glucose inside the reactor turns into coke for both cases in (Figure 4.3.1 (d) and (h)).

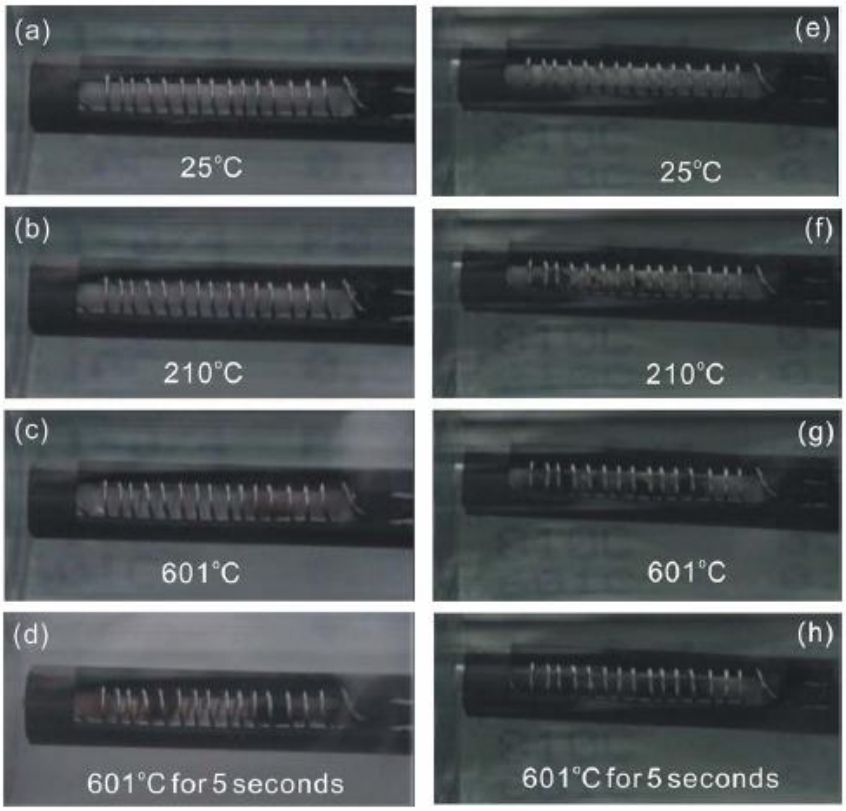

Figure 4.3.1 Comparison of glucose fast pyrolysis (a, b, c, and d) and glucose/ZSM-5 pyrolysis (e, f, g, and h; catalyst to feed ratio = 19).

4.4 Thermal Decomposition of Glucose: FTIR results

To further investigate the thermal decomposition of glucose in the presence of ZSM-5, ex-situ FTIR was performed at various temperature steps. Glucose with ZSM-5 (catalyst : feed ratio = 1.5) was pyrolyzed with a heating rate of 100 °C s^{-1} to various final temperatures. Upon reaching the final reaction temperature, the probe was quenched with room temperature helium flow. FTIR was performed on the residues left in the quartz reactor. Figure 4.4.1 (I) shows the infrared spectra (1200-2000 cm^{-1} region) of the reaction mixture obtained at various temperatures. Figure 4.4.1(II) shows the CH stretching region (2700-4000 cm^{-1}) of the same spectra. Ramping to a final temperature of 100 or 200 °C does not alter the glucose composition significantly as the CH_2 bending

modes are of similar intensity. However, it can be seen from the disappearance of the C-H bending modes of glucose at 1340, 1379 and 1460 cm^{-1} (Figure 4.4.1(I)) that the glucose decomposes between 200 and 300 °C. Similarly, in Figure 4.4.1(II) the three aliphatic C-H modes at 2890, 2914 and 2945 cm^{-1} are lost between 200 and 300 °C.

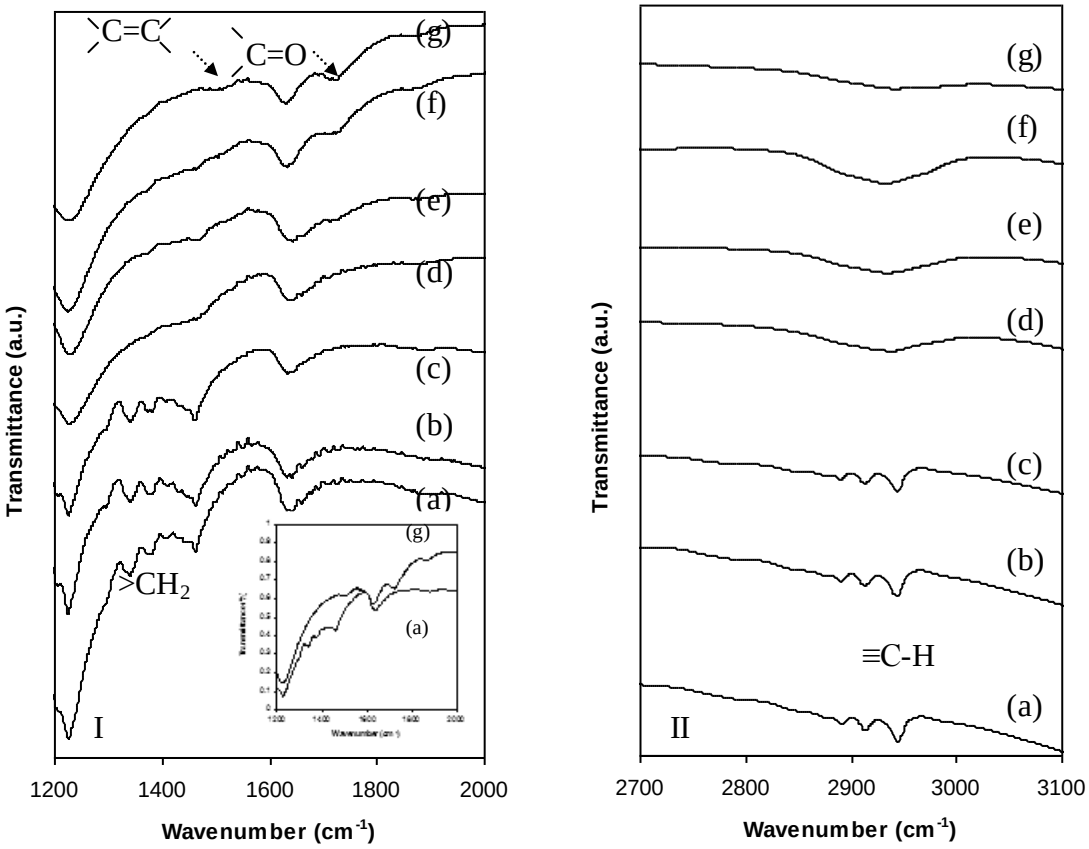

Figure 4.4.1 IR spectra for glucose pyrolysis in the presence of ZSM-5 (catalyst to feed ratio = 1.5) at 100 ˚C s^{-1} to a final temperature of: (a) unreacted (b) 100˚C, (c) 200˚C, (d) 300˚C, (e) 400˚C, (f) 500˚C, (g) and 600˚C. (I) 1200-2000 cm^{-1} region and (II) 2700-3100 cm^{-1} region. Spectra are off-set to show the bands.

From Figure 3.4.1 (I) it can be seen that there is a new composition formed at temperatures above 400°C from the new peaks at 1492 and 1706 cm^{-1}. At 600 ˚C, the presence of C=C bonds (C=C vibrations at ca. 1500 cm^{-1}) and carbonyl groups (C=O, ca. 1700 cm^{-1}) are evident. Sarbak et al.[70] who studied coke formation on HX zeolite

attributes the bands at 1500 and 1589 cm^{-1} to presence of naphthalenes. Band positions for these spectra in Figure 3.4.1 are assigned in Table 4.4.1.

Table 4.4.1 Infrared band positions (cm-1) and assignments for the fast pyrolysis of glucose with ZSM-5 (catalyst:feed ratio = 1.5) at various temperatures.

glucose	100˚C	200˚C	300˚C	400˚C	500˚C	600˚C	Assignment[71-73]
433	445	442	436	437	439	439	Si-O-Si external deformation (ZSM-5)
553	541	540	536	539	539	538	Si-O-Si internal deformation (ZSM-5)
	612	611	606				D6R ring mode (ZSM-5)
621							
647	641	632	699				
727	730	725					
775	775	774	779	782	781	786	Si-O sym stretch (ZSM-5)
	790	793					Si-O sym stretch (ZSM-5)
838	834	836					
914	912	912	897				
996							C-O
1023		1022					
1052		1046					
1080	1071	1068	1068	1072	1068	1072	Si-O anti-sym stretch (ZSM-5)
1111		1094					C-O
1148		1138					Ring mode (glucose)
1202	1216	1194					
1225		1217	1215	1217	1216	1216	Si-O anti-sym stretch (ZSM-5)
1295		1284					
1340	1334	1328					CH bend
1379	1363	1365	1355	1352			Sym CH bend
1460	1453	1449	1453	1457	1455		Asym. CH bend
					1492	1492	C=C
	1631	1628	1629		1625	1618	HOH bend (adsorbed water)
			1703h	1703	1706	1706	C=O (acid carboxyl)
	1869	1866	1858	1858	1854	1858	
2890	2886	2887					CH aliphatic (glucose)
2914	2908	2910	2917	2917b	2917b	2922b	CH aliphatic
2945	2935	2941					CH aliphatic (glucose)
3356							OH (glucose)
3412							OH (glucose)

4.5 Effect of Reaction Time on Catalytic Fast Pyrolysis: Pyroprobe Results

To investigate the effect of reaction time on the yield of the catalytic fast pyrolysis products, the carbon yield of aromatics, CO and CO_2 were measured at various total reaction times from 1 and 240 s at 600 °C. Figure 4.5.1 shows the carbon yield as a function of reaction time for the optimized reaction conditions. Initially, after 1 s of reaction, CO and CO_2 comprise the main products and increase little throughout the reaction. After 3 s reaction aromatic is higher than CO or CO_2 and increases rapidly as

the reaction proceeds. After 240 s the aromatic yield appears to be level off at a maximum carbon yield of 32%. Reaction times as little as 2 minutes give aromatic yields in excess of 30carbon%.

The aromatic selectivity as a function of reaction time for CFP of glucose with ZSM-5 is shown in Figure 4.5.2. Apart from the yield of naphthalenes and indenes, the selectivity of all other aromatics decreases between 1 and 3 seconds of reaction time at 600 °C. During this same period, the naphthalenes selectivity dramatically increases from 18 to 40%. Naphthalenes are the major products between 3 and 240 s and there is little selectivity change for reaction greater than 3 s.

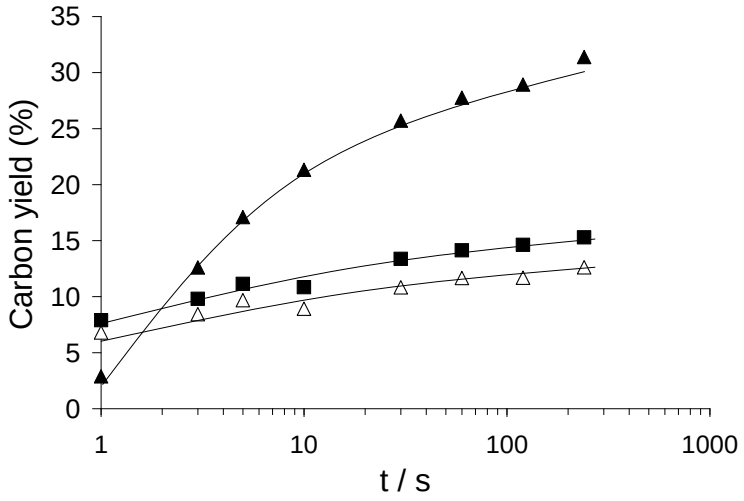

Figure 4.5.1 Carbon yield as a function of reaction time for catalytic fast pyrolysis of glucose with ZSM-5. Reaction conditions: catalyst to feed weight ratio = 19; catalyst ZSM-5 (Si/Al = 15), nominal heating rate 1000 °C s-1, reaction temperature 600 °C. Key: ■: carbon monoxide ▲: aromatics Δ: carbon dioxide.

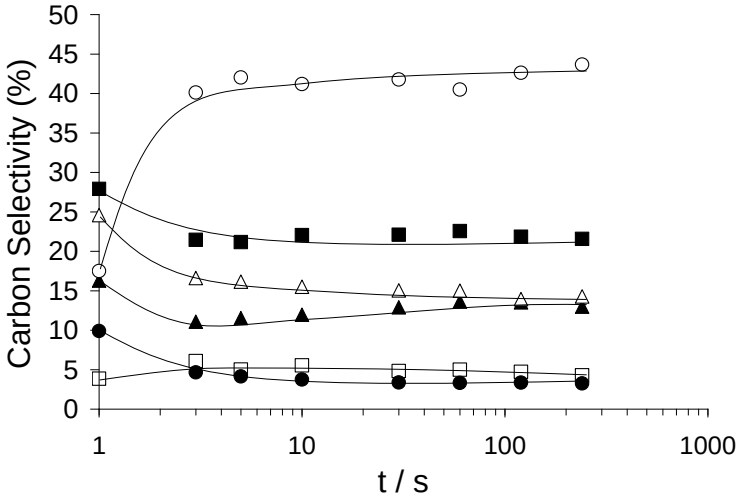

Figure 4.5.2 Aromatic selectivity as a function of reaction time for catalytic fast pyrolysis of glucose with ZSM-5. Reaction conditions: catalyst to feed weight ratio = 19; catalyst ZSM-5 (Si/Al = 15), nominal heating rate 1000 °C s-1, reaction temperature 600 °C. Key: ■: toluene ▲: benzene Δ: xylenes, ethyl-benzene ●: methyl-ethyl-benzene and trimethyl-benzene □: indanes ○: naphthalenes

4.6 Effect of Reaction Time on Catalytic Fast Pyrolysis of Glucose: FTIR Results

Figure 4.6.1 shows the infrared spectra of pure glucose after pyrolysis at 600 °C for 1 s and 120 s compared to unreacted glucose. Assignments of the bands are given in Table 4.6.1. After 1 s reaction time the CH_2 deformation modes of glucose are no longer present indicating that little unreacted glucose remains. Furthermore, the lost of the band at 1148 cm^{-1} shows that the 6-carbon ring mode is not present after 1 s reaction. The new band that appears at 1703 cm^{-1} after1 second is characteristic of C=O stretching vibration. Therefore, the decomposition of glucose appears to go through a compound with carboxyl character.[70] 1703 cm^{-1} is in the carboxylic acid range for C=O stretching vibrations. After even the short time of 1 s there is very little material left in the pyroprobe reactor, only a residue film.

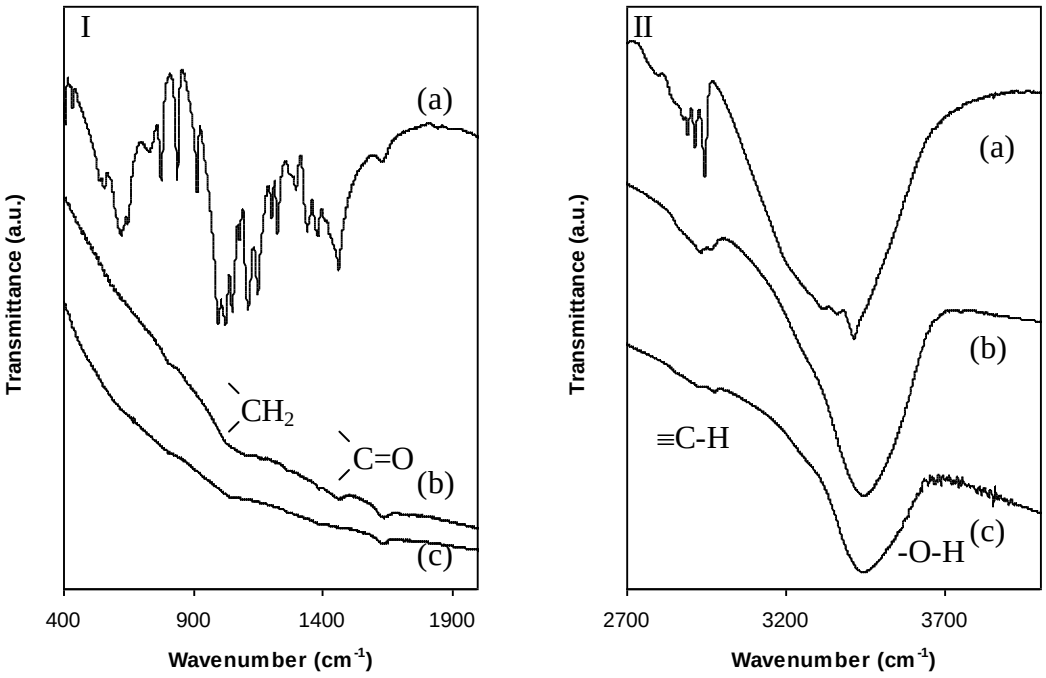

Figure 4.6.1 FTIR spectra of pure glucose (a) unreacted and pyrolyzed at 600 °C for (b) 1 s and (c) 120 s. (I, region 400-2000 cm-1 and II, CH and OH stretching region 2700-4000 cm-1).

Table 4.6.1 Infrared band positions (cm-1) and assignments for the pyrolysis of glucose 600 ˚C.

Glucose	1 s	120 s	Assignment[70, 73]
433			Framework mode (glucose)
553			Framework mode (glucose)
621			C-C, C-O stretch (glucose)
647			C-C, C-O stretch (glucose)
727			C-C, C-O stretch (glucose)
775			CH deformation (glucose)
	797	787	CH deformation
838			CH2CH deformation (glucose)
	873		
914			C-OH and CH deformation (glucose)
996			
1023	1021	1027	C-OH deformation (glucose)
1052			CH deformation (glucose)
1080			CH, COH deformation (glucose)
1111			CH, COH bend (glucose)
1148			Ring mode (glucose)
1202			C-O (glucose)
1225	1257		CH2 (glucose)
1295	1374	1374	CH2 bend, C-OH (glucose)
1340			CH bending (glucose)
1379			CH bending (glucose)
1460	1443		CH2 bend, COH (glucose)
	1620	1621	HOH bend (adsorbed water)
	1703		C=O stretch (carboxylic)
2890	2841		CH stretch (glucose)
2914	2910	2910	CH stretch (glucose)
2945	2951	2957	CH stretch (glucose)
3356			OH stretch (glucose)
3412			OH stretch (glucose)

Figure 4.6.2(I) and (II) show the infrared spectra of glucose-ZSM-5 at a low catalyst to feed ratio (1.5) reacted at 600 °C for various time periods between 1-120 s. The assignments of the bands are given in Table 4.6.2. After 3 s reaction the bands from the glucose (including, 1460, 2890, 2914 and 2945 cm^{-1}) have completely disappeared indicating the decomposition of glucose. A longer reaction time 3 s (compared to 1 s) is required to fully decompose the glucose, which is likely due to the larger mass of glucose present. The infrared spectra of the sample after 3s reaction at 600 °C shows two new bands at 1571 And 1711 cm^{-1} along with a broad band in the C-H stretching regions centered at 2950 cm^{-1}. The former two bands are assigned to C=C stretch and C=O stretch. The C=O stretch is in the characteristic wave number region for diketonics[74],

while the C=C stretch may be from aromatics. Therefore, the coke present after 3 s reaction has aromatic and ketone characteristics. The broad band in the C-H region indicates a broad range of organic compounds/compositions present. With further reaction time up to 120 s, these bands decrease until 120 s sample indicating these intermediates have been decomposed.

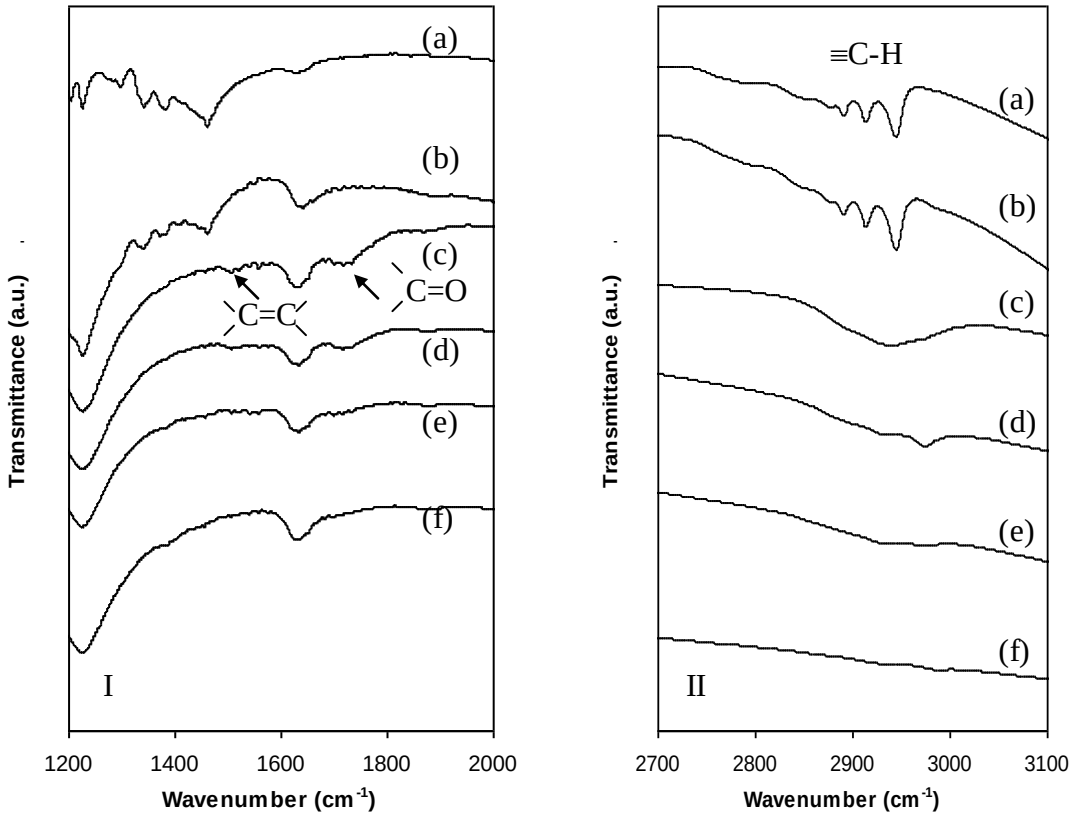

Figure 4.6.2 Infrared spectra of (a) pure glucose and glucose with ZSM-5 (catalyst : feed ratio = 1.5) and reacted at 600 °C for various times (b) unreacted (c) 1 s, (d) 3 s, (e) 5 s and (f) 120 s. (I) 400-2000 cm-1 region and (II) CH stretching region (2700-3100 cm-1) .

Table 4.6.2 Infrared band positions (cm-1) and assignments for the fast pyrolysis of glucose with ZSM-5 (catalyst : feed ratio = 1.5) at various temperatures compared to polyfurfuryl alcohol.

glucose	Polyfurfuryl alcohol on HY zeolite[74]	Assignment	Polyfurfuryl alcohol on HY zeolite heated to 673K[74]	Assignment	Glucose on ZSM-5 heated to 600˚C for 1s	Glucose on ZSM-5 heated at 600˚C for 3s	Glucose on ZSM-5 heated at 600˚C for 120s	Assignment[71-73]
1225					1216			Si-O anti-sym stretch (ZSM-5)
1295							1284	
1340								CH bend
1379	1375	CH bend	1350	C=C carbon			1381	Sym CH bend
1460	1422	CH bend						Asym. CH bend
	1487	Oligomeric C=C			1492			C=C
	1575	Oligomeric C=C				1571	1589	
	1628	HOH bend and carbon C=C	1630	C=C carbon	1618			HOH bend (adsorbed water)
	1710	Diketonic C=O			1706	1711		C=O (carbonyl)
	~2500				1858			
2890						2885	2912	CH (glucose)
2914	2924	C-H			2922b	2912		CH
2945						2962	2971	CH (glucose)
	3120	C-H						
3356								OH (glucose)
3412								OH (glucose)

4.7 Conversion of Oxygenated Intermediates by Catalytic Fast Pyrolysis: Pyroprobe Results

Using low (1.5) catalyst-to-feed ratio, mainly furan-based oxygenates are produced (Section 3.4). The partially deoxygenated species detected are likely intermediates in the formation of aromatics, since at low catalyst-to-feed ratios, the high quantities of oxygenates leave the reactor before they can react further to form aromatics. Using these oxygenates as feedstocks at the same reaction conditions as glucose CFP may shed light on the heterogeneous chemistry in glucose conversion to aromatics. The oxygenated intermediates; acetic acid, furan, furfural, methyl-furan, as well as the aromatic products; toluene and benzene were chosen as feedstocks for this study. These represent the dominant products observed at low (1.5) catalyst-to-feed ratios.

Figure 4.7.1 shows the products yields of catalytic pyrolysis of acetic acid, furan, furfural, methyl-furan, furfuryl alcohol, toluene and benzene. A catalyst-to-feed ratio of 19, 240 second reaction time and 600 °C final reaction temperature were used in this set of experiments. As shown in Figure 4.7.1 the oxygenates form of aromatics, CO, CO_2 and coke. Acetic acid produces mainly CO_2 through decarboxylation, however, almost all of the remaining carbon goes to aromatics (~30% carbon yield). In the case of furan-based feedstocks, it is shown in Figures 4.7.1 and 4.7.2 that similar yields (between 35-50%) and selectivity of aromatics were produced from furfural, furfuryl alcohol, furan and 2-methyl furan. The yields of gases were also similar for the furans with the exception being the increased amount of decarbonylation with the furfural feed.

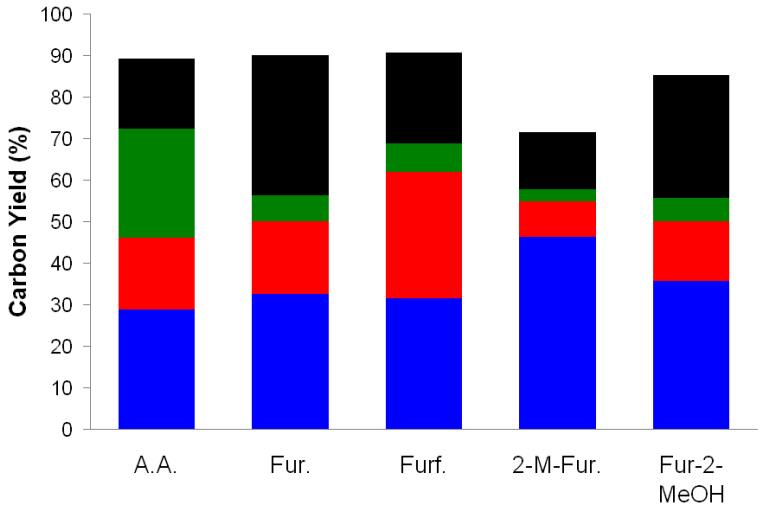

Figure 4.7.1 Distribution of product yields as a function of intermediate compounds reacted using catalytic fast pyrolysis. Reaction conditions: nominal heating rate 1000 °C s-1, final reaction temperature 600 °C, reaction time 240 s. Key : aromatics (blue), carbon monoxide (red), carbon dioxide (green), and coke (black). Abbreviations for the intermediate species are: acetic acid (A.A.), furfural (Fur.), 2-methyl furfural (2-M-Fur.) and furan 2-methanol (Fur-2-MeOH).

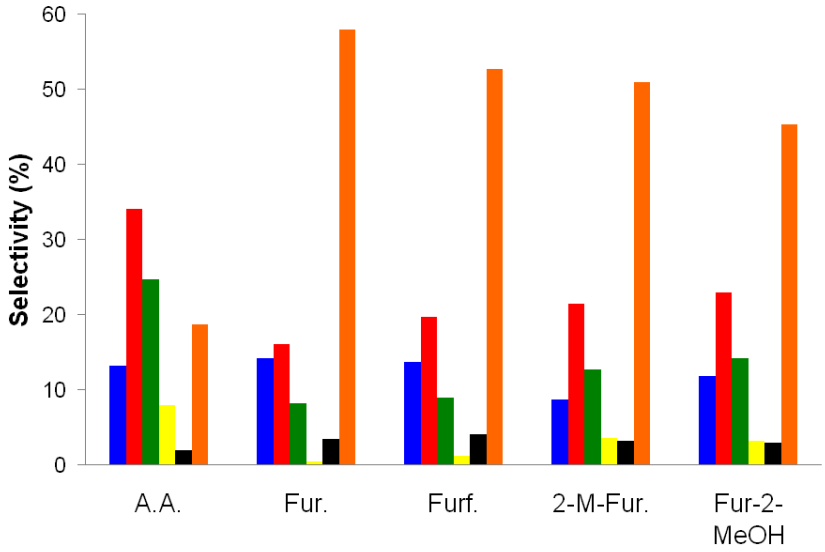

Figure 4.7.2 Selectivity of conversion of intermediate compounds reacted using catalytic fast pyrolysis. Reaction conditions: nominal heating rate 1000°C s-1, final reaction temperature 600 °C, reaction time 240 s. Key : benzene (blue), toluene (red), xylene and ethyl-benzene (green), methyl-ethyl-benzene and trimethyl-benzene (yellow), indenes (black), and Naphthalenes (orange). Abbreviations for the intermediate species are: acetic acid (A.A.), furfural (Fur.), 2-methyl furfural (2-M-Fur.) and furan 2-methanol (Fur-2-MeOH).

4.8 Isotopic Labeling of Glucose Feeds: Pyroprobe Results

In the first set of experiments a 1:1 wt% mixture of pure ^{12}C and ^{13}C glucose was pyrolyzed at two different catalyst to feed ratios (2.3 and 19 catalyst to feed weight ratio). In a second set of experiments a 1:1 wt% mixture of ^{12}C benzene and ^{13}C glucose was pyrolyzed in order to determine the role of single ring aromatics in the formation of polycyclic aromatics. In the last set of experiments, a 1:1 wt% mixture of ^{12}C naphthalene and ^{13}C glucose was pyrolyzed to determine whether naphthalene is susceptible to alkylation reactions.

When mixtures of ^{13}C and ^{12}C glucose were reacted at a low catalyst to feed ratio (2.3 ZSM-5:glucose ratio), the oxygenates detected in the effluent (including anhdyrosugars, furan, furfural, acetic acid) were either all ^{12}C or all ^{13}C. The single ring aromatic products are all intramolecular mixtures of ^{13}C and ^{12}C for reactions of ^{13}C and ^{12}C glucose, as shown in Figure 4.8.1. The relative amounts of ^{13}C and ^{12}C in the single ring aromatic species (Figure 4.8.1a-c) are normally distributed with the maximum abundance corresponding to a 1:1 isotopic mix. This suggests that the single ring aromatics are products from the hydrocarbon pool that exists within the zeolite formed from the dehydrated species. Inside this hydrocarbon pool, oxygen is removed from the dehydrated species as a combination of CO, CO_2 and H2O. The reported carbon scrambling is similar with previously reported reactions of isotopically labeled propane[75, 76] and methanol[68, 77, 78] on ZSM-5.

The data indicates that naphthalene is formed through another route. The isotopic distribution for naphthalene (Figure 4.8.1d) is composed of two distinct groups of peaks. The bimodal distribution indicates that a molecule with a random distribution (e.g.

benzene) oligomerized with a monoisotopic molecule to form naphthalene. Furthermore, the center of each of the groups (m/z =130 and 134) are separated by four suggesting the monoisotopic reactant is four carbons.

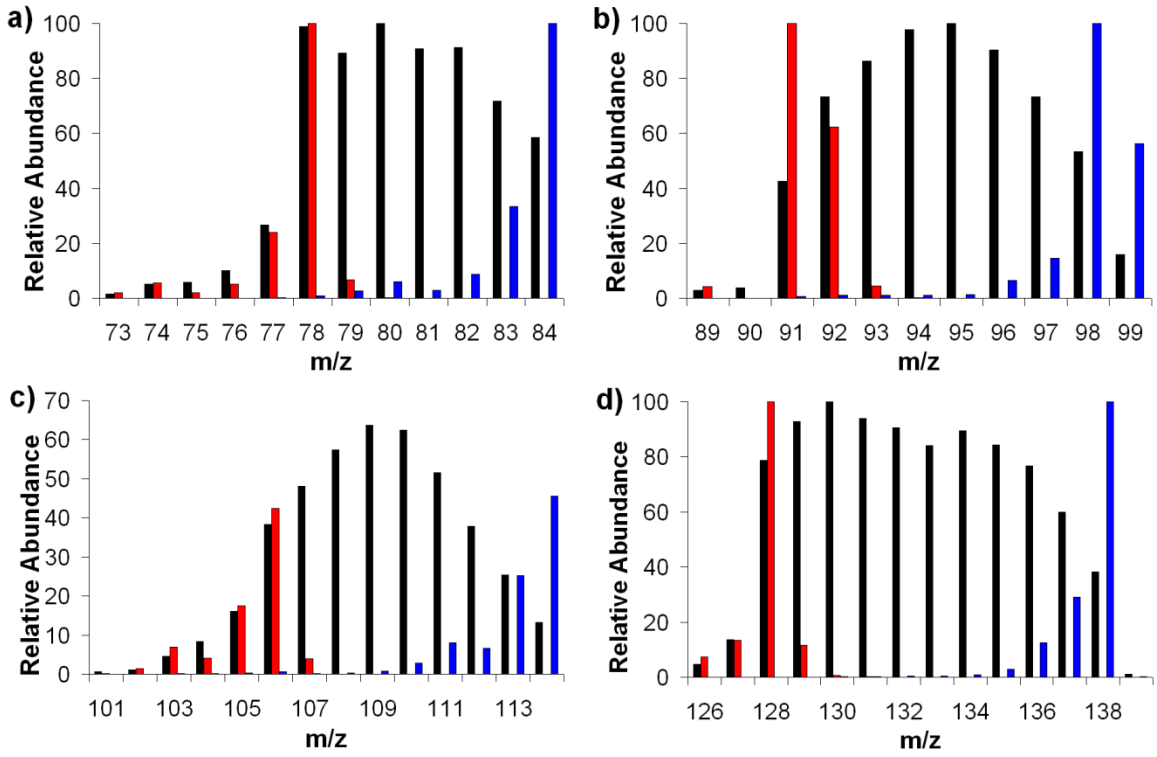

Figure 4.8.1 The isotopic distributions for: a) benzene, b) toluene, c) xylene and d) naphthalene from the pyrolysis of a 1:1 wt% mix of ^{12}C glucose and ^{13}C glucose. Pure ^{12}C and ^{13}C spectrums for the given molecule are shown in red and blue, respectively. Reaction conditions: catalyst to feed weight ratio = 19; catalyst ZSM-5 (Si/Al = 15), nominal heating rate 1000°C s-1, reaction temperature 600°C, reaction time 240 s.

To further investigate how naphthalene is formed, we performed experiments with ^{12}C benzene and ^{13}C glucose. As shown in Figure 4.8.2A two different types of naphthalene are formed. One type of naphthalene is formed only from the ^{13}C glucose. The other naphthalene is formed from a reaction of ^{12}C benzene and ^{13}C glucose (or products from ^{13}C glucose). Importantly this shows that the amount of undesired naphthalenes can be reduced by decreasing the concentrations of aromatics or oxygenates

in the reactor. The naphthalene formed from glucose is two times higher than the naphthalene from a mixture of benzene and glucose. Similar results were obtained for the methyl and dimethyl-naphthalene (Figure 4.8.2B-C).

In contrast, only small amounts of the single ring aromatics are formed by alkylation of the benzene (Figure 4d-f). This indicates that benzene does not re-enter the hydrocarbon pool inside the zeolite. Over 90 % of the toluene and xylenes are formed from the ^{13}C glucose as shown in Figures 4.8.2D-E. However, the benzene can be alkylated by the hydrocarbon pool. The relative intensity of mixed xylene is lower than the relative intensity of mixed toluene. This is because xylene has to be alkylated twice as opposed to one alkylation for toluene. However, as seen in Figure 4.8.2F the relative intensity for mixed isotope ethyl-benzene compared to the pure ^{13}C species is much higher meaning alkylation of benzene is an important route for the formation of ethyl benzene.

We studied catalytic fast pyrolysis of ^{12}C naphthalene with ^{13}C glucose to study the rate of alkylation of naphthalene. The spectra of methyl-naphthalene, dimethly-naphthalene and trimethyl-naphthalene are shown in Figure 4.8.3. As shown in Figure 4.8.3a, the relative intensity of the methyl naphthalene formed from the ^{12}C naphthalene reacting with the oxygenate is 40% compared to the ^{13}C methyl-naphthalene from the oxygenate. This suggests that naphthalene can be formed first in this reaction and then undergo alkylation from species in the hydrocarbon pool.

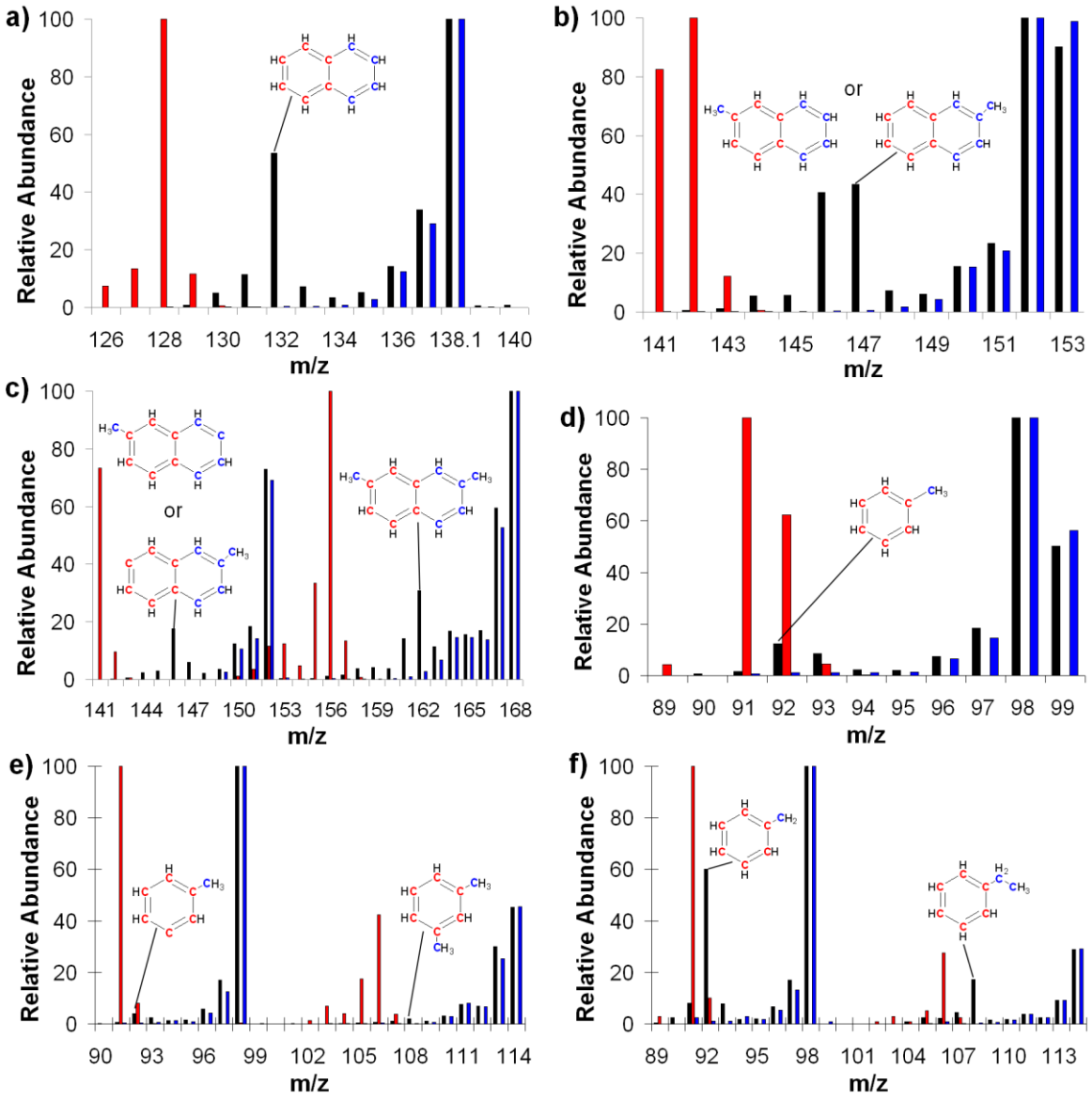

Figure 4.8.2 The isotopic distributions for: a) naphthalene, b) methyl-naphthalene, c) dimethyl-naphthalene, d) toluene, e) xylene and f) ethyl-benzene from the pyrolysis of a 1:1 wt% mix of ^{12}C benzene and ^{13}C glucose. Blue and red labeled carbons represent 13C and 12C carbons, respectively. Pure ^{12}C, and ^{13}C spectrums for the given molecule are shown in red and blue, respectively. Reaction conditions: catalyst to feed weight ratio = 19; catalyst ZSM-5 (Si/Al = 15), nominal heating rate 1000°C s-1, reaction temperature 600°C, reaction time 240 s.

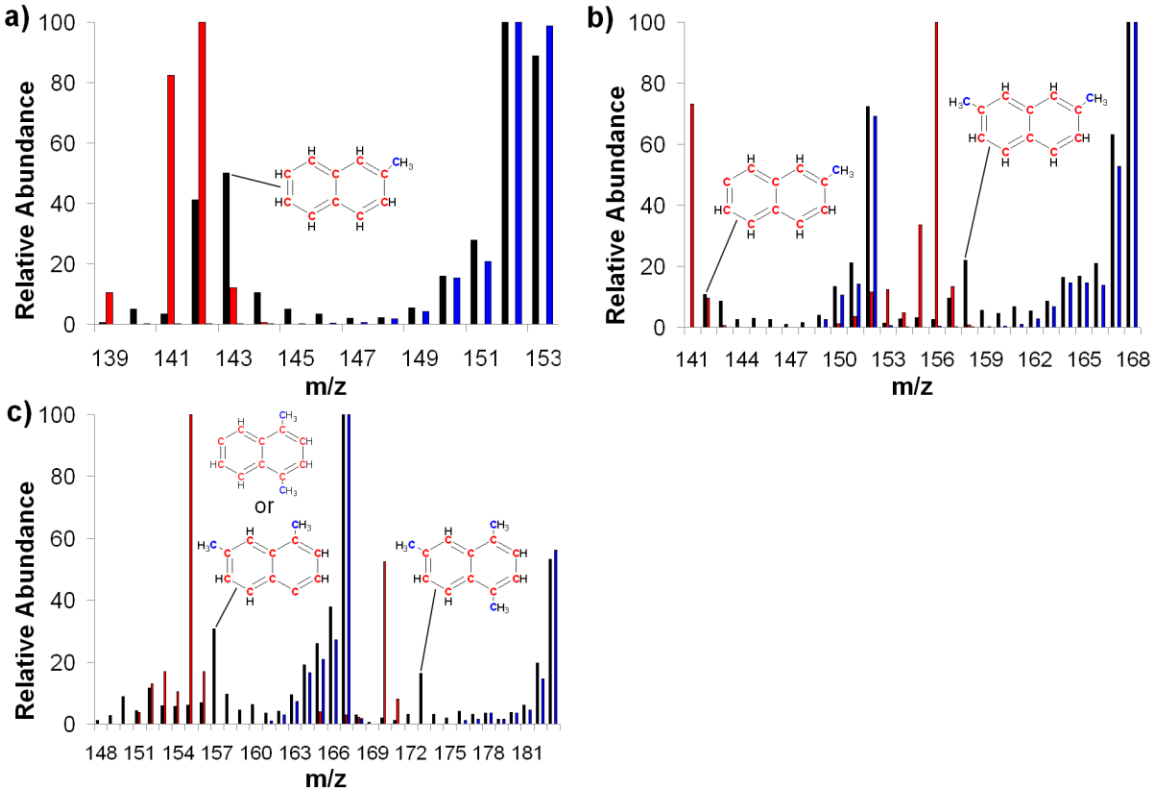

Figure 4.8.3 The isotopic distributions for a) methyl-naphthalene, b) dimethyl-naphthalene, c) trimethyl-naphthalene from the pyrolysis of a 1:1 wt% mix of ^{12}C naphthalene and ^{13}C glucose. Blue and red labeled carbons represent ^{13}C and ^{12}C carbons, respectively. Pure ^{12}C, and ^{13}C spectrums for the given molecule are shown in red and blue, respectively. Reaction conditions: catalyst to feed weight ratio = 19; catalyst ZSM-5 (Si/Al = 15), nominal heating rate 1000°C s-1, reaction temperature 600°C, reaction time 240 s.

4.9 Effect of Coke on Catalytic Activity: Pyroprobe Results

To investigate the effect of coke on the activity of ZSM-5 for the conversion of glucose the spent catalyst was recycled and pyrolized again with fresh glucose. As shown in Figure 4.9.1, the aromatic yield does not decrease with the repeated use of coked ZSM-5 indicating that the active sites of ZSM-5 remain despite of the coke on the catalyst phase. In fact, the aromatic yield slightly increases with subsequent cycles. It appears that the coke deposited on the catalyst has the active form which can be an intermediate for aromatic production. The aromatic selectivity observed for the coked

catalyst after 1 and 2 times reuse is shown in Figure 4.9.2. There is a small decrease in the selectivity for benzene and toluene and a small increase indenes and naphthalenes with increasing coke content. The ethyl benzenes and methyl, ethyl benzenes are unaffected by the increase in coke level.

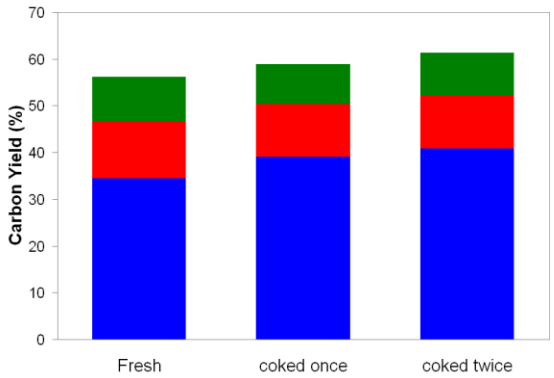

Figure 4.9.1 Product yields in the conversion of glucose with spent catalysts at 600 °C and a catalyst to feed ratio of 19. Key: aromatics (blue), carbon monoxide (red), and carbon dioxide (green).

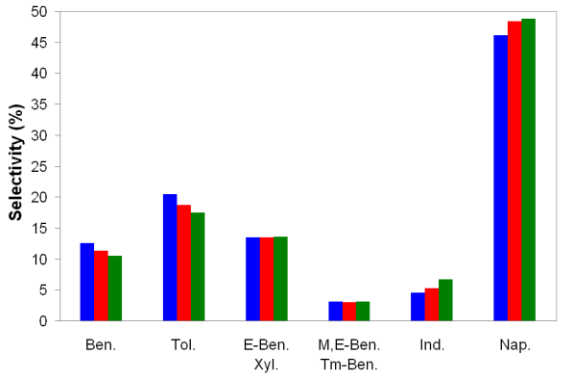

Figure 4.9.2 Selectivity of conversion of glucose with spent catalysts at 600 °C and a catalyst to feed ratio of 19. Key: Fresh ZSM-5 (blue), 1 time coked ZSM-5 (red), and 2 times coked ZSM-5 (green).

4.10 Effect of Coke on Catalytic Activity: N_2 adsorption Results

Coke is the major product in the conversion of glucose over ZSM-5. The yield of coke is 33% at a catalyst-to-feed ratio of 19 (600 ˚C for 240 s) and increases with decreasing catalyst concentration. To ascertain whether the coke is deposited on the outer

surface of the catalyst particles and/or within the pores of ZSM-5, nitrogen adsorption was performed on ZSM-5 before reaction, after reaction at 19:1 catalyst-to-feed ratio and after reaction at 1.5:1 catalyst-to-feed ratio. Figure 4.10.1 shows the high resolution adsorption isotherm of fresh and coked ZSM-5. The surface area and pore volume calculated from isotherms are summarized in Table 3.10.1. It can be seen that, compared to fresh ZSM-5, the amount of adsorbed nitrogen (micropore volume) decreases from 0.12 to 0.067 cm^3g^{-1} as the coke level increases from zero to 0.7 wt% carbon, indicating that some coke is deposited inside the zeolite pores. Further, increasing the amount of coke from 0.7 to 5 wt% does not significantly reduce the micropore volume which suggests further coking may take place outside of the pores on the catalyst surface. Interestingly, the external surface area does not change greatly between fresh and coked samples. This could be due to the low total quantity of coke on the catalyst. The BET surface area decreases with increasing weight percent of coke, indicating that higher coke levels decrease micropore surface area. It should be noted however, that the BET theory is not strictly valid for microporous materials and hence the C_{BET} constants are negative.

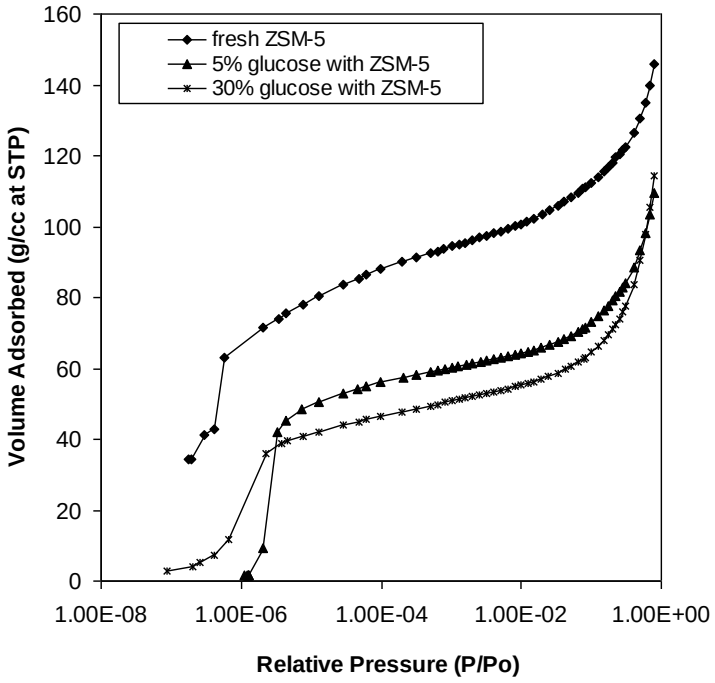

Figure 4.10.1 High resolution adsorption isotherms (N2 at 77 K) of fresh ZSM-5 and coked ZSM-5 at the catalyst to feed weight ratio of 19 and 2.3.

Table 4.10.1 External surface area and micropore volume for fresh and coked ZSM-5.

Catalyst	BET Surface area and Constant (C_{BET}) (m^2g^{-1})	External surface area (m^2g^{-1})[a]	Micro pore volume (cm^3g^{-1})[b]	Carbon content (ICP analysis) (wt%)[c]
ZSM-5 (Si/Al=15)	372, -62	140	0.120	-
Coked ZSM-5 (from 5wt% glucose at 600˚C, reacted 1x)	255, -81	125	0.067	0.69
Coked ZSM-5 (from 30wt% glucose at 600˚C)	236, -151	138	0.049	5

[a]calculated based on the t-method
[b]calculated using the t-method
[c]From ICP analysis. Calculation assumes organic component is primarily carbon.

4.11 Discussion

4.11.1 Chemistry of Glucose Pyrolysis

Figure 4.11.1 shows the reaction pathways that occur during catalytic fast pyrolysis of glucose. As we discovered in this study, there are two pathways for the thermal decomposition of glucose. Both pathways occur very rapidly with complete glucose decomposition in about one second at 600 °C. At low temperatures glucose decomposes via retro-aldol and Grob fragmentation reactions to form small oxygenates such as; hydroxyl-acetaldehyde, hydroxyl acetone, dihydroxyacetone and d-glyceraldehyde. Other researchers have also shown that these small oxygenates are formed from pyrolysis of carbohydrates.[26, 27, 79]

At high temperatures, dehydration of glucose is favored. First, glucose is dehydrated to anhydrosugars with levoglucosan as the major product. These anhydrosugars are further dehydrated to furans such as furfural, furfuryl alcohol, furan and 2-methyl furan. Both of these decomposition pathways can occur either homogenously or on acid sites of ZSM-5. From the FTIR results (Figure 4.4.1) there are carboxylic acids present during decomposition which could homogeneously catalyze dehydration. In the literature, it has been shown that furfuryl aldehyde, furfuryl alcohol, and 5-hydroxymethyl furfural are prominent dehydration products from the fast pyrolysis of glucose, cellulose and hemicellulose.[25, 79] In addition, Lourvanij et al. reported that aqueous glucose can be dehydrated with acidic zeolites to yield hydroxymethyl furfural.[80]

Williams and Besler also showed that glucose has two thermal decomposition peaks between 200 and 400°C using thermogravimetric analysis.[81] However, these

workers concluded glucose decomposes to a polymeric intermediate which then undergoes secondary degradation. Hence, two transitions are observed in the DTG at ~260 and 360 °C (for a heating rate of 40 °Cmin^{-1}). Further, Ramos-Sanchez et al. reported the TGA in air of sugars including glucose.[82] Glucose showed an onset temperature in the TGA at 192 °C with two weight losses at 227 and 321 °C.

When ZSM-5 is added to the reactor the temperatures at which the thermal decomposition reactions occur are lowered. From the visual observations, it can be seen that coke can be formed at low temperatures (<210°C) from the retro-aldol/Grob fragmentation products as well as at high temperatures from the dehydration products. However, coke formation is more favorable at low temperature since for pure glucose pyrolysis (section 4.1) as well as catalytic fast pyrolysis of glucose (section 3.3) coke yield is higher at low heating rates.

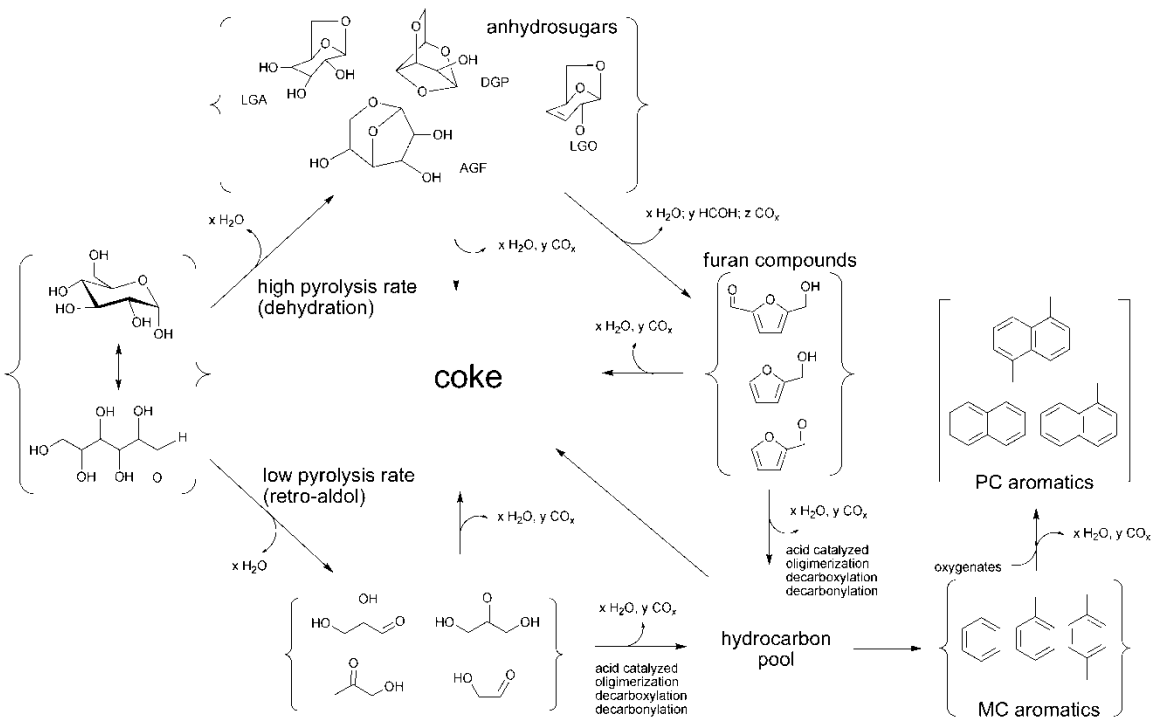

Figure 4.11.1 Reaction chemistry for the catalytic fast pyrolysis of glucose with ZSM-5.

4.11.2 Chemistry of Glucose Conversion to Aromatics

In this study, we showed that oxygenates produced from the thermal decomposition of glucose are intermediates in the conversion of glucose to aromatics. Furan, furfural, methyl-furan and furfuryl alcohol as well as acetic acid, are all converted to aromatics with similar selectivity under the same pyrolysis conditions (600 °C for 240 s). The pathway for conversion of the intermediate oxygenates to aromatics is shown in Figure 4.11.1. From the FTIR and pyroprobe reaction time results (Figures 4.5.1, 4.6.1 and 4.6.2) it can be seen that the formation of aromatics is the slow step in the reaction pathway. Glucose decomposes quickly in less than one second while aromatic formation takes 2 minutes. To form aromatics, oxygenates diffuse into the ZSM-5 pores and through a series of decarbonylation, decarboxylation, dehydration, and oligomerization reactions form aromatics. It has been proposed that, for the conversion of methanol to

aromatics with ZSM-5, the reaction proceeds through a common intermediate or "hydrocarbon pool" within the zeolite framework.[68, 77, 78, 83] The methanol enters this hydrocarbon pool where it reacts with other hydrocarbons to form aromatics and olefins. The exact nature of this hydrocarbon pool has been the subject of much debate,[83] but it is thought that the active species inside the hydrocarbon pool is a polymethylbenzene.[68, 77, 78] The isotopic labeling studies (section 4.8) suggest that similar hydrocarbon pool chemistry occurs during glucose conversion to aromatics over ZSM-5.[28] The presence of monoisotopic oxygenates indicates some of the oxygenates (about 15% of the total carbon) leave the reactor before they enter into the hydrocarbon pool. Furthermore, these monoisotopic intermediates indicate that only dehydration and rearrangement reactions occur before these intermediate oxygenates enter the hydrocarbon pool within the zeolite. The isotopic studies show that the single ring aromatic products from this hydrocarbon pool are a random mixture of ^{12}C and ^{13}C carbon, indicating that the partial dehydrated products lose their identity during this reaction. The isotopic mix of naphthalene suggests it is produced from two different steps with one step involving the combination of monocyclic aromatics with oxygenated fragments. Furthermore, the aromatic product selectivity (Figure 4.5.2) shifts from monocyclic aromatics to naphthalenes with increasing reaction time indicating that naphthalenes are probably formed from monocyclic aromatics in second series reaction. These results suggest that the ratio of benzene, toluene and xylene (BTX) to naphthalene can be adjusted in CFP technology because naphthalene and BTX are formed from two different mechanisms. Both benzene and naphthalene are susceptible to alkylation from the hydrocarbon pool

although the rate of alkylation of naphthalene is high and the rate of alkylation of benzene is low.

The major competing reaction to the formation of aromatics is the formation of coke. It is likely that during CFP of glucose the intermediate furans polymerize to form resins which further decompose to form coke on the catalyst. The acid catalyzed dehydration polymerization of furfuryl alcohol has been well documented in the literature.[74, 84, 85] The FTIR reaction time data (Figure 4.6.2, Table 4.6.2) shows at 3 seconds carbonyl species (band at 1711 cm^{-1}) are present. Bertarione et al.,[74] Choura et al.[84] and Conley et al.[85] identified 1710-1715 cm^{-1} as the characteristic band of the diketonic carbonyl present in furfuryl alcohol resins. These furan resins are probably coke precursors as the band at 1711 cm^{-1} is no longer present at long reaction times. Bertarione et al. reported that the furfuryl alcohol resin is decomposed on the acidic zeolite HY when heated to 400 °C to form amorphous carbon. Our FTIR results also show that unsaturated carbon is present at long reaction times (bands at 1492, 1571 and 1589 cm^{-1}).

When compared to fresh catalyst the coked catalyst pore volume is decreased significantly, however, with increasing coke levels there is no additional change in the pore volume. This initial decrease in pore volume is likely due to the formation of the hydrocarbon pool within the zeolite framework. Once the hydrocarbon pool is formed additional carbon is deposited on the surface not within the pores. Several researchers studying the conversion of methanol to hydrocarbons (MTH) over ZSM-5 have reported that catalyst deactivation occurs from highly unsaturated coke on the external surface of the catalyst and not from large species within the pores.[68, 86, 87] In contrast, larger caged

zeolites such as HSAPO-34 and β-zeolite are mainly deactivated by the formation of polyaromatic species within the pore systems.[77, 88] The results herein suggest that the primary coking mechanism is the formation of oxygenate resins on the surface of the catalyst which ultimately decompose to unsaturated coke.

4.11.3 Design of Improved Reactors for Catalytic Fast Pyrolysis

There are several important parameters involved in maximizing the yield of aromatics from the catalytic fast pyrolysis of oxygenates over ZSM-5. High heating rates must be obtained to decrease the amount of time spent at low temperatures. At low temperatures the primary product formed is coke. In addition, as shown in Figure 3.5.1, moderately high reaction temperatures are required to minimize coke formation. However, the aromatic yield does not significantly increase above 600 °C, and more energy would be required for heating, hence a reaction temperature of 600 °C is the optimum. Reactor temperature can also be used to adjust the selectivity for various aromatics as shown in Figure 3.5.2. Lastly, the concentration of oxygenates in the reactor should be low to reduce coking reactions. In addition, to reducing coke it is also desirable to reduce the amount of naphthalene produced as it is of less value than the monocyclic aromatics.

4.12 Conclusions

The catalytic fast pyrolysis of glucose involves two steps. The first step involves the rapid thermal decomposition of glucose. Glucose can decompose through two different pathways. At low temperature glucose is decomposed to small oxygenates through retro-aldol condensation reactions. At high temperatures glucose is dehydrated to form anhydrosugars and furans. Both decomposition pathways can occur homogenously or on

catalyst active sites. Addition of ZSM-5 to the reactor lowers the temperature at which both the decomposition reactions occur. The second step in CFP is the formation of aromatics within the pores of the zeolite. The monocyclic aromatic compounds are formed from random hydrocarbon fragments which are most likely produced from a hydrocarbon pool within the zeolite structure. Naphthalene is produced from two different steps with one step involving the combination of monocyclic aromatics with oxygenated fragments. Both benzene and naphthalene are susceptible to alkylation from the hydrocarbon pool although the rate of alkylation of naphthalene is high and the rate of alkylation of benzene is low. The aromatics formation step is far slower than the preceding thermal decomposition reactions.

The oxygenates produced from thermal decomposition are likely the intermediates in the formation of aromatics as furans and acetic acid produce similar aromatic products under the same pyrolysis conditions (600 °C for 240 s). The main competing reaction with aromatic production is the formation of unsaturated coke on the surface of the catalyst. Coke is formed through intermediate furan polymers which ultimately decompose to unsaturated coke. To achieve maximum aromatic yields pyrolysis should proceed with rapid decomposition of glucose to oxygenates to react with the catalyst. The concentration of oxygenates should remain low to avoid formation of coke and less desirable polycyclic aromatics.

CHAPTER 5

CONTINUOUS CATALYTIC FAST PYROLYSIS OF REAL BIOMASS FEEDS

5.1 Introduction

The yield and selectivity for aromatics from the CFP of glucose in the pyroprobe show the potential for the CFP process, however, it would be desirable to demonstrate CFP on a larger scale using real biomass feeds. Using optimized conditions in the pyroprobe micro reactor 32 % of the carbon in the glucose can be converted into aromatics, however, the micro pyroprobe reactor cannot economically be scaled up into a larger reactor. In order to demonstrate larger scale a continuously fed fluidized bed reactor was constructed. Fluidized bed reactors have been proven in a vast number of processes across industry due to their excellent mass and heat transfer properties, scalability and simplicity of operation. [39, 89-91] Using the fluidized bed reactor we have determined the dependence of space velocity, temperature and time on stream for catalytic fast pyrolysis of pine wood with ZSM-5 catalyst.

Several researchers have also performed catalytic pyrolysis in continuous fluidized bed reactors.[15, 19, 20, 23, 45, 92] In early studies aromatics were produced by first pyrolyzing wood in a non-catalytic fluidized bed reactor followed by a secondary fixed bed catalytic reactor to convert the primary pyrolysis vapors. [15, 45, 92] In general the two reactor approaches yielded more coke and less aromatics when compared with the later single stage studies. Of the single stage studies Olazar and coworkers[20] reported aromatic yields of 12% carbon in a canonical spouted bed reactor using ZSM-5 catalyst.

In this reactor setup the bottom section of the reactor is conical in shape and a high velocity stream of gas (the spout) induces circulation within the catalyst bed. Aho et al. [23] tested several types of zeolites for the catalytic pyrolysis of softwood in a cylindrical bubbling fluidized bed reactor. They reported that β-zeolite, mordenite, Y-zeolite, and ZSM-5 all produced different product spectra in the resulting bio-oil. The addition of ZSM-5 significantly decreased the amount of acids and alcohols in the bio-oil while the amount of ketones increased. Lappas and collaborators [19] reported on the use of a lab scale FCC riser reactor for the catalytic pyrolysis of pine wood with a commercial fluid catalytic cracking catalyst and a commercial ZSM-5 additive. They reported that addition of catalyst increased the yield of water, non-condensable gases and char. The bio-oil obtained was of lower oxygen content and therefore they proposed of better quality.

The objective of this portion of the thesis is to study CFP of pine wood in a bubbling fluidized bed reactor and compare these results with CFP in a fixed bed reactor and a pyroprobe reactor. The effects of temperature, and biomass weight hourly space velocity (WHSV) reaction time on the product yield and selectivity are studied. In addition, we test the catalytic properties before and after reaction to determine if impurities in the biomass poison catalytic sites. Biomass contains minerals that may poison zeolite catalysts during CFP.[93] None of the previous researchers studied the effect of the minerals on the catalyst stability. In the fixed bed reactor we study furan conversion over ZSM5 and compare these results to CFP in a fluidized bed reactor. The effects of co-feeding olefins in both the fluidized bed and fixed bed reactors were also

studied. The fluidized bed and fixed bed results are also compared to a pyroprobe micro reactor to show how CFP can change with different reactor types and catalysts.

5.2 Fluidized Bed Results

5.2.1 Product Yields as a Function of Time on Stream

Figure 5.2.1 shows the concentration of aromatics exiting the condenser train as a function of time on stream during catalytic fast pyrolysis. As shown the product concentration first increases during the first 40 minutes of operation at the reaction conditions shown in Figure 5.2.1. After 40 minutes the concentration begins to decrease due to coke buildup on the catalyst surface. Thus all the data was collected in a 30 minute time on stream period where the catalyst activity did not decrease with time.

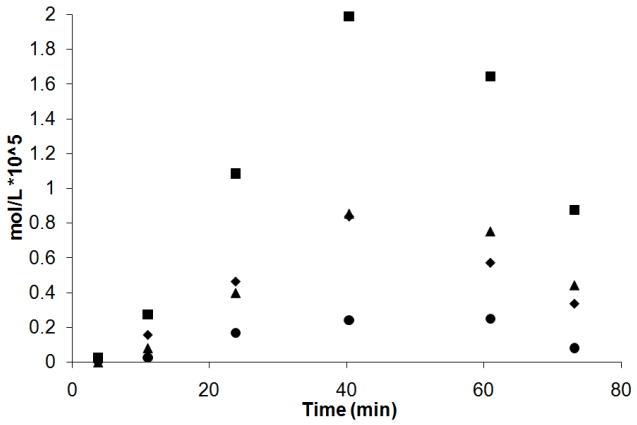

Figure 5.2.1 Gas phase aromatic concentrations as a function of time on stream for catalytic fast pyrolysis of pine sawdust. Reaction conditions: pine wood feed at 0.1 WHSV, 1200 mL min^{-1} He fluidization flow rate, 600 °C reactor temperature. Key: ♦: benzene, ▲: toluene, ●: xylenes, ■: total aromatics.

5.2.2 Gas Residence Time Distribution

Carbon monoxide was used as a tracer in our fluidized bed reactor, as shown in Figure 5.2.2. This figure shows the normalized concentration of carbon monoxide tracer

gas measured at the outlet of the reactor as a function of time. Also shown in figure 3.1.6, are the calculated concentrations for an ideal plug flow reactor (PFR) and an ideal continuously stirred tank reactor (CSTR). The ideal residence time distribution was calculated using the actual reactor volume of 515 mL, the piping volume leading to the reactor of 49 mL and and inlet gas flow rate of 1200 cm3 sec-1. The calculated gas residence time of the reactor is therefore about 26 sec. It can be seen that the actual measured distribution looks more like a CSTR which indicates that there is good gas mixing within the reactor.

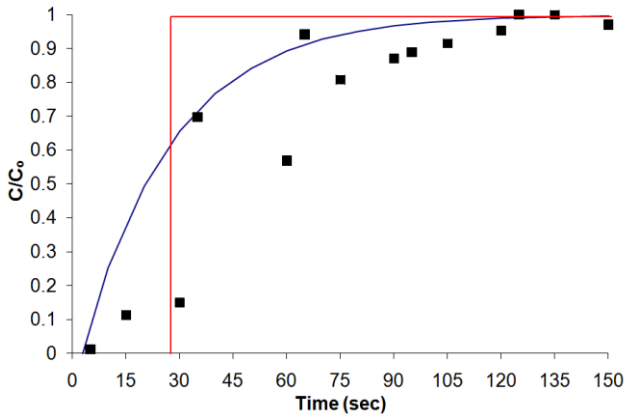

Figure 5.2.2 Normalized gas concentration in the fluidized bed reactor after a step change in inlet concentration. The red lines are the calculated concentrations for an ideal PFR (red) and an ideal CSTR (blue).

5.2.3 Effect of Biomass Weight Hourly Space Velocity

Figure 5.2.3 shows the product yield for CFP of pine sawdust at 600 °C as a function of weight hourly space velocity (WHSV). WHSV is defined as the mass flow rate of feed divided by the mass of catalyst in the reactor. The aromatic and coke yield both decrease with increasing space velocity. The highest aromatic yield of 14 % carbon was obtained at a space velocity of 0.1 hr^{-1}. The amount of unidentified carbon increases with increasing space velocity. The unidentified carbon could be from either unconverted

intermediate oxygenates or from the small amount of insoluble tar that accumulates in the transfer lines at higher space velocities. The olefin yield increases steeply from 5 % carbon at 0.1 hr^{-1} to 8 % carbon at 0.2 hr^{-1} then decreases slowly to 7 % carbon over the rest of the range. The methane yield increases with increasing WHSV from 3 % to 8 % carbon.

Table 5.2.1 gives a detailed carbon yield and selectivity as a function of WHSV. Methane and ethylene are the primary light hydrocarbon species. At low WHSV ethylene is the most abundant light hydrocarbon with a selectivity of 59 % carbon selectivity followed by methane with a carbon selectivity of 34.2 %. At high biomass WHSV methane becomes the dominant light hydrocarbon product (57 % carbon selectivity) while ethylene selectivity decreases to 37.0 %. The selectivity for toluene and xylene are both strong functions of biomass WHSV. Toluene and xylenes (total of meta, ortho and para) carbon selectivity both decrease with increasing WHSV appreciably from 34.1 % to 17.2 % and 15.4 % to 2.9 %, respectively. Benzene and naphthalene show the opposite trend. Benzene increases from 24.8 % to 33.4 % carbon selectivity while naphthalene increases from 14.9 % to 26.1 % carbon selectivity as WHSV increases.

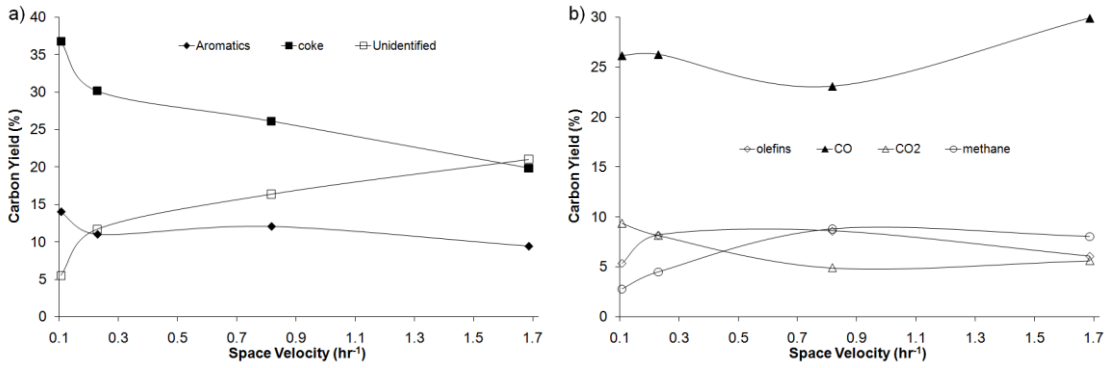

Figure 5.2.3 Carbon yields as a function of biomass WHSV for CFP of pine sawdust. Reaction conditions: ZSM-5 catalyst, 600 °C, 1.2 SLM helium fluidization flow rate, 30 min total reaction time. Key: a) ♦: aromatics ■: coke □: unidentified, b) ▲: CO Δ: CO2, ○: methane ◊: olefins.

Table 5.2.1 Detailed yield distribution and product selectivity for CFP of pine wood. Aromatic selectivity is defined as the moles of carbon in the product divided by the total moles aromatic carbon. Light hydrocarbon selectivity is defined as the moles of carbon in the product divided by the total moles olefin carbon.

	WHSV (hr^{-1})			
	0.1	0.2	0.8	1.7
Overall Yields				
Aromatics	14.0	11.0	12.1	9.5
Olefins	5.4	8.2	8.6	6.1
Methane	2.8	4.5	8.8	8.0
Carbon Monoxide	26.2	26.3	23.1	29.9
Carbon Dioxide	9.4	8.1	4.9	5.6
Coke	36.8	30.2	26.1	19.9
Aromatic Selectivity				
Benzene	24.8	23.1	29.1	33.4
Toluene	34.1	30	21.9	17.2
Ethyl-Benzene	0.6	1.2	0.5	0.2
m-Xylene and p-Xylene	12.9	12	5	2.6
o-Xylene	2.5	1.9	0.8	0.3
Styrene	3.3	4.4	5.9	5.2
Phenol	1.1	4	8.1	5.1
Indene	1.4	7.1	8.9	8.4
Benzofuran	4.3	1.6	2.1	1.4
Napthalene	14.9	14.7	17.7	26.1
Light Hydrocarbon Selectivity				

Methane	34.2	35.4	50.6	57
Ethylene	59.8	41	41.3	37
Propylene	5.4	16.6	6.1	4.3
Butene	0.2	1.9	0.4	0.3
Butadiene	0.4	5	1.7	1.5

5.2.4 Effect of Reaction Temperature

The product yields for the catalytic fast pyrolysis of pinewood in the fluidized bed reactor at different temperatures are shown in Figure 5.2.4. The coke and unidentified oxygenates yield decreases with increasing temperature. The CO and methane yield increase with temperature. These results indicate that the chemistry shifts to gasification like reactions at higher temperatures temperature. The aromatic yield goes through a slight maximum of 11 % carbon at 600 °C. Further increasing the temperature to 670 °C decreases the yield slightly to 9 % carbon. Temperature has little effect on the total yield of olefins. However, as shown in Table 5.2.2 the selectivity for the olefins shows an interesting trend. Propylene selectivity is high (22.1 % carbon) at low temperature but then decreases to almost zero at the highest temperature. Ethylene exhibits a minimum at 600 °C. Methane increases in selectivity from 25.7 to 54.1 % carbon over the temperature range tested. Increasing the reactor temperature from 500 to 670 °C changes the product distribution of aromatics. The selectivity for xylenes and toluene decrease from 41.5 % to 14.6 % and 12.6 % to 1.2 % carbon, respectively as the temperature increases. Benzene and naphthalene increase in selectivity from 26.1 % to 45.7 % and 4.5 % to 31.7 %, respectively as the temperature increases.

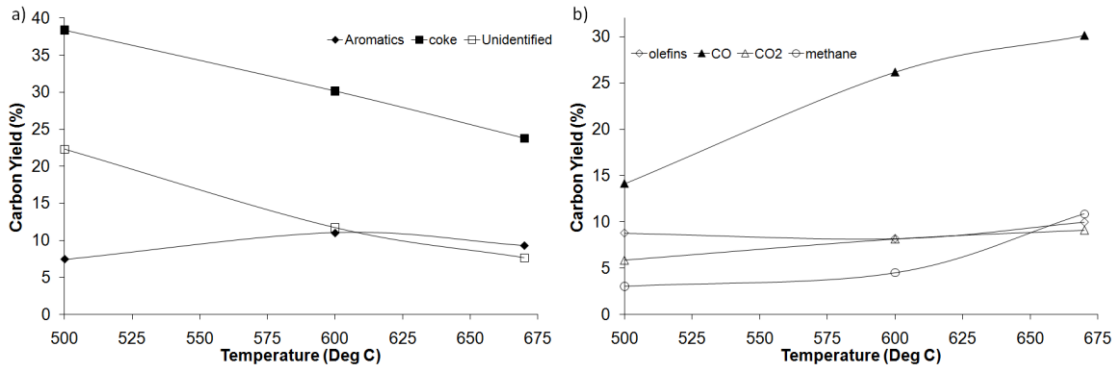

Figure 5.2.4 Effect of temperature on the carbon yield for CFP of pine sawdust. Reaction conditions: ZSM-5 catalyst, 0.2 wood WHSV, 1.2 SLM helium fluidization flow rate, 30 min total reaction time. Key: a) ♦: aromatics ■: coke □: unidentified, b) ▲: CO Δ: CO_2, ○: methane ◊: olefins.

Table 5.2.2 Detailed yield distribution and product selectivity for CFP of wood at various temperatures. Aromatic selectivity is defined as the moles of carbon in the product divided by the total moles aromatic carbon. Olefin selectivity is defined as the moles of carbon in the product divided by the total moles olefin carbon.

	Temperature (°C)		
	500	600	670
Overall Yields			
Aromatics	7.4	11.0	9.3
Olefins	8.8	8.2	9.2
Methane	3.1	4.5	10.9
Carbon Monoxide	14.1	26.3	30.1
Carbon Dioxide	5.9	8.1	9.1
Coke	38.4	30.2	23.8
Aromatic Selectivity			
Benzene	26.1	23.1	45.7
Toluene	41.5	30	14.6
Ethyl-Benzene	3.1	1.2	0.1
m-Xylene and p-Xylene	8.8	12	1.1
o-Xylene	3.8	1.9	0.1
Styrene	2.9	4.4	3.3
Phenol	4.8	4	0.5
Indene	3.2	7.1	2.5

Benzofuran	1.2	1.6	0.4
Naphthalene	4.5	14.7	31.7
Light Hydrocarbon Selectivity			
Methane	25.7	35.4	54.1
Ethylene	45.7	41	44.8
Propylene	22.1	16.6	0.8
Butene	4	1.9	0.1
Butadiene	2.4	5	0.2

5.2.5 Olefin Recycle

Olefin co-feed experiments were conducted using the reaction parameters outlined in Table 5.2.3. All reactor parameters were held constant except for the concentration of olefin in the inlet fluidization gas. As shown in Table 5.2.3 propylene is consumed in this process since the moles of olefin exiting the reactor for propylene is about half of the amount fed. When ethylene is used as co-feed there is a net production of ethylene during the reaction which suggests that ethylene is a stable product and is non-reactive.

Table 5.2.3 Reaction conditions for catalytic fast pyrolysis of pine sawdust with olefins as a co feed. Reaction conditions: Grace ZSM-5 catalyst, 1.4 SLM total gas flow rate, 0.2 wood WHSV, 30 min total reaction time, 600 °C reaction temperature. The low olefin co feed runs correspond to 0.2 mol% olefin in the gaseous feed. The high olefin co feed runs correspond to 2 mol% olefin in the gaseous feed. The runs with zero furan WHSV were run with 2 mol% olefin in the gaseous feed.

	Propylene Feed		Ethylene Feed		No Co-Feed
WHSV of wood (hr^{-1})	0.24	0.24	0.26	0.27	0.21
grams olefin/grams wood	0.16	0.04	0.08	0.02	0.00
olefin/wood (carbon amount)	0.30	0.09	0.15	0.05	0.00
Moles olefin out / in	0.50	0.45	0.96	1.33	Na

Figure 5.2.4 shows the overall yields for the different products from the CFP of wood with propylene co-feed. In Figure 5.2.5 the carbon yield is the single pass yield e.g. it is calculated as the amount of carbon in the given product divided by the total amount of carbon fed to the reactor (wood and olefin). Increasing the amount of propylene co-feed

slighly increases the aromatic yield from 11 % to 12.4 % carbon while the coke yield decreases from 30 to 25%. The yield of carbon dioxide and carbon monoxide also decrease at higher propylene feed concentration. The carbon monoxide and carbon dioxide yields increase from 26.3 to 35.1 % carbon and 8.1 to 9.4 % carbon, respectively.

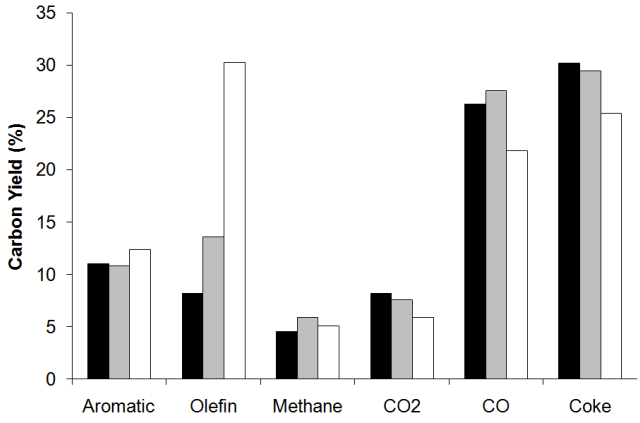

Figure 5.2.5 Single pass yields for catalytic fast pyrolysis of pine wood with propylene as a co-feed. The yield based on total carbon fed to the reactor. Reaction conditions: ZSM-5 catalyst, 0.2 wood WHSV, 1.2 SLM helium fluidization flow rate, 30 min total reaction time. Key: Black: no co feed, grey: 0.09 propylene/wood carbon ratio, white: 0.3 propylene/wood carbon ratio. The aromatics quantified include: benzene, toluene, xylene, ethyl-benzene, styrene, indene, phenol and naphthalene. The olefins quantified include: ethylene, propylene, butene and butadiene. The aromatic species quantified include: benzene, toluene, xylene (all three isomers), ethyl-benzene, styrene, indene, naphthalene and 1-methyl-naphthalene.

Table 5.2.4 shows how the selectivity for the aromatic species changes with the addition of propylene co-feed. In general the aromatic selectivity does not change significantly with the addition of propylene. The selectivity for benzene is the highest (30.4 % carbon) at intermediate propylene concentration. The toluene selectivity is highest (33.3 %) at the high propylene concentration. At the intermediate propylene concentration toluene exhibits a minimum selectivity of 28 % carbon. The total selectivity for xylenes remains relatively constant at ~12-14% carbon selectivity for low and high propylene concentration, however, at intermediate concentration far more o-

xylene is produced. The benzofuran selectivity is a strong function of propylene concentration and increases from 1.6 % to 11.0 % carbon as the propylene concentration increases. The selectivity for naphthalene decreases at the higher concentration of propylene.

Table 5.2.4 Detailed yield distribution and product selectivity for aromatic and olefin species for various propylene feed amounts. Reaction conditions: ZSM-5 catalyst, 0.2 wood WHSV, 1.2 SLM helium fluidization flow rate, 30 min total reaction time. Aromatic selectivity is defined as the moles of carbon in the product divided by the total moles aromatic carbon. Olefin selectivity is defined as the moles of carbon in the product divided by the total moles olefin carbon.

	Propylene/wood ratio (mol/mol carbon)		
	wood only	0.09	0.3
Overall Yields			
Aromatics	11.0	10.8	12.4
Olefins	8.2	13.6	30.2
Methane	4.5	5.9	5.0
Carbon Monoxide	26.3	27.6	21.8
Carbon Dioxide	8.1	7.5	5.9
Coke	30.2	29.4	25.4
Aromatic Selectivity			
Benzene	23.1	30.4	24.8
Toluene	30.0	28.0	33.3
Ethyl-Benzene	1.2	0.7	1.3
m-Xylene and p-Xylene	12.0	6.9	11.2
o-Xylene	1.9	4.7	2.1
Styrene	4.4	1.2	3.6
Phenol	4.0	1.6	1.3
Indene	7.1	2.4	0.3
Benzofuran	1.6	9.0	11.0
Naphthalene	14.7	15.1	11.0
Light Hydrocarbon Selectivity			
Methane	42.5	46.0	31.0
Ethylene	49.2	48.7	58.5
Propylene	na	na	na
Butene	2.3	1.6	6.3
Butadiene	6.0	3.7	4.2

Figure 5.2.6 shows the single pass yield for the various products with ethylene co-fed with wood to the reactor. As shown in Figure 5.2.6increasing the ethylene in the feed slightly decreases the aromatic and coke yields. The decrease in aromatic yield indicates the ethylene is not reacting to form additional aromatics, which, is consistent with the conversion of ethylene in Table 5.2.5. The yield of carbon dioxide slightly decreases with increasing ethylene concentration. The carbon monoxide yield goes through a maximum at intermediate ethylene concentration.

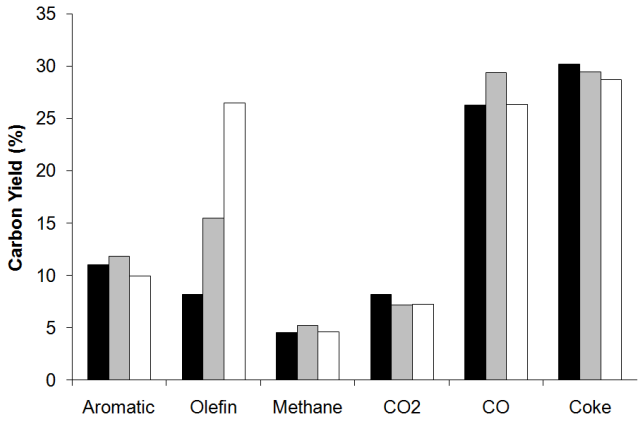

Figure 5.2.6 Catalytic fast pyrolysis of pine wood with ethylene as a co-feed. The yield is calculated from the total carbon fed to the reactor. Reaction conditions: ZSM-5 catalyst, 0.2 wood WHSV, 1.2 SLM helium fluidization flow rate, 30 min total reaction time. Key: Black: no co feed, grey: 0.05 ethylene/wood carbon ratio, white: 0.15 ethylene/wood carbon ratio. The aromatics quantified include: benzene, toluene, xylene, ethyl-benzene, styrene, indene, phenol and naphthalene. The olefins quantified include: ethylene, propylene, butene and butadiene. The aromatic species quantified include: benzene, toluene, xylene (all three isomers), ethyl-benzene, styrene, indene, naphthalene and 1-methyl-naphthalene.

Table 3.1.5 shows how the selectivity for the aromatic species changes with the addition of ethylene co-feed. The aromatic selectivities do not change significantly with ethylene concentration. The benzene selectivity increases from 23.1 to 27.4 % as the ethylene concentration increases. The total selectivity for xylenes decreases with increasing ethylene concentration from 13.9 to 9.3 % carbon. Similar to the propylene

co-feed at intermediate concentrations of olefin the ratio of ortho-xylene to meta and para-xylene is higher. Benzofuran selectivity is also strong function of ethylene concentration. It increases from 1.6 % to 12.0 % carbon while going through a maximum of 13.8 % at the intermediate concentration. The selectivity for naphthalene (14.7 %) is not a strong function of ethylene concentration. The propylene selectivity does not change significantly with ethylene concentration. The selectivity for larger olefins such as butane and butadiene decreases with increasing ethylene concentration.

Table 5.2.5 Detailed yield distribution and product selectivity for aromatic and olefin species for various ethylene feed amounts. Reaction conditions: ZSM-5 catalyst, 0.2 wood WHSV, 1.2 SLM helium fluidization flow rate, 30 min total reaction time. Aromatic selectivity is defined as the moles of carbon in the product divided by the total moles aromatic carbon. Olefin selectivity is defined as the moles of carbon in the product divided by the total moles olefin carbon.

	Ethylene/wood ratio (mol/mol carbon)		
	wood only	0.05	0.15
Overall Yields			
Aromatics	11.0	11.8	10.0
Olefins	8.2	15.5	26.4
Methane	4.5	5.2	4.6
Carbon Monoxide	26.3	29.4	26.4
Carbon Dioxide	8.1	7.2	7.2
Coke	30.2	29.4	28.7
Aromatics Selectivity			
Benzene	23.1	23.6	27.4
Toluene	30	24.1	26.6
Ethyl-Benzene	1.2	0.9	0.8
m-Xylene and p-Xylene	12	7.2	7.4
o-Xylene	1.9	4.7	1.9
Styrene	4.4	8.7	4.5
Phenol	4	1.5	1.7
Indene	7.1	2.6	3.1
Benzofuran	1.6	13.8	12
Naphthalene	14.7	12.8	14.5
Light Hydrocarbon Selectivity			

Methane	60	64.2	61.8
Ethylene	na	na	na
Propylene	28.2	26.7	29.6
Butene	3.2	2.1	1.8
Butadiene	8.5	7	6.7

5.3 3.2 Catalyst Characterization

To study the stability of the catalyst during CFP, the catalyst was subjected to ten reaction/regeneration cycles. For each cycle the reaction was performed with a WHSV of 0.2 hr^{-1} at 600 °C for 30 min followed by a 30 min purge. After reaction and purge the catalyst was regenerated in air for approximately 3 hours. Figure 5.3.1 shows the powder diffraction patterns of the Grace ZSM-5 catalyst before and after 10 reaction/regeneration cycles. The ZSM-5 crystal structure appears to slightly change after 10 reaction regeneration cycles as the intensities of some of the peaks change. An increase in the intensity of the peak at ~8 2Θ after reaction indicates an increase in ZSM-5 crystalinity or a increase in the framework Si/Al ratio.[94, 95] However, it has been previously shown that a decrease in intensity for the peak at 24 2Θ indicates if aluminum is removed from the framework. [95, 96] As seen in the inset of Figure 3.2.1 the peak at 24 2Θ does not change in intensity, therefore, the increase in Si/Al ratio of the zeolite is probably small.

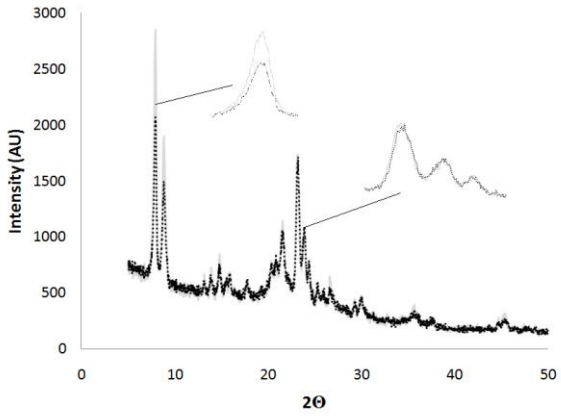

Figure 5.3.1 X-ray diffraction patterns before reaction (dotted line) and after 10 reaction-regeneration cycles (grey line). Cu anode material; K-Alpha1 wavelength = 1.540598 Å; K-Alpha2 wavelength = 1.544426 Å; Ratio K-Alpha2/K-Alpha1 = 0.5; Fixed divergence slit at 0.10 mm.

To qualitatively determine the loss of catalyst fines and attrition SEM imaging was used before and after reaction. The SEM images of the fresh catalyst (a) and the catalyst after ten reaction/regeneration cycles (b) are shown in Figure 5.3.2. The average particle size was measured using ImageJ image processing and analysis software. The average particle size was found to increase from 45 to 63 µm after 10 reaction regeneration cycles. The increase in particle size suggests there is a loss of catalyst fines. This is probably because of loss of catalyst from the fluidized bed reactor due to entrainment. The entrained catalyst was not recycled from the cyclone back to the reactor. The image of the used catalyst also shows some signs of physical damage. More broken pieces of catalyst can be seen in Figure 5.3.2b compared to Figure 5.3.2a.

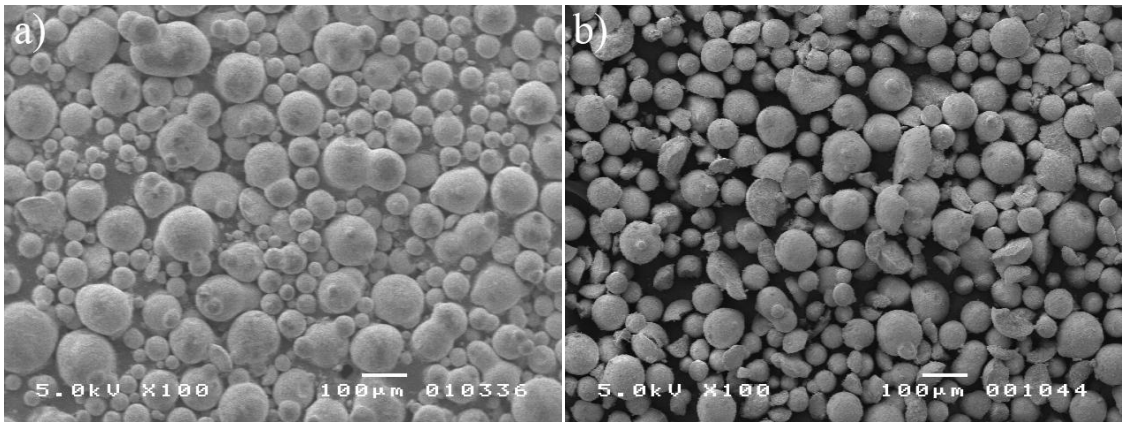

Figure 5.3.2 SEM images of the fluidized bed catalyst before (a) and after 10 reaction-regeneration cycles (b).

The DRIFT spectra of adsorbed ammonia at 100 °C are shown in Figure 5.3.3. The assignments of the bands and relative areas are reported in Table 5.3.1. It can be seen that the area of the bands at 3675 and 3610 cm^{-1} which correspond to Lewis and Brønstead acids do not change much after 10 reaction regeneration cycles. The ratio of Brønstead to Lewis acid sites increases slightly from 1.4 to 1.6 after the repeated reaction-regeneration. The disappearance of the band at 3745 cm^{-1} indicates that the number of surface hydroxyl groups decreases after the reaction-regeneration cycles.

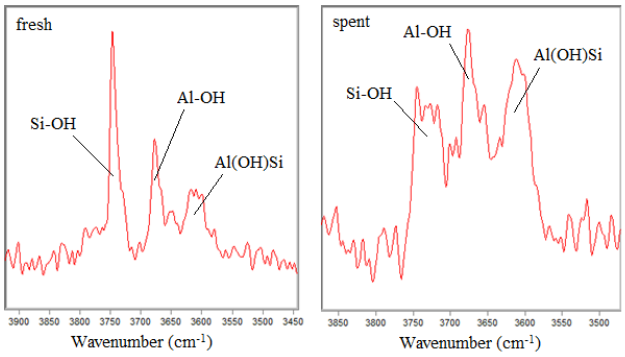

Figure 5.3.3 DRIFT spectra of adsorbed ammonia on the fluidized bed catalyst at 500 °C. Fresh is the catalyst as received after calcining and spent is the catalyst after 10 reaction regeneration cycles.

Table 5.3.1 Band assignments for the 3500-3900 cm-1 region of the DRIFT spectra.

Band (cm^{-1})	Assignment	Fresh Catalyst Area	Spent Catalyst Area
3745	Si-OH	1.3	0.5
3675	Al-OH (Lewis)	1	1.2
3610	Al(OH)Si (Brønsted)	1.4	1.9

In addition to the distribution of acid sites the total number of acid sites was measured using ammonia temperature programmed desorption (TPD). The TPD curves for the fresh and spent catalysts are shown in Figure 5.3.4. It can be seen that there are two peaks with centers at ~275 °C and ~475°. The low temperature peak corresponds to the weakly bound ammonia on non framework Lewis acid sites whereas the high temperature peak corresponds to the more strongly bound ammonia on Brønstead acid sites.[97] As reported in Table 5.3.2 the total acidity of the catalyst decreases after the 10 reaction-regeneration cycles. From the TPD curve it appears that the loss in acidity is due to a decrease of the low temperature peak intensity as the high temperature peak does not change much.

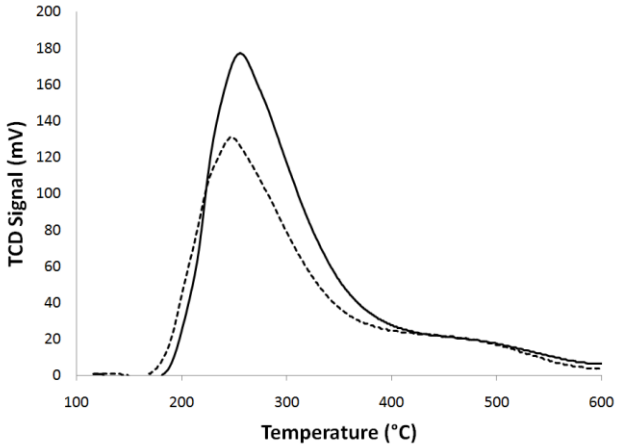

Figure 5.3.4 Temperature programmed desorption of ammonia for the fresh (solid line) and spent (dotted line) catalysts.

Table 5.3.2 Total acidity of the fresh catalyst and the catalyst after 10 reaction-regeneration cycles.

	Total Acidity (mmol NH3/g catalyst)
Fresh	0.49
Spent	0.36

To determine whether metals found in the biomass are deposited on the catalyst during reaction, the spent catalyst was subjected to ICP-EOS to measure the elements present. It can be seen from Table 5.3.3 that ppm levels of four common biomass metals are found in the spent catalyst. It can also be seen that the bulk weight percentage of silicon and aluminum stays relatively the same after the 10 reaction regeneration cycles. The ratio of silicon to aluminum is also constant at a value of 2. The other primary element in the catalyst is phosphorous. The weight percentage of phosphorous in the catalyst also only changes slightly from 4.75 to 4.5 wt% after ten reaction regeneration cycles. Typically spray dried catalysts contain above 40 wt% zeolite, 3-15 wt% phosphorus (P_2O_5), 15-45% kaolin ($Al_2Si_2O_5(OH)_4$) and above 10 wt% alumina.[98] The low Si/Al ratio is

probably due to other additives such as kaolin and alumina as ZSM-5 catalysts typically have a Si/Al ratio above 10.

Table 5.3.3 Elemental analysis of the fresh catalyst and the catalyst after ten reaction regeneration cycles.

	Fresh	Spent
Element Present		
Aluminum (wt %)	13.4	13.2
Silicon (wt %)	26.2	27.5
Phosphorous (wt %)	4.75	4.5
Calcium (ppm)	0	642
Potassium (ppm)	0	812
Magnesium (ppm)	0	308
Manganese (ppm)	0	88

5.4 Pyroprobe

Since the Zeolyst catalyst sample is unsuitable for use in the fluidized bed reactor the pyroprobe was used to compare the two catalysts tested. The pyroprobe reactor is a semi-batch reactor where small samples of biomass and catalyst are mixed together. The pyroprobe reactor is then rapidly heated and the products are analyzed by GCMS. The pyroprobe reactor can screen large numbers of catalysts in a short time with each reaction taking less than 30 minutes to complete. Figure 5.4.1 shows the performance of the two catalysts for the conversion of wood and furan[24]. It can be seen that the aromatic yield of 18 % carbon from wood with the Grace catalyst is higher than the best yield of 14 % aromatic yield obtained in the fluidized bed reactor. Using the pure ZSM-5 Zeolyst catalyst the aromatic yield from wood is 24 % carbon. This demonstrates that the pure ZSM-5 catalyst is more selective than the spray dried catalyst. The coke yield was higher on the Grace catalyst (42%) compared to the pure ZSM-5 (28%) catalyst. The carbon

dioxide yields from the two catalysts are quite similar while the carbon monoxide yield was higher for the Zeolyst catalyst. For the reaction of furan with the Zeolyst ZSM-5 the aromatic yield was 33 % carbon. The coke yield for the furan feed was 37 % carbon. These results illustrate that furan has similar yields for CFP as wood, and therefore is a good probe molecule. Furthermore, furan has been shown to be an important reaction intermediate in CFP.[24]

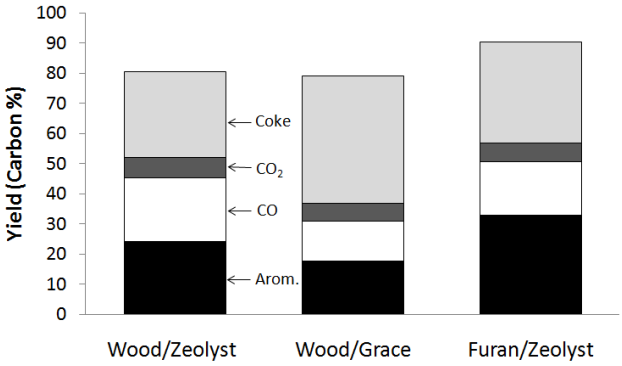

Figure 5.4.1 Product yields for the pyrolysis of wood and furan with the two different catalysts. Reaction conditions: catalyst to feed weight ratio 19, nominal heating rate 1000 °C s-1, reaction temperature 600 °C, reaction time 240 s. Key: aromatics (black), carbon monoxide (white), carbon dioxide (dark grey), coke (grey).

As shown in Table 5.4.1 the aromatic selectivity for the pyrolysis of wood is different for the two catalyst tested. The Grace catalyst produced more naphthalene, indene and phenol. The Zeolyst catalyst produced more of the monocyclic aromatics. The aromatic selectivity for the conversion of furan with the Zeolyst catalyst is quite different from wood. The selectivity for benzene and naphthalene are higher for furan than wood. The toluene and xylene selectivity was lower for furan than for wood. These results demonstrate that the catalyst tested in the fluidized bed reactor is far from the optimal catalyst for CFP.

Table 5.4.1 Aromatic selectivity for the feed and catalyst combinations tested.

	Feed/Catalyst Combination		
	Wood/Zeolyst ZSM-5	Wood/Grace ZSM-5	Furan/Zeolyst ZSM-5
Overall Yields			
Aromatics	24.1	17.7	33.0
Carbon Monoxide	21.3	13.2	17.6
Carbon Dioxide	6.8	6.0	6.3
Coke	28.3	42.2	33.6
Aromatic Selectivity			
Benzene	9.7	5.2	14.0
Toluene	19.5	14.5	15.8
Xylene + Ethyl Benzene	20.8	19.0	8.0
Trimethyl-benzene + Ethyl-methyl-Benzene	6.2	4.0	0.4
Phenol	0.4	5.3	0.0
Benzofuran	0.0	0.0	1.6
Indene	4.2	6.2	3.3
Naphthalene	39.3	45.8	57.0

5.5 Fixed bed

5.5.1 Effect of Furan WHSV

The conversion of furan with a zeolite was tested in the fixed bed reactor at furan WHSV range of 1.9 to 98.4 hr^{-1}. As shown in Figure 5.5.1 the total aromatic carbon yield decreases as WHSV increases. The yield is defined as moles of carbon in the product divided by moles of furan converted. A maximum aromatic yield of 27 % carbon is obtained at the lowest WHSV. This yield decreases to 7.2 % carbon as the WHSV increases. The furan conversion varies greatly over the WHSV range tested. At low WHSV the furan conversion is 96.9 % then decreases to 17.2 % at the highest WHSV tested.

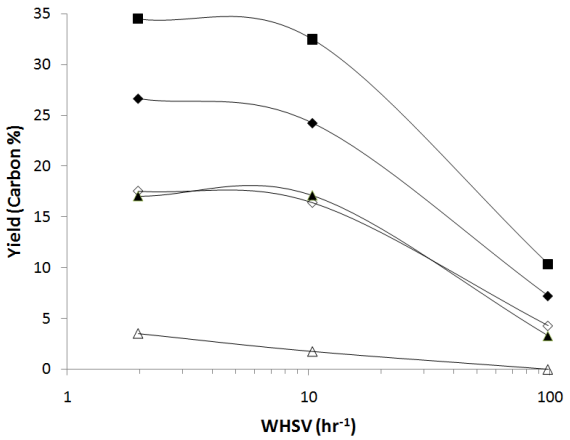

Figure 5.5.1 Carbon yield for furan conversion over ZSM5. Reaction conditions: Zeolyst ZSM-5 catalyst, 204 sccm helium flow rate, 600 °C reactor temperature, 4.5 min total reaction time. Yield is defined as moles of carbon in the product divided by moles of furan carbon converted. Key: ♦: aromatics ■: coke, □: unidentified, ▲: CO, Δ: CO_2, ○: methane and ◊: olefins.

In the fixed bed, the aromatic selectivity is also a function of WHSV. The selectivity for toluene and xylene decreases from 37.0 % to 25.7 % carbon and 10.3 to 0.0 % carbon, respectively. Unlike the fluidized bed, the selectivity for benzene decreases over the range tested from 37.0 % to 27.2 % carbon. The selectivity for the intermediate size aromatics indene and benzofuran changes the most over the range tested. Indene increases from 7.5% to 24.2% while benzofuran increases from 0.6% to 12.2%. The selectivity for naphthalene is relatively constant over the range.

Table 5.5.1 Product selectivities for aromatic and olefin species for various weight hourly space velocities. Aromatic selectivity is defined as the moles of carbon in the product divided by the total moles aromatic carbon. Olefin selectivity is defined as the moles of carbon in the product divided by the total moles olefin carbon.

	WHSV (hr^{-1})		
	1.9	10.4	98.4
Furan Conversion	96.9	43.3	17.2
Overall Yields			
Aromatics	26.7	24.3	7.2
Olefins	17.5	16.4	4.3
Carbon Monoxide	17.0	17.1	3.3
Carbon Dioxide	3.5	1.8	0.0
Coke	34.5	32.5	10.3
Aromatic Selectivity			
Benzene	37.0	33.5	27.2
Toluene	37.0	30.0	25.7
Ethyl-Benzene	0.0	0.0	0.0
Xylenes	10.3	5.4	0.0
Styrene	5.5	9.2	7.7
Indene	7.5	13.7	24.2
Benzofuran	0.6	3.6	12.2
Napthalene	2.1	4.6	2.9
Light Hydrocarbon Selectivity			
Ethylene	54.0	50.2	61.8
Propylene	41.3	45.4	38.2
Butene	4.7	4.4	0.0

5.5.2 Effect of Reactor Temperature

Figure 5.5.2 shows the product yields as a function of reactor temperature for furan conversion over ZSM5. The maximum aromatic yield (24% carbon) from furan was measured at 600 °C. Unlike the fluidized bed the yield of olefins is a strong function of temperature for furan conversion. The olefin yield increases from 5% carbon to 19% carbon when the temperature was increased from 450 to 650 °C. The yield of carbon monoxide increases from 8 % to 17 % carbon over the range tested. Carbon dioxide yield exhibits a slight maximum at 600 °C.

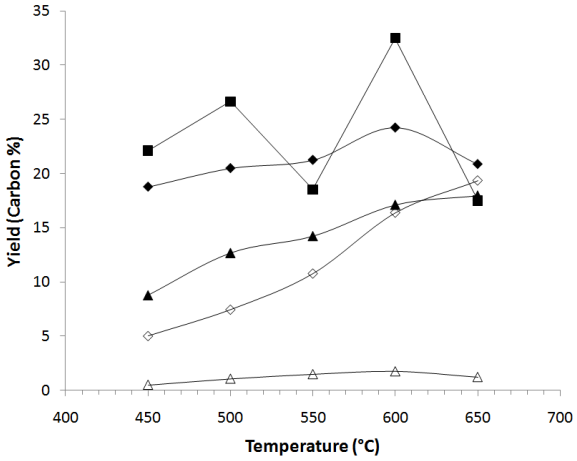

Figure 5.5.2 Conversion of furan as a function of temperature over a zeolite catalyst. Reaction conditions: Zeolyst ZSM-5 catalyst, 204 sccm helium flow rate, 10.4 WHSV, 4.5 min total reaction time. Carbon yield defined as moles of carbon in the product divided by moles of furan converted. Key: ♦: aromatics ■: coke, □: unidentified, ▲: CO, Δ: CO_2, ○: methane and ◊: olefins

The aromatic selectivity is also a strong function of temperature. The selectivity for benzene increases from 14.9% to 39.7% carbon as the temperature increases. The selectivity for toluene increases with temperature from 17.4% to 29.0% carbon. Xylene and naphthalene go through a maximum selectivity at 500 °C and 550 °C, respectively. At low temperature benzofuran is the most abundant product with a selectivity of 51.5 carbon percent, however, the selectivity decreases to 11.3% when the temperature is increased to 650 °C.

Table 5.5.2 Product selectivity for aromatic and olefin species for various temperatures. Aromatic selectivity is defined as the moles of carbon in the product divided by the total moles aromatic carbon. Olefin selectivity is defined as the moles of carbon in the product divided by the total moles olefin carbon.

	Temperature (°C)				
	450	500	550	600	650
Overall Yields					
Aromatics	18.8	20.5	21.3	24.3	20.9
Olefins	5.0	7.5	10.8	16.4	19.4
Carbon Monoxide	8.8	12.7	14.2	17.1	18.0
Carbon Dioxide	0.5	1.1	1.5	1.8	1.2
Coke	22.1	26.6	18.5	32.5	17.5
Aromatic Selectivity					
Benzene	14.9	19.1	26.0	33.5	39.7
Toluene	17.4	24.2	28.5	30.0	29.0
Ethyl-Benzene	0.0	0.0	0.0	0.0	0.0
Xylenes	5.0	6.6	5.9	5.4	4.9
Styrene	1.8	5.2	7.7	9.2	7.4
Indene	9.5	13.3	14.0	13.7	4.1
Benzofuran	51.5	29.6	13.1	3.6	11.3
Naphthalene	0.0	2.1	4.7	4.6	3.7
Light Hydrocarbon Selectivity					
Ethylene	61.6	56.8	51.5	50.2	55.5
Propylene	38.4	43.2	47.6	45.4	38.9
Butene	0.0	0.0	0.9	4.4	5.6

5.5.3 Olefin Co-feed

The effect of co-feeding olefins with furan was tested in the fixed bed reactor. As shown in Table 5.5.3 the co-feeding of ethylene and proplylene both increase the conversion of furan. Without olefin co-feed the conversion of furan under the same reaction conditions is 43 % carbon. When olefins are co-feed to the reactor the furan conversion was increased from 43% carbon to 62% for propylene and 49% for ethylene. Similar to the fluidized bed results propylene is more reactive than ethylene. The moles olefin out/moles olefin values indicate propylene is consumed during reaction and

ethylene has a net production. The synergistic effect of propylene feeding can clearly be seen from the propylene consumption since the conversion of propylene increases with the furan feed compared to 2 % propylene alone.

Table 5.5.3 Reaction Parameters and olefin conversion for the CFP of wood with olefin co feed. Reaction conditions: Zeolyst ZSM-5 catalyst, 200 sccm total gas flow rate, 10.4 furan WHSV, 4.5 min total reaction time, 600 °C reaction temperature. The low olefin co feed runs correspond to 0.2 mol% olefin in the gaseous feed. The high olefin co feed runs correspond to 2 mol% olefin in the gaseous feed. The runs with zero furan WHSV were run with 2 mol% olefin in the gaseous feed.

	Propylene Feed			Ethylene Feed		
Furan WHSV (h^{-1})	10.7	10.7	0	10.5	10.6	0
Furan conversion (carbon amount)	48.7	62.7	na	46.3	49.3	na
Olefins/furan (mass)	0.2	1.7	∞	0.1	1.1	∞
Olefins/furan (carbon)	0.18	1.8	na	0.13	1.24	na
Moles of olefins out/in	0.98	0.82	0.91	1.34	1.06	1.05

Figure 5.5.3 shows the single pass yields of the various products as a function of ethylene co-feed amount. The single pass yield for 2 mol% ethylene without furan feed is also shown. The yield of aromatics increases slightly at the intermediate ethylene amount then decreases at higher ethylene concentration. This is from the low reactivity of ethylene as more carbon is being fed to the reactor without greatly increasing the total amount of aromatics produced.

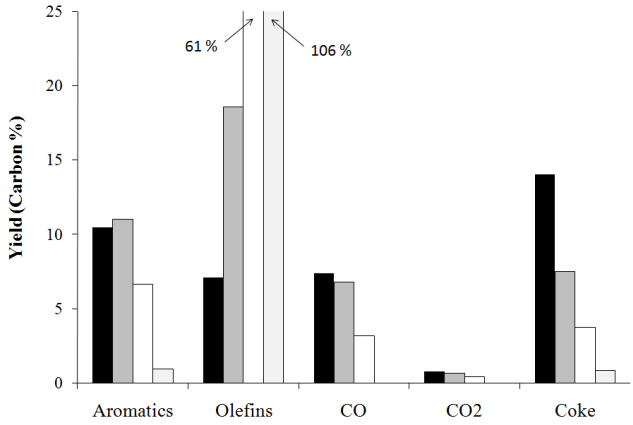

Figure 5.5.3 Yields for the reaction of furan with ethylene co-feed over ZSM-5. The yield is calculated from the total carbon fed to the reactor. Key: Black: no co feed, grey: 0.13 ethylene/furan carbon ratio, white: 1.24 ethylene/furan carbon ratio, light gray: 2% ethylene only.

The selectivity for the various aromatic products is also a function of the amount of ethylene in the co-feed as shown in Table 5.5.4. The selectivity for both toluene and xylenes increase at the higher ethylene feed amounts. Benzene, benzofuran and naphthalene all decrease slightly from no co-feed to high ethylene co-feed. However, benzene goes through a minimum at intermediate ethylene feed while benzofuran and naphthalene go through a maximum. The primary olefin produced other than ethylene is propylene with a selectivity of 91.1 % at no ethylene co-feed. At the highest ethylene feed amount the propylene selectivity decreases to 87.1 % carbon while butene increases from 8.9% to 12.9 % carbon.

Table 5.5.4 Overall yield and product selectivity for the CFP of furan with various ethylene co-feed amounts. Aromatic selectivity is defined as the moles of carbon in the product divided by the total moles aromatic carbon. Olefin selectivity is defined as the moles of carbon in the product divided by the total moles olefin carbon.

	Ethylene/furan ratio (mol/mol carbon)			
	0.13	1.24	Furan only	2% Ethylene only
Overall Yields				
Aromatics	11.0	6.6	10.5	1.0
Olefins	18.6	61.4	7.1	106.1
Carbon Monoxide	6.8	3.2	7.4	0.0
Carbon Dioxide	0.7	0.4	0.8	0.0
Coke	7.5	3.7	14.1	0.8
Aromatic Selectivity				
Benzene	30.2	31.3	33.5	46.6
Toluene	29.4	33.4	30.0	25.1
Xylenes	6.6	9.1	5.4	14.7
Styrene	9.4	8.1	9.2	0.0
Indene	15.1	11.5	13.7	13.6
Benzofuran	4.4	2.8	3.6	0.0
Napthalene	4.9	3.7	4.6	0.0
Light Hydrocarbon Selectivity				
Ethylene	na	na	na	na
Propylene	91.5	87.1	91.1	56.1
Butene	8.5	12.9	8.9	43.9

Figure 5.5.4 shows the single pass yields of the various products for different propylene co-feed amount. The single pass yield for 2 mol% propylene without furan feed is also shown. The yield of aromatics increases from 10.5 % to 16.3 % carbon. A synergistic effect can clearly be seen in Figure 5.5.4 as this aromatic increase is higher than the sum of the aromatic yields from the furan and 2 mol% propylene. Like ethylene the

propylene co-feed decreases the coke yield. The coke yield is decreased from 14.0 % to 3.7 % carbon.

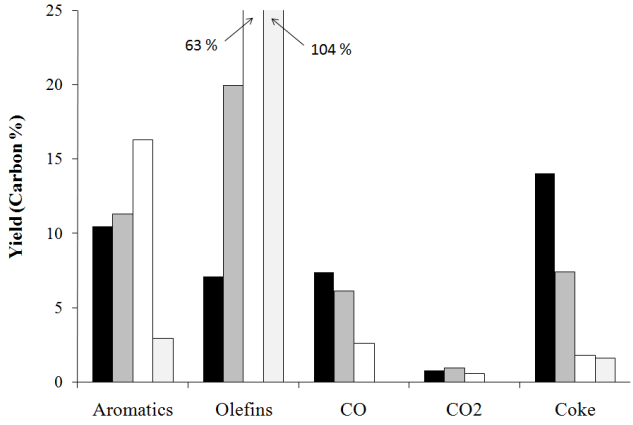

Figure 5.5.4 Yields for the reaction of furan with propylene co-feed over ZSM-5. The yield is calculated from the total carbon fed to the reactor, b) yield based on furan fed to the reactor. Key: Black: no co feed, dark grey: 0.18 propylene/furan carbon ratio, white: 1.83 propylene/furan carbon ratio, light gray: 2% propylene only.

As shown in Table 5.5.5 propylene co-feed effect the selectivity of aromatics more than the ethylene co-feed. The selectivity for benzene decreases from 33.5 % 16.2 % carbon to with increasing olefin amount. Interestingly for the propylene run without furan feed benzene is the most selective product at 39.1 % carbon selectivity. Toluene selectivity doubles from 30.0 % to 60.4 % carbon at the highest propylene/furan ratio. Xylenes also increase with propylene feed from 5.4 % to 15.2 %. Styrene, indene, benzofuran and naphthalene selectivity all decrease with propylene feed. The propylene co-feed also has an effect on the other olefins. The ethylene selectivity decreases from 91.9 % to 64.8 % carbon while butene increases from 8.1 % to 35.2 % carbon.

Table 5.5.5 Detailed yields and Product selectivity for the CFP of furan with various propylene feed amounts. Aromatic selectivity is defined as the moles of carbon in the product divided by the total moles aromatic carbon. Olefin selectivity is defined as the moles of carbon in the product divided by the total moles olefin carbon.

	Propylene/furan ratio (mol/mol carbon)			
	0.18	1.83	Furan only	2% Propylene only
Overall Yields				
Aromatics	11.3	16.3	10.5	3.0
Olefins	19.9	62.9	7.1	104.2
Carbon Monoxide	6.1	2.6	7.4	0.0
Carbon Dioxide	1.0	0.6	0.8	0.0
Coke	7.4	1.8	14.1	1.6
Aromatic Selectivity				
Benzene	28.7	16.2	33.5	39.1
Toluene	39.9	60.4	30.0	35.4
Xylenes	8.1	15.2	5.4	14.7
Styrene	7.7	4.5	9.2	1.4
Indene	9.7	2.3	13.7	6.0
Benzofuran	2.1	0.6	3.6	0.0
Napthalene	3.8	0.9	4.6	3.4
Light Hydrocarbon Selectivity				
Ethylene	84.2	64.8	91.9	51.4
Propylene	na	na	na	na
Butene	15.8	35.2	8.1	48.6

5.6 Discussion

5.6.1 Reactor Design

In this paper three different reactor configurations and two different feedstocks were tested. Figure 5.6.1 shows the optimized yields for the three reactors. For the

continuous reactors the lowest WHSV run is shown. Both feeds showed a higher yield of aromatics in the pyroprobe reactor than the continuous reactors with the same catalyst. The coke yield is also higher in the pyroprobe reactor. No olefins were detected in the pyroprobe reactor. Furthermore, larger amounts of napthalenes are observed in the pyroprobe reactor. The olefins plus aromatic yields is higher in the continuous reactors than the pyroprobe reactor. The differences in the three reactors may arise from differences in mass transfer. In the continuous reactors there is a high gas flux through the catalyst bed while the pyroprobe reactor has no gas flow though the bed. In the pyroprobe reactor the gas residence time and concentration are likely much higher. With a long gas residence time the rate of naphthalene formation could be higher as it is probably formed by secondary reactions.[28] The absence of olefins in the product from the pyroprobe could also be linked to low rates of mass transfer in the pyroprobe as olefins can oligomerize to form aromatics.[68, 77]

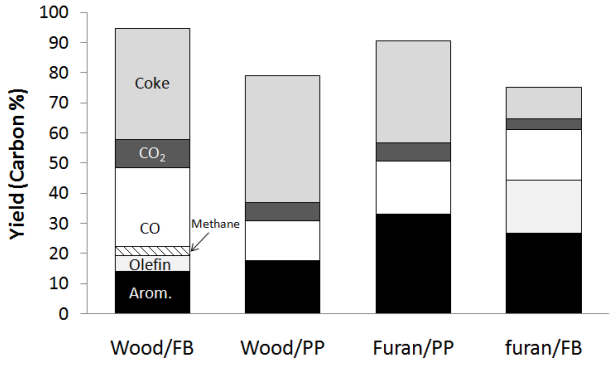

Figure 5.6.1 Comparison of all three reactors with optimized reaction conditions. Key: aromatics (black), carbon monoxide (white), carbon dioxide (dark grey), coke (medium grey), olefins (dark grey), methane (hatched lines).

Table 5.6.1 Detailed yield distribution and product selectivity for catalytic fast pyrolysis of wood and furan in the various reactors. Aromatic selectivity is defined as the moles of carbon in the product divided by the total moles aromatic carbon. Olefin selectivity is defined as the moles of carbon in the product divided by the total moles olefin carbon.

	Feed/Reactor Combination			
	Wood/Fluidized Bed	Wood/Pyroprobe	Furan/Pyroprobe	Furan/Fixed Bed
Overall Yields				
Aromatics	14.0	17.7	33.0	26.7
Olefins	5.4	0.0	0.0	17.6
Methane	2.8	0.0	0.0	0.0
Carbon Monoxide	26.2	13.2	17.6	17.1
Carbon Dioxide	9.4	6.0	6.3	3.5
Coke	36.8	42.2	33.6	10.3
Aromatic Selectivity				
Benzene	24.8	5.2	14.0	37.0
Toluene	34.1	14.5	15.8	37.0
Xylene + Ethyl Benzene	19.4	19.0	8.0	15.8
Trimethyl-benzene + Ethyl-methyl-Benzene	0.0	4.0	0.4	0.0
Phenol	1.1	5.3	0.0	0.0
Benzofuran	4.2	0.0	1.6	0.6
Indene	1.4	6.2	3.3	7.5
Naphthalene	14.9	45.8	57.0	2.1

Aside from reactor configuration temperature and weight hourly space velocity have the largest effect on aromatic yield and selectivity. It may be advantageous to operate at temperatures below 600 °C as this temperature maximizes the monocyclic aromatics. Higher temperatures shift the selectivity toward naphthalenes. The olefin selectivity exiting the reactor is a strong function of temperature. In the fluidized bed at temperatures below 600 °C propylene is selectively produced and could be recycled to form more aromatics. In the fixed bed with furan the maximum selectivity for propylene is at 550 °C. Operation at low temperature also decreases the amount of methane generated during wood pyrolysis. The methane is likely from the lignin portion of the pinewood as only trace amounts of methane were measured during the conversion of furan.

In addition to temperature the biomass WHSV can be used to maximize the yield of toluene and xylene. As seen in Table 5.2.1 both of these aromatics have high selectivity at low WHSV. Furthermore, when using wood is the feedstock the selectivity for the undesired naphthalene and methane decreases at low WHSV. If the objective is to use the aromatics as a gasoline additive toluene and xylene would be the best aromatics to produce as they are higher octane than benzene and naphthalene.[58] Additionally EPA regulations limit benzene to 0.8 vol % in gasoline while the other aromatics can make up to 25 % of the total volume.[56] However, benzene is more valuable than toluene due to its use in the chemical industry.

The major competing reaction to the formation of aromatics is the formation of coke. The time on stream study shows that catalyst activity goes through a maximum. This initial increase in aromatic concentration is likely due to the formation of the

hydrocarbon pool within the zeolite. It is possible that this hydrocarbon pool acts as a catalyst to selectively produce the aromatics. When the maximum rate is obtained the hydrocarbon pool is likely fully formed within the zeolite, however, at the same time the coking of the catalyst begins to deactivate the activity. Therefore, the aromatic concentration decreases in the outlet gas. To be industrially feasible fresh catalyst would need to be continuously feed to the reactor while spent catalyst is withdrawn and regenerated in a separate vessel. The process heat from regeneration could be used to provide energy for the pyrolysis reactor.

In addition to reversible catalyst deactivation by coking, irreversible deactivation by loss of zeolite crystal structure, active sites and attrition of the catalyst particles could occur. Several researchers have shown that ZSM-5 is susceptible to loss of acid sites by dealumination under steam treatment.[99-102] It is likely that the water concentration in the reactor is too low to see this kind of deactivation as the XRD data before and after reaction show that the crystal structure of the zeolite is relatively unchanged. The TPD data shows the total acidity of the composite catalyst decreases with repeated reaction/regeneration cycles, however, this loss in acidity appears to be from a loss of the weak non framework Lewis acid sites in the non zeolite components of the catalyst (such as alumina).[97] The actual zeolite acid sites are not likely lost as the high temperature TPD peak and the ratio of Brønstead to Lewis acid sites in the zeolite measured by DRIFTS remain constant. From the ICP-OES the metals; calcium, potassium, magnesium and manganese are deposited on the catalyst after the repeated reaction regeneration cycles. The deactivation of zeolite catalyst from these metals has not been documented in the literature, however, other metals such as nickel and vanadium have

been well studied.[103-106] Vanadium affects the crystalininty of the catalyst while Ni promotes coke deposition on the catalyst. Nevertheless, little change in catalyst activity was observed before and after exposure to the wood.

The surface hydroxyl groups appear to be removed after repeated reaction-regeneration cycles. From the SEM images the spent catalyst shows signs of particle attrition and loss of fines. According to Werther and Reppenhagen[107] the main source of attrition in low superficial velocity (<0.55 m/s) fluidized bed systems is from the gas jets near the distributor plate and from bubbling within the bed. At higher gas velocities (>0.55 m/s) the main source of attrition comes from the cyclone. Future reactor design should focus on optimization for catalyst lifetime as well as aromatic yield.

5.6.2 Olefin Recycle

One of the major products from catalytic fast pyrolysis is olefins. For wood the highest olefin yield is about 8 % carbon and for furan the highest olefin yield is about 17 % carbon. It would be desirable to recycle the product olefins to increase the overall aromatic yield of the process. Propylene is easier to convert into aromatics than ethylene because the carbocation of propylene is more stable than that of ethylene.[108] For the conversion of methanol to aromatics over ZSM-5 it has been proposed that ethylene is an end product formed from the hydrocarbon pool concurrently with aromatics. Propylene is suspected to be an intermediate in a separate cycle which forms higher alkenes. [68] These higher alkenes ultimately oligomerize to form aromatics.[68, 77] The results from Table 5.2.1 also suggest that propylene is an intermediate as is exhibits a maximum yield at intermediate biomass WHSV.

The feasibly of recycling olefins to the reactor can be assessed by simple mass balance on the model system shown in Figure 5.6.2. The wood (labeled biomass in Stream 1) is mixed with a recycle stream (Stream 3) containing the olefins, CO, and CO2, and fed into the fluidized bed reactor . Inside the reactor the wood (dry basis) can either react to form aromatics and olefins by reactions (1) and (2), respectively. The olefins in the reactor can be converted to additional aromatics by equation (3).

$$C_{3.8}H_{5.8}O_{2.7} \rightarrow 0.36\ C_7H_8 + 1.45\ H_2O + 1.25\ CO \quad (1)$$

$$C_{3.8}H_{5.8}O_{2.7} \rightarrow 0.67\ C_3H_6 + 0.9\ H_2O + 1.8\ CO \quad (2)$$

$$C_3H_6 \rightarrow \tfrac{3}{7}C_7H_8 + \tfrac{9}{7}H_2 \quad (3)$$

The balance of biomass not converted into aromatics or olefins is converted into coke and gasses. The spent coked catalyst is then sent to a regenerator and regenerated by burning the coke in a secondary regeneration reactor. Most likely, the catalyst recirculation is adjusted to control the temperature of the reactor and regenerator.[109] In our system the coke yield is quite high and heat removal from the regenerator may be necessary to avoid high temperatures in the regenerator. The excess heat could be utilized elsewhere in the process. The product stream from the reactor (Stream 3) is separated into the condensable aromatic product (Stream 4), water and water soluble compounds and non-condensable olefins and gases. The separation system would include a condenser system that removes condensable compounds from the recyclable gases. The liquefied product would contain a mixture of water, aromatics and water soluble compounds. The aromatic product would be decanted and further refined. The water and water soluble products would go to waste water treatment. From the separation system the olefins are then recycled to the reactor with a molar recycle ratio defined as moles of olefin in the recycle

(Stream 6) divided by moles of olefin in the purge stream (Stream 5). The purge stream is necessary to remove the CO and CO2 and avoid accumulation of any other non reactive species in the system.

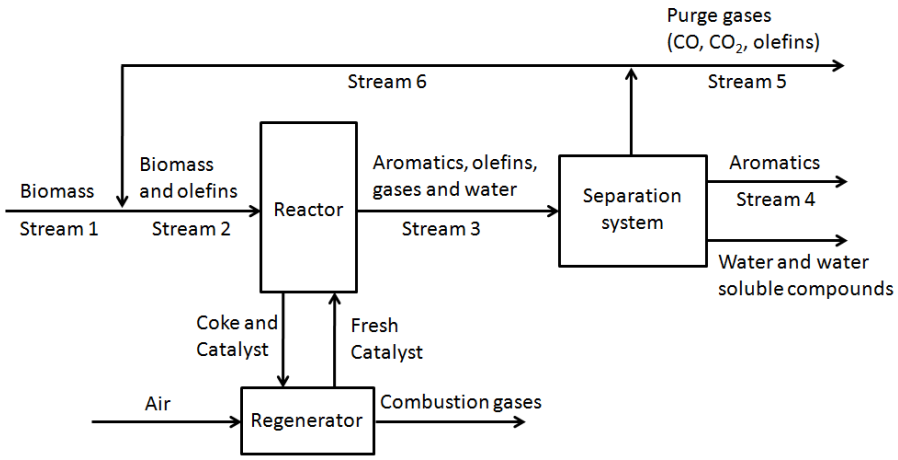

Figure 5.6.2 Block flow diagram for aromatic production by catalytic fast pyrolysis.

Figure 5.6.3 shows the effect of adjusting the olefin conversion and recycle ratio for CFP. Each line in Figure 5.6.3 corresponds to a different extent of reaction for Equation 3. The extent of reactions for Equations 1 and 2 were both fixed at 0.17 to match the experimental yield for olefins and aromatics at zero olefin co-feed in the fluidized bed reactor. As shown in Figure 5.6.3, the yield of aromatics increases with increasing the recycle ratio and also increasing the extent of reaction for Reaction 3. It can be seen that using recycle ratios in excess of 10 and having high extents of reaction for Reaction 3 could lead to a two fold increase in aromatic yield for the system.

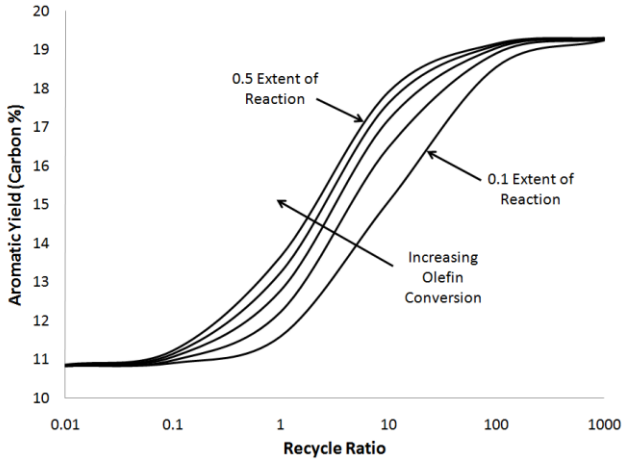

Figure 5.6.3 Aromatic yield as a function of recycle ratio for the model process depicted in Figure 4.2.1. Solid lines are drawn for various extents of olefin reaction (Equation 3 above). The extents of reaction plotted are; 0.1, 0.2, 0.3, 0.4 and 0.5.

Recycling the olefins back into the reactor may also allow operation of the fluidized bed reactor at higher space velocities. As shown in the results from Section 5.5.3 there is higher conversion of intermediate furans in the presence of the olefin co-feed. This suggests that co-feeding of olefins at higher biomass WHSV could increase the conversion which otherwise would be low at those conditions.

Shown in Figure 5.6.4 is the volume yield of aromatics per metric ton of feed that could be produced. The volume of aromatics produced at 100 % theoretical yield was calculated from equations 4 and 5 using toluene as the product. For the calculation it was assumed that the wood is dry and half of the toluene produced is through equation 4 and half though equation 5.

$$C_{3.8}H_{5.8}O_{2.7} \rightarrow 0.36\ C_7H_8 + \ 1.45\ H_2O + \ 1.25\ CO \qquad (4)$$

$$C_{3.8}H_{5.8}O_{2.7} \rightarrow 0.43\ C_7H_8 + \ 1.16\ H_2O + \ 0.77\ CO_2 \qquad (5)$$

The aromatic yield in our fluidized bed reactor was 17% higher than the aromatic yield obtained by Olazar et al.[20] in a spouted bed reactor. If the product olefins are recycled

then the yield of aromatics can be increased to 23 gallons per ton. The aromatic yield from wood in the pryroprobe is higher than either of the fluidized bed results. This shows that there is still potential for the optimization of the fluidized bed reactor and the fluidized bed catalyst. The results from Figure 5.6.1 show that the pure zeolite catalyst performs better than the spray dried composite catalyst suggesting further improvements in this process can come by further catalyst improvement. As shown in Figure 5.6.4 the aromatic yield for cellulose CFP is much higher than with wood (~30 gal ton^{-1}). This suggests that another option for increasing aromatic yield in CFP is to optimize the biomass feedstock by increasing the amount of cellulose and hemicellulose and decrease the amount of lignin. This results also suggest that the lignin content of the wood decreases the yield of aromatics as we have previously reported for the CFP of maple wood and maple wood with lignin removed.[110] In addition, a recent international study involving 14 laboratories concluded that lignin pyrolyses differently than whole biomass and current reactor designs are not sufficient to pyrolyze lignin by itself.[111] It has also been shown that for non-catalytic pyrolysis the type of the feedstock can greatly affect the composition of the primary pyrolysis vapors.[13] Another way to further increase aromatic yield is to inhibit coke forming reactions as it has been previously shown that coke formation and aromatic production are competing reactions.[24] On an energy basis the yield of aromatics from CFP in our current fluidized bed reactor is about half of the projected yield of other biomass conversion technologies such as fermentation and gasification. Ethanol production from wood via hydrolysis and fermentation can yield 85 gal ton^{-1}.[5] On an energy basis this volume of fuel yields 7.5 GJ ton^{-1}. It has been projected that up to 56 gal ton^{-1} liquid alkanes can be produced via Fischer–Tropsch

Synthesis.[5] The energy yield for this volume of fuel is about 8 GJ ton^{-1}. However, it should be noted that large amounts of resources have been devoted to optimize hydrolysis/fermentation technologies and Fischer-Tropsch Synthesis whereas few resources have been devoted to the study of CFP.[5] Furthermore, CFP is only 25-35% of the theoretical yield today. There is no thermodynamic limitation to the yield that we have obtained as these reactions are thermodynamically favorable. It is likely that advances in catalysis combined with reaction engineering studies to design fluidized bed reactors that are optimized for CFP technology will allow us to obtain energy yields that are comparable to other biomass conversion technologies.

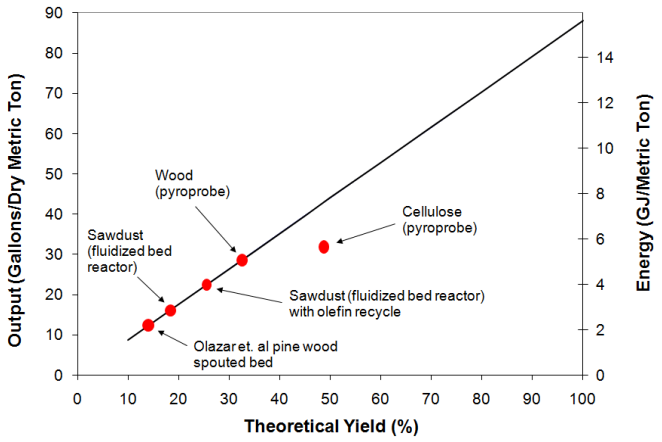

Figure 5.6.4 Volume of aromatics that could be produced from one ton of feed for various yields.

5.7 Conclusions

The general conclusion from this study is that aromatics and olefins can be produced directly from wood in a continuous fashion in a fluidized bed reactor that contains zeolite catalysts. The olefins that are produced can be recycled to the reactor to produce additional aromatics. Propylene is more reactive than ethylene leading to a higher conversion of feed and a higher yield of aromatics when it is co-fed to the reactor.

Temperature and WHSV can be used to adjust both the yield and selectivity for the aromatic products. When wood is reacted at low space velocities the more valuable monocyclic aromatics are produced and the formation of lower value polycyclic aromatics is inhibited. The more valuable aromatics are also favored at lower temperature. Lowering the temperature also decreases the amount of methane produced. Mineral impurities from the biomass can be found on the zeolite catalyst after the reaction. However, the concentration of acid sites on the zeolite did not change after exposure to the mineral impurities. The spray dried composite catalyst is not as selective to aromatics as the pure ZSM-5 catalyst suggesting that modifying the properties of the spray dried catalyst would increase the aromatic yield. Of the three reactors tested the batch pyroprobe reactor produces the most aromatics. The pyroprobe reactor also produces more naphthalene and does not produce olefins. The combined yield of aromatic plus olefin products is higher in the fixed and fluidized bed reactors with the same feeds and catalysts.

CHAPTER 6

CONCLUSIONS

The general conclusion from this study is that high quality aromatic fuel additives can be produced directly from solid biomass feedstocks by catalytic fast pyrolysis in a single catalytic reactor at short residence times. This reaction involves homogeneous thermal decomposition of the biomass to smaller oxygenates. These oxygenates are then dehydrated. The dehydrated oxygenates then diffuse into the zeolite catalysts where they undergo a series of oligomerization, decarbonylation, and dehydration reactions to produce aromatics, CO, CO_2, and water. The major challenge with catalytic fast pyrolysis is undesired coke formation, which can be produced from both homogeneous and heterogeneous reactions. Coke formation can be minimized and aromatic formation can be maximized by three important parameters:

(1) fast heating rates

(2) high catalyst to feed ratios, and

(3) proper catalyst selection (both active site and pore structure).

The fast heating rates and high catalyst feed ratios are necessary to avoid undesired thermal decomposition reactions in the homogeneous phase. The pore structure and active sites of the catalyst can be tuned to control the product selectivity. The aromatics produced include benzene, toluene, xylenes, substituted benzenes, indanes, and napthalenes. The pyroprobe reactor used in this study offers a convenient method to study the fundamental science of catalytic fast pyrolysis and for screening catalysts in order to scale up to real systems. It is likely that advances in understanding the chemistry of catalytic fast pyrolysis combined with the development of improved catalytic

materials, which are specifically designed for biomass conversion, will lead to further process improvements.

The catalytic fast pyrolysis of glucose involves two steps. The first step involves the rapid thermal decomposition of glucose. Glucose can decompose through two different pathways. At low temperature glucose is decomposed to small oxygenates through retro-aldol condensation reactions. At high temperatures glucose is dehydrated to form anhydrosugars and furans. Both decomposition pathways can occur homogenously or on catalyst active sites. Addition of ZSM-5 to the reactor lowers the temperature at which both the decomposition reactions occur. The second step in CFP is the formation of aromatics within the pores of the zeolite. The monocyclic aromatic compounds are formed from random hydrocarbon fragments which are most likely produced from a hydrocarbon pool within the zeolite structure. Naphthalene is produced from two different steps with one step involving the combination of monocyclic aromatics with oxygenated fragments. Both benzene and naphthalene are susceptible to alkylation from the hydrocarbon pool although the rate of alkylation of naphthalene is high and the rate of alkylation of benzene is low. The aromatic formation step is far slower than the preceding thermal decomposition reactions.

The oxygenates produced from thermal decomposition are likely the intermediates in the formation of aromatics as furans and acetic acid produce similar aromatic products under the same pyrolysis conditions (600 °C for 240 s). The main competing reaction with aromatic production is the formation of coke on the surface of the catalyst. Coke is formed through intermediate furan polymers which ultimately decompose to unsaturated coke. To achieve maximum aromatic yields pyrolysis should proceed with rapid

decomposition of glucose to oxygenates to react with the catalyst. The concentration of oxygenates should remain low to avoid formation of coke and less desirable polycyclic aromatics.

In addition to elucidating the chemistry of CFP we have also shown that aromatics and olefins can be produced directly from wood in a continuous fashion in a fluidized bed reactor that contains zeolite catalysts. The olefins that are produced can be recycled to the reactor to produce additional aromatics. Propylene is more reactive than ethylene leading to a higher conversion of feed and a higher yield of aromatics when it is co-fed to the reactor. Temperature and WHSV can be used to adjust both the yield and selectivity for the aromatic products. When wood is reacted at low space velocities, the more valuable monocyclic aromatics are produced and the formation of lower value polycyclic aromatics is inhibited. The more valuable aromatics are also favored at lower temperature. Lowering the temperature also decreases the amount of methane produced. Mineral impurities from the biomass can be found on the zeolite catalyst after the reaction. However, the concentration of acid sites on the zeolite did not change after exposure to the mineral impurities. The spray dried composite catalyst is not as selective to aromatics as the pure ZSM-5 catalyst suggesting that modifying the properties of the spray dried catalyst would increase the aromatic yield. Of the three reactors tested the batch pyroprobe reactor produces the most aromatics. The pyroprobe reactor also produces more naphthalene and does not produce olefins. The combined yield of aromatic plus olefin products is higher in the fixed and fluidized bed reactors with the same feeds and catalysts.

The CFP process is still relatively in its infancy compared to other conversion technologies and there is much room for improvement. For example, on an energy basis, ethanol production through enzymatic pretreatment and hydrolysis of wood can provide about 50% of the theoretical yield of the CFP process. Similarly, on an energy basis, Fisher-Tropsch synthesis of liquid alkanes from biomass derived synthesis gas can only yield about 50% of the theoretical yield of CFP. There have been large amounts of resources devoted to these other conversion technologies compared to CFP. It is likely that advances in catalysis combined with reaction engineering studies to design fluidized bed reactors that are optimized for CFP technology will allow us to obtain energy yields that are comparable to other biomass conversion technologies.

BIBLIOGRAPHY

[1] L. R. Lynd, C. E. Wyman, T. U. Gerngross, *Biotechnology Progress* **1999**, *15*, 777.

[2] C. E. Wyman, *Annual Review of Energy and the Environment* **1999**, *24*, 189.

[3] C. E. Wyman, B. E. Dale, R. T. Elander, M. Holtzapple, M. R. Ladisch, Y. Y. Lee, *Bioresource Technology* **2005**, *96*, 1959.

[4] D. L. Klass, *Biomass for Renewable Energy, Fuels, and Chemicals*, Academic Press, San Diego, **1998**.

[5] G. W. Huber, S. Iborra, A. Corma, *Chemical Reviews* **2006**, *106*, 4044.

[6] G. W. Huber, J. A. Dumesic, *Catalysis Today* **2006**, *111*, 119.

[7] P. J. Dauenhauer, B. J. Dreyer, N. J. Degenstein, L. D. Schmidt, *Angewandte Chemie, International Edition* **2007**, *46*, 5864.

[8] A. V. Bridgwater, *Chemical Engineering Journal (Amsterdam, Netherlands)* **2003**, *91*, 87.

[9] H. B. Goyal, D. Seal, R. C. Saxena, *Renewable & Sustainable Energy Reviews* **2007**, *12*, 504.

[10] A. Demirbas, *Energy Sources, Part A: Recovery, Utilization, and Environmental Effects* **2007**, *29*, 753.

[11] A. V. Bridgwater, *Energy & Fuels* **1992**, *6*, 113.

[12] M. Wright, Robert C. Brown, *Biofuels, Bioprod. Bioref.* **2007**, *1*, 191.

[13] D. Mohan, C. U. Pittman, P. H. Steele, *Energy & Fuels* **2006**, *20*, 848.

[14] J. Adam, E. Antonakou, A. Lappas, M. Stoecker, M. H. Nilsen, A. Bouzga, J. E. Hustad, G. Oye, *Microporous and Mesoporous Materials* **2006**, *96*, 93.

[15] P. A. Horne, P. T. Williams, *Fuel* **1996**, *75*, 1043.

[16] M. I. Nokkosmaki, E. T. Kuoppala, E. A. Leppamaki, A. O. I. Krause, *Journal of Analytical and Applied Pyrolysis* **2000**, *55*, 119.

[17] T. R. Carlson, G. A. Tompsett, W. C. Conner, G. W. Huber, *Topics In Catalysis* **2009**, *52*, 241.

[18] T. R. Carlson, T. R. Vispute, G. W. Huber, *Chemsuschem* **2008**, *1*, 397.

[19] A. A. Lappas, M. C. Samolada, D. K. Iatridis, S. S. Voutetakis, I. A. Vasalos, *Fuel* **2002**, *81*, 2087.

[20] M. Olazar, R. Aguado, J. Bilbao, A. Barona, *AIChE Journal* **2000**, *46*, 1025.

[21] D. Fabbri, C. Torri, V. Baravelli, *Journal of Analytical and Applied Pyrolysis* **2007**, *80*, 24.

[22] A. Pattiya, J. O. Titiloye, A. V. Bridgwater, *Journal of Analytical and Applied Pyrolysis* **2008**, *81*, 72.

[23] A. Aho, N. Kumar, K. Eraenen, T. Salmi, M. Hupa, D. Y. Murzin, *Fuel* **2008**, *87*, 2493.

[24] T. R. Carlson, J. Jae, Y.-C. Lin, G. A. Tompsett, G. W. Huber, *Journal Of Catalysis* **2010**, *270*, 110.

[25] J. B. Paine, Y. B. Pithawalla, J. D. Naworal, *Journal Of Analytical And Applied Pyrolysis* **2008**, *83*, 37.

[26] J. B. Paine, Y. B. Pithawalla, J. D. Naworal, *Journal Of Analytical And Applied Pyrolysis* **2008**, *82*, 10.

[27] J. B. Paine, Y. B. Pithawalla, J. D. Naworal, *Journal Of Analytical And Applied Pyrolysis* **2008**, *82*, 42.

[28] T. R. Carlson, J. Jae, G. W. Huber, *Chemcatchem* **2009**, *1*, 107.

[29] N. Y. Chen, T. F. Degnan, Jr., L. R. Koenig, *Chemtech* **1986**, *16*, 506.

[30] M. I. Hanniff, L. H. Dao, *Energy from Biomass and Wastes* **1987**, *10*, 831.

[31] M. I. Hanniff, L. H. Dao, *Applied Catalysis* **1988**, *39*, 33.

[32] M. C. Samolada, W. Baldauf, I. A. Vasalos, *Fuel* **1998**, *77*, 1667.

[33] J. D. Adjaye, N. N. Bakhshi, *Fuel Processing Technology* **1995**, *45*, 161.

[34] R. K. Sharma, N. N. Bakhshi, *Canadian Journal of Chemical Engineering* **1993**, *71*, 383.

[35] A. V. Bridgwater, M. L. Cottam, *Energy & Fuels* **1992**, *6*, 113.

[36] L. H. Dao, M. Haniff, A. Houle, D. Lamothe, *Preprints of Papers - American Chemical Society, Division of Fuel Chemistry* **1987**, *32*, 308.

[37] K. Bilba, A. Ouensanga, *Journal Of Analytical And Applied Pyrolysis* **1996**, *38*, 61.

[38] R. K. Sharma, J. B. Wooten, V. L. Baliga, M. R. Hajaligol, *Fuel* **2001**, *80*, 1825.

[39] J. I. Kroschwitz, Kirk-Othmer Encyclopedia of Chemical Technology, 5ed., Wiley Interscience, Hoboken, NJ, **2004**.

[40] A. H. Corma, G. W. Huber, L. Sauvanaud, P. O'Connor, *Journal of Catalysis* **2007**, *247*, 307.

[41] D. M. Ruthven, B. K. Kaul, *Ind. Eng. Chem. Res.* **1993**, *32*, 2053.

[42] M. Cook, W. C. Conner, *Proceedings of the International Zeolite Conference, 12th, Baltimore, July 5-10, 1998* **1999**, *1*, 409.

[43] G. Fremont, *Journal of Catalysis* **1992**, *9*, 1.

[44] Q. H. Xia, S. C. Shen, J. Song, S. Kawi, K. Hidajat, *Journal of Catalysis* **2003**, *219*, 74.

[45] P. A. Horne, N. Nugranad, P. T. Williams, *Journal of Analytical and Applied Pyrolysis* **1995**, *34*, 87.

[46] P. B. Weisz, W. O. Haag, P. G. Rodewald, *Science (Washington, DC, United States)* **1979**, *206*, 57.

[47] L. H. Dao, (Institut National de la Recherche Scientifique, Can.). Application: CA CA, **1986**, p. 10 pp.

[48] L. H. Dao, M. Haniff, A. Houle, D. Lamothe, *ACS Symposium Series* **1988**, *376*, 328.

[49] A. Aho, N. Kumar, K. Eranen, T. Salmi, M. Hupa, D. Y. Murzin, *Process Safety and Environmental Protection* **2007**, *85*, 473.

[50] E. F. Iliopoulou, E. V. Antonakou, S. A. Karakoulia, I. A. Vasalos, A. A. Lappas, K. S. Triantafyllidis, *Chemical Engineering Journal (Amsterdam, Netherlands)* **2007**, *134*, 51.

[51] H. J. Park, J.-I. Dong, J.-K. Jeon, K.-S. Yoo, J.-H. Yim, J. M. Sohn, Y.-K. Park, *Journal of Industrial and Engineering Chemistry (Seoul, Republic of Korea)* **2007**, *13*, 182.

[52] V. V. Alferov, O. S. Misnikov, O. V. Kislitsa, E. M. Sul'man, D. Y. Murzin, N. Kumar, *Kataliz v Promyshlennosti* **2006**, 42.

[53] E. M. Sulman, V. V. Alferov, Y. Y. Kosivtsov, A. I. Sidorov, O. S. Misnikov, A. E. Afanasiev, N. Kumar, D. Kubicka, J. Agullo, T. Salmi, D. Y. Murzin, *Chemical Engineering Journal (Amsterdam, Netherlands)* **2007**, *134*, 162.

[54] G. W. Huber, S. Iborra, A. Corma, *Chemical Reviews (Washington, DC, United States)* **2006**, *106*, 4044.

[55] S. Ernst, M. Hartmann, S. Sauerbeck, T. Bongers, in *App. Catal. A Vol. 200*, **2000**, pp. 117.

[56] Clean Air Act of 1990 report of the committee on Energy and Commerce, U. S. C. H. C. o. E. a. Commerce, U.S.G.P.O., 1990

[57] C. L. Yaws, *Chemical Properties Handbook*, McGraw Hill, New York, **1999**.

[58] W. G. Lovell, *Industrial and Engineering Chemistry* **1948**, *40*, 2388.

[59] *Petrochemical Evaporation Loss From Storage Tanks*, First Edition, Bulletin No. 2523, American Petroleum Institute, Washington, D.C., 1969.

[60] A. Baysar, K. J. Johnson, J. L. Kuester, *Res. Thermochem. Biomass Convers., [Ed. Rev. Pap. Int. Conf.]* **1988**, *680*, 680.

[61] B. Krieger-Brockett, *Research on Chemical Intermediates* **1994**, *20*, 39.

[62] Y. Yoshizawa, T. Fujita, N. Iwamatsu, *Nippon Kikai Gakkai Ronbunshu, B-hen* **1996**, *62*, 2874.

[63] M. Miura, H. Kaga, T. Yoshida, K. Ando, *Journal of Wood Science* **2001**, *47*, 502.

[64] A. M. Sarotti, R. A. Spanevello, A. G. Suarez, *Green Chemistry* **2007**, *9*, 1137.

[65] M. Graef, G. G. Allan, B. B. Krieger, *Preprints - American Chemical Society, Division of Petroleum Chemistry* **1979**, *24*, 432.

[66] F. Yu, K. W. Hennessy, S. Deng, P. Chen, R. Ruan, *Abstracts of Papers, 234th ACS National Meeting, Boston, MA, United States, August 19-23, 2007* **2007**, IEC.

[67] F. Yu, S. Deng, P. Chen, Y. Liu, Y. Wang, A. Olsen, D. Kittelson, R. Ruan., *Applied Biochemistry and Biotechnology* **2007**, *136-140*, 957.

[68] M. Bjorgen, S. Svelle, F. Joensen, J. Nerlov, S. Kolboe, F. Bonino, L. Palumbo, S. Bordiga, U. Olsbye, *Journal Of Catalysis* **2007**, *249*, 195.

[69] D. R. Lide, *CRC Handbook of Chemistry and Physics: A Ready-Reference Book of Chemical and Physical Data*, 89 ed., CRC Press, Boca Raton, Fla, **2008**.

[70] Z. Sarbak, *Reaction Kinetics and Catalysis Letters* **2000**, *69*, 177.

[71] A. Miecznikowski, J. Hanuza, *Zeolites* **1987**, *7*, 249.

[72] P. Walther, *Zeitschrift fuer Physikalische Chemie (Leipzig)* **1988**, *269*, 809.

[73] H. A. Wells, Jr., R. H. Atalla, *Journal of Molecular Structure* **1990**, *224*, 385.

[74] S. Bertarione, F. Bonino, F. Cesano, A. Damin, D. Scarano, A. Zecchina, *Journal Of Physical Chemistry B* **2008**, *112*, 2580.

[75] J. A. Biscardi, E. Iglesia, *Journal Of Physical Chemistry B* **1998**, *102*, 9284.

[76] J. A. Biscardi, E. Iglesia, *Journal Of Catalysis* **1999**, *182*, 117.

[77] J. F. Haw, W. G. Song, D. M. Marcus, J. B. Nicholas, *Accounts Of Chemical Research* **2003**, *36*, 317.

[78] D. M. McCann, D. Lesthaeghe, P. W. Kletnieks, D. R. Guenther, M. J. Hayman, V. Van Speybroeck, M. Waroquier, J. F. Haw, *Angewandte Chemie-International Edition* **2008**, *47*, 5179.

[79] R. J. Evans, T. A. Milne, *Energy & Fuels* **1987**, *1*, 123.

[80] K. Lourvanij, G. L. Rorrer, *Journal of Chemical Technology & Biotechnology* **1997**, *69*, 35.

[81] P. T. Williams, S. Besler, *Advances in thermochemical biomass conversion* **1994**, *2*, 771.

[82] C. Ramos-Sanchez, F. J. Rey, L. Rodriguezmendez, F. J. Martin-Gil, *Thermochimica Acta* **1988**, *134*, 55.

[83] M. Stocker, *Microporous And Mesoporous Materials* **1999**, *29*, 3.

[84] M. Choura, N. M. Belgacem, A. Gandini, *Macromolecules* **1996**, *29*, 3839.

[85] R. T. Conley, I. Metil, *Journal of Applied Polymer Science* **1963**, *7*, 37.

[86] D. Mores, E. Stavitski, M. H. F. Kox, J. Kornatowski, U. Olsbye, B. M. Weckhuysen, *Chemistry-A European Journal* **2008**, *14*, 11320.

[87] N. K. Bar, F. Bauer, D. M. Ruthven, B. J. Balcom, *Journal Of Catalysis* **2002**, *208*, 224.

[88] M. Bjorgen, U. Olsbye, S. Kolboe, *Journal Of Catalysis* **2003**, *215*, 30.

[89] J. M. Matsen, *Powder Technology* **1996**, *88*, 237.

[90] S. S. Chauk, L.-S. Fan, *Heat Transfer in Packed and Fluidized Beds*, 3rd ed., McGraw-Hill, New York, **1998**.

[91] T. M. Knowlton, S. B. R. Karri, A. Issangya, *Powder Technology* **2005**, *150*, 72.

[92] J. Diebold, J. Scahill, *Preprints of Papers - American Chemical Society, Division of Fuel Chemistry* **1987**, *32*, 297.

[93] Y. Tsuchiya, H. Shimogaki, H. Abe, A. Kagawa, *Journal of Wood Science* **2010**, *56*, 53.

[94] Y. T. Kim, K. D. Jung, E. D. Park, *Microporous And Mesoporous Materials* **2010**, *131*, 28.

[95] C. H. Ding, X. S. Wang, X. W. Guo, S. G. Zhang, *Catalysis Communications* **2008**, *9*, 487.

[96] J. L. S.J. Wang, G.W. Guo, L.Q. Zhao, R.H. Wang, *Chinese Journal Of Catalysis* **1992**, *13*.

[97] G. L. Woolery, G. H. Kuehl, H. C. Timken, A. W. Chester, J. C. Vartuli, *Zeolites* **1997**, *19*, 288.

[98] G. M. Smith, B. K. Speronello, *Vol. US 7547813 B2* (Ed.: USPO), BASF Catalysts LLC, United States, **2009**.

[99] T. Sano, N. Yamashita, Y. Iwami, K. Takeda, Y. Kawakami, *Zeolites* **1996**, *16*, 258.

[100] I. Wang, T. J. Chen, K. J. Chao, T. C. Tsai, *Journal Of Catalysis* **1979**, *60*, 140.

[101] V. R. Choudhary, D. B. Akolekar, *Journal Of Catalysis* **1990**, *125*, 143.

[102] S. M. Campbell, D. M. Bibby, J. M. Coddington, R. F. Howe, R. H. Meinhold, *Journal Of Catalysis* **1996**, *161*, 338.

[103] E. Rautiainen, R. Pimenta, M. Ludvig, C. Powels, *Catalysis Today* **2009**, *140*, 179.

[104] C. A. Trujillo, U. N. Uribe, P. P. KnopsGerrits, L. A. Oviedo, P. A. Jacobs, *Journal Of Catalysis* **1997**, *168*, 1.

[105] E. L. Kugler, D. P. Leta, *Journal Of Catalysis* **1988**, *109*, 387.

[106] M. T. Xu, X. S. Liu, R. J. Madon, *Journal Of Catalysis* **2002**, *207*, 237.

[107] J. Werther, J. Reppenhagen, *Aiche Journal* **1999**, *45*, 2001.

[108] C. Pereira, G. T. Kokotailo, R. J. Gorte, *Journal of Physical Chemistry* **1991**, *95*, 705.

[109] *Kirk-Othmer encyclopedia of chemical technology, Vol. 3*, 5 ed., Wiley-Interscience, Hoboken, NJ, **2004**.

[110] J. H. Jae, G. A. Tompsett, Y. C. Lin, T. R. Carlson, J. C. Shen, T. Y. Zhang, B. Yang, C. E. Wyman, W. C. Conner, G. W. Huber, *Energy & Environmental Science* **2010**, *3*, 358.

[111] D. J. Nowakowski, A. V. Bridgwater, D. C. Elliott, D. Meier, P. de Wild, *Journal Of Analytical And Applied Pyrolysis* **2010**, *88*, 53.